UNIVERSITY OF CALIFORNIA

Los Angeles

Simultaneous global extraction of transverse momentum-dependent distribution functions

A dissertation submitted in partial satisfaction of

the requirements for the degree Doctor of

Philosophy in Physics

by

Fidele Johnson Twagirayezu

2025

ABSTRACT OF THE DISSERTATION

Simultaneous global extraction of transverse momentum-dependent distribution functions

by

Fidele Johnson Twagirayezu

Doctor of Philosophy in Physics

University of California, Los Angeles, 2025

Professor Zhongbo Kang, Chair

Scientific investigations show that nucleons are the building blocks of atomic nuclei, which constitute nearly all the mass of visible matter in the universe. Unlike electrons, which are fundamental particles, nucleons have an internal structure composed of quarks and gluons. While much has been learned about nucleon structure, many details remain to be understood. There is broad consensus that understanding the fundamental properties of matter requires understanding the nucleon's internal structure in terms of its constituents. In Quantum Chromodynamics (QCD), the theory of strong interactions, the nucleon is described as a relativistic bound state of quarks and gluons, interacting strongly through the exchange of gluons. These partons are permanently confined within hadrons due to the property of color confinement, which prevents their direct isolation but still allows their dynamics to be studied through high-energy scattering experiments. However, at sufficiently small distance scales, QCD exhibits the property of asymptotic freedom [1, 2], where the strong coupling becomes significantly weaker. This allows QCD factorization to be used in perturbative calculations, enabling the study of nucleon structure [3].

One of the key challenges in QCD is the full understanding the spin structure of the nucleon in terms of its constituents. A nucleon is known to be a fermion with a spin of 1/2, and while we understand how to distribute the nucleon's spin between the orbital angular momentum and the spins of quarks and gluons, the exact numerical values of each contribution remain uncertain, especially when it comes to the orbital angular momentum. In this context, three-dimensional distributions of quarks and gluons in momentum space are crucial tools, as they capture all possible spin-orbit and spin-spin interactions between the proton and its constituents. A thorough understanding of these distributions can offer valuable insights into the roles of quarks and gluons in determining the nucleon's spin. The early studies focused on processes involving collinear functions to understand the nucleon spin structure. While these functions offer valuable insight into the internal composition of nucleons, it was quickly realized that they were not sufficient since they only provide a one-dimensional and, therefore, partial perspective on the complex structure of the nucleon.

The search for alternative methods beyond collinear factorization to fully describe the nucleon internal structure has led to the development of a robust transverse momentum dependent (TMD) factorization framework. This framework allows to acquire the three-dimensional (3D) dynamics of quarks and gluons within a colliding nucleon. These new and precise data provide the means to determine transverse momentum dependent parton distributions, often referred to as TMDs. In this dissertation, we develop TMD formalisms to perform simultaneous global analysis of Sivers asymmetries and Collins asymmetries. The TMD Sivers formalism allows us to extract simultaneously the Sivers function from semi-inclusive deep inelastic scattering, Drell-Yan production, and jet production in proton-proton collisions. The TMD Collins formalism allows us to extract simultaneously the Collins fragmentation function from semi-inclusive deep inelastic scattering, e^+e^- annihilation, and hadron production inside jets in proton-proton collisions.

The dissertation of Fidele Johnson Twagirayezu is approved.

Stuart Brown

Huan Z. Huang

James Rosenzweig

Zhongbo Kang, Committee Chair

University of California, Los Angeles

2025

Dedication

To my mom, Félicité

Contents

List of Figures

List of Tables

Preface

I would like to express my heartfelt gratitude to my dissertation committee for their unwavering support and guidance throughout my research journey. I am especially thankful to Prof. Zhongbo Kang, whose expert advice, continuous encouragement, and invaluable insights were essential to the development of this dissertation. My sincere appreciation also goes to Prof. Stuart Brown, Prof. Huan Z. Huang, and Prof. James Rosenzweig for their thoughtful feedback, constructive criticism, and generous contributions of time and expertise, which have greatly enriched this work. It has been an honor to work with such distinguished scholars, and I am truly grateful for the opportunity to learn from each of you.

I would also like to express my sincere gratitude to Dr. Erik Bochove for his dedicated mentorship and the independent work we've undertaken together. Our frequent discussions have greatly enhanced my ability to grasp advanced physics concepts. Lastly, I extend my heartfelt thanks to Prof. Wilhelmus J. Geerts for his expert guidance, encouragement and invaluable teaching, which have significantly contributed to my academic growth and education. Additionally, I would like to express my gratitude to Dr. Luisa M. Scolfaro for kindly agreeing to work with me and providing the opportunity to learn about computational physics.

Curriculum Vitae

Recent Education:

Texas State University, San Marcos, TX, USA *2014-2016*

M.S. student in physics

Thesis defense: June 2017

University of California, Los Angeles, CA, USA *September 2018-Present*

Ph.D. student in Physics

Dissertation defense: December 2024

Recent Experience:

Air Force Research Laboratory, Albuquerque, NM, USA *Summer 2015*

AFRL Scholar

NASA Ames Research Center, Moffett Field, CA, USA *Summer 2016*

Research Associate

Recent Awards:

NASA fellowship (Texas Space Grant Consortium Fellowship) *2016-2017*

Competitive Edge Grant (UCLA) *2018-2019*

Eugene V. Cota-Robles Fellowship (UCLA) *2018-2022*

Honor Societies:

The Honor Society of Phi Kappa Phi

Alpha Chi Honor Society

Publications:

Here is a list of some recent articles:

1. Zhong-Bo Kang, John Terry, and Fidele J. Twagirayezu,
   Simultaneous global analysis of the Sivers Asymmetry in SIDIS, Drell-Yan, and Jet Production, in preparation to submit to JHEP.

2. Zhong-Bo Kang, Fidele J. Twagirayezu, and Yiyu Zhou,
   A simultaneous global extraction of the Collins function in e^+e^- collisions, semi-inclusive DIS, and hadron-in-jet production, in preparation to submit to JHEP.

3. Fidele J. Twagirayezu,
   On magnetic monopole and Dirac quantization condition in the minimal length formalism, Can.J.Phys. 101 (2023) 4, 195-202.

4. Fidele J. Twagirayezu,
   Effect of minimal length uncertainty on neutrino oscillation, Z.Naturforsch.A 78 (2023) 5, 405-410.

5. Fidele J. Twagirayezu,
   Quantum gravity modifications of magnetized ideal gas thermodynamics, Physica A: Statistical Mechanics and its Applications 580 (2021) 126159.

6. Fidele J. Twagirayezu,
   On generalized quantum scattering theory: Rayleigh scattering and Thomson scattering with a minimal length, Phys.Lett.A 400 (2021) 127323.

7. Fidele J. Twagirayezu,
   Generalized uncertainty principle corrections on atomic excitation, Annals Phys. 422 (2020) 168294.

For a complete list of publications, please refer to iNSPIRE and the ORCID database.

Outline

In this dissertation, after introducing the origin of quark theories in Chapter (1) we quickly proceed to introduce the notion of transverse single spin asymmetry (TSSA) in the same Chapter (1) because of its essential utility to extract TMD functions of interest. In Chapter (2) we discuss the SCET due to its capability to provide a systematic framework for describing processes where different types of modes are present, especially in the context of high-energy hadronic physics. In other words, The SCET provides an effective description of a theory. Since Wilson lines appear frequently in gauge theories, we discuss their importance for non-local operators in gauge theories and present different types of Wilson lines and some physical interpretations in Chapter (3). Since our TMD formalisms involve the use of twist-2 and twist-3 functions, we discuss the derivations of these functions from correlation functions (correlators) in Chapter (4). We also discuss the TMD factorization theorems, a powerful tool in quantum field theory (QFT), which allow us to express cross sections in terms of perturbatively calculable quantities and non-perturbative quantities. In addition, we discuss one of different regulators to eliminate rapidity divergences. Since our TMD formalisms involve QCD evolutions, we discuss derivations of evolution equations and solutions to evolution equations in Chapter (5). Because of the importance of SCET, we also discuss TMD factorization and TMD evolution in SCET in Chapter (5). The Sivers formalism and results are presented in Chapter (6). The Collins formalism is presented in Chapter (7). Finally, the dissertation is summarized in Chapter (8).

Chapter 1

Introduction

1.1 Origin of quark model

In search for understanding of nature, mankind has made some remarkable progress. Nowadays, it is known that all elements which are building blocks of nature are made of protons of positive charges and neutrons of neural charges, forming atomic nucleus, surrounded by orbiting electrons of negative charges to form atoms. In the early 20th century, experiments with particle accelerators revealed a plethora of subatomic particles beyond the proton, neutron, and electron. Physicists found a bewildering array of particles, leading to a desire to understand their underlying structure and organization. The discovery of the strange mesons suggested that that there might be more fundamental building blocks underlying the known particles.

Various classification schemes were developed to organize the ever-growing list of observed particles. The constituent quark model which is based on an $SU(3)$ flavor symmetry, proposed by Murray Gell-Mann [20, 21] and independently by George Zweig [22, 23], was one such scheme that provided insight into the underlying structure of hadrons (particles like protons and neutrons). The quark model, suggests the presence of fundamental particles termed quarks. These quarks are believed to exhibit a fundamental symmetry described

by the $SU(3)$ group theory, leading to the identification of three elementary particles: up, down, and strange quarks. Experimental validation of this model came from measurements conducted by SLAC [24, 25], where electron-proton and electron-neutron collisions in deep-inelastic scattering (DIS) experiments provided evidence supporting the existence of up and down quarks. Additional quarks were predicted and their existence was also confirmed by experiments.

Later, it was realized that quarks are bound inside nucleons. Since quarks carry an electric charge, their presence raised the question of how nucleons could remain bound together despite electrostatic repulsion. This led to the proposal of a strong, short-range force that overcomes the electromagnetic force at nuclear scales. The first significant theory of the strong interaction was put forward by Yukawa, who proposed that the proton and neutron are held together by the exchange of a force-mediating particle. This exchange particle is now known as the pion.

1.2 Quantum Chromodynamics

Quantum Chromodynamics (QCD) is the fundamental theory describing the strong interaction, one of the four known forces of nature. It explains how quarks and gluons, the building blocks of protons, neutrons, and other hadrons, interact through the exchange of force-carrier particles called gluons. QCD is a type of quantum field theory, and it operates under the principle that quarks possess a property known as color charge, a fundamental property of quarks and gluons, analogous to electric charge in quantum electrodynamics(QED) and comes in three types, traditionally referred to as red, green, and blue. Unlike the electromagnetic force (which involves electric charge), the strong force is incredibly powerful at short distances but becomes weaker at longer ranges due to a phenomenon called asymptotic freedom, where the interaction strength between quarks and gluons decreases at higher energies. This theory is central to understanding particle physics, as it governs the behavior of matter at the small-

est scales, playing a key role in high-energy processes such as those occurring in particle accelerators and the early universe. The QCD Lagrangian density [26] is usually expressed as

$$\begin{aligned}\mathcal{L}_{\rm QCD} = &-\frac{1}{4}G^a_{\mu\nu}G^{a\mu\nu} + i\sum_{j=1}^{n}\bar{\psi}^\alpha_j\gamma^\mu(D_\mu)_{\alpha\beta}\psi^\beta_j - \sum_{j=1}^{n}m_j\bar{\psi}^\alpha_j\psi_{j,\alpha} - \frac{1}{2\alpha_G}\partial^\mu A^a_\mu\partial_\mu A^\mu_a \\ &- \partial_\mu\bar{\phi}_a D^\mu\phi^a,\end{aligned} \tag{1.1}$$

where $G^a_{\mu\nu} \equiv \partial_\mu A^a_\nu - \partial_\nu A^a_\mu + g_s f_{abc}A^b_\mu A^c_\nu \quad (a \equiv 1, 2, ..., 8)$ are the Yang-Mills strength tensors expressed in terms of gluon fields $A^a_\mu(x)$. The quark field of flavor j and mass m_j is represented by ψ_j and $\phi^a(x)$ represents eight Grassmann-valued fields in the $\overline{8}$ representation of SU(3). These ghost fields $\phi^a(x)$ are associated with the gauge fixing procedure and ensure the correct treatment of redundancies in the gauge theory. The covariant derivative D_μ is expressed as

$$(D_\mu)_{\alpha\beta} = \delta_{\alpha\beta}\partial_\mu - ig_s\sum_a\frac{1}{2}t^a_{\alpha\beta}A^a_\mu\,. \tag{1.2}$$

The covariant derivative D_μ acts on the quark color component α, β. The 3×3 color matrices $t^a_{\alpha\beta}$ are the eight generators of the SU(3) gauge group, and f^{abc} represents the fully antisymmetric structure constants of the gauge group, defined by the commutation relation $[T^a, T^b] = if^{abc}T^c$, where $(T^a)_{\alpha\beta} = (1/2)t^a_{\alpha\beta}$ in the fundamental color $\overline{3}$ representation, and $(T_a)_{bc} = -if_{abc}$ in the adjoint $\overline{8}$ representation. The last two terms in the Lagrangian density are the gauge-fixing term for a covariant quantization in the gluon sector, $\alpha_G = 1(0)$ in the Feynman (Landau) gauge respectively, and the Faddeev-Popov ghost term [27] to remove nonphysical degrees of freedom. The parameter g_s is the interaction strength and it is related to the more conventional strong coupling constant α_s as follows

$$\alpha_s = \frac{g_s^2}{4\pi}\,. \tag{1.3}$$

The asymptotic freedom is one of the essential characteristics of QCD. The discovery of asymptotic freedom earned D. Gross, H. Politzer, and F. Wilczek the Nobel Prize in Physics

in 2004 [28, 29]. This behavior is captured by the renormalization group equation for the strong coupling constant $\alpha_s(\mu)$, [30] given by

$$\mu^2 \frac{\partial \alpha_s}{\partial \mu^2} = \frac{\partial \alpha_s}{\partial \ln \mu^2} = \beta(\alpha_s)\,, \quad \beta(\alpha_s) = -\alpha_s^2 \left(b_0 + b_1 \alpha_s + b_2 \alpha_s^2 + \dots\right)\,, \tag{1.4}$$

where b_0 is the 1-loop coefficient of the β-function, and $b_1, b_2, \dots$ are the 2-loop and 3-loop coefficients, respectively. The coefficient b_0 is given by

$$b_0 = \frac{11 C_A - 4 n_f T_R}{12\pi} = \frac{33 - 2 n_f}{12\pi}\,, \tag{1.5}$$

where $C_A = 3$, $T_R = 1/2$, and n_f denotes the number of quark flavors. With six quark flavors (u, d, s, c, b, t), we have $n_f = 6$, resulting in $b_0 > 0$. The negative sign in Eq. (1.4) is responsible for asymptotic freedom, indicating that $\alpha_s(\mu)$ decreases as μ increases. For a given physical process, the renormalization scale μ is typically chosen to match the momentum transfer Q in that process, so $\alpha_s(\mu^2 = Q^2)$ reflects the effective strength of the strong interaction involved. Figure (1.1) displays the running coupling α_s measured as a function

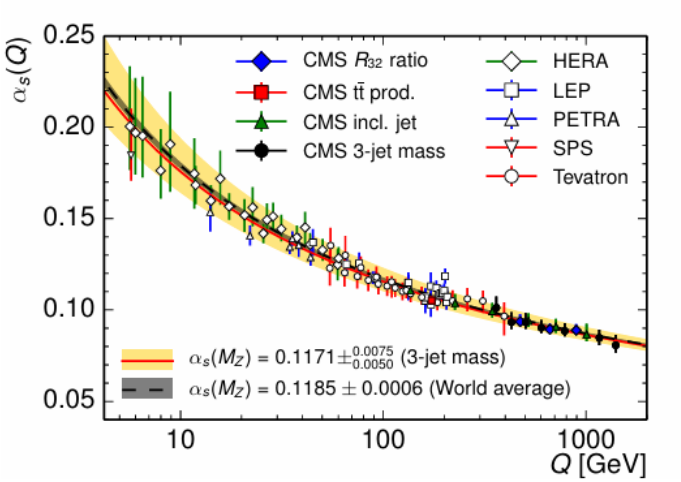

Figure 1.1: The result for the running coupling $\alpha_s(Q)$ is shown as a function of the energy scale Q in [4]. The running coupling $\alpha_s(Q)$, determined with CT10 – NLO, is compared with the world average of $\alpha_s(M_z) = 0.1185 \pm 0.0006$ [5]. The error bars on the data points correspond to the total uncertainty.

of the energy scale Q , taken from [4]. The figure shows measurements of the running $\alpha_s(Q)$ from different experiments. For high Q values, the coupling α_s is weak which allows the use of perturbation methods. The coupling α_s increases at low energies and becomes divergent at the scale Λ_{QCD}. As a result, QCD becomes strongly interacting at scales around and below 1 GeV. In this energy regime, perturbative methods are no longer reliable.

1.3 Transverse spin asymmetries

In high-energy nuclear and particle physics, understanding the spin structure of hadrons is essential for uncovering the complex dynamics of strong interactions. A key observable in this area is the transverse single spin asymmetry (TSSA), which refers to the asymmetry in the distribution of particles produced in a scattering process when one of the colliding particles is transversely polarized. Unlike longitudinal polarization, which is more commonly studied in hadronic physics, transverse polarization provides unique insights into the internal structure and dynamics of hadrons.

Transverse single spin asymmetry arises when the spin of a hadron is oriented perpendicular to the direction of motion, and it is observed as an imbalance in the distribution of final-state particles, such as in the azimuthal angle of produced particles relative to the spin axis. This asymmetry has been experimentally observed in various processes, particularly in high-energy scattering experiments involving protons and hadronic collisions, such as in proton-proton (pp) or proton-nucleus (pA) interactions. In general, the TSSA for an inclusive process such as $A^{\uparrow}B \to C + X$ is expressed as

$$A_N = \frac{d\sigma^{\uparrow} - d\sigma^{\downarrow}}{d\sigma^{\uparrow} + d\sigma^{\downarrow}} \tag{1.6}$$

where $d\sigma^{\uparrow(\downarrow)}$ is the differential cross section for the production of a hadron C when A is transversely polarized in the upward or the downward direction. For illustration purposes, Figure (1.2) shows the measured x_F-dependent TSSA for the production of $\pi^{\pm}$ [6]. The study

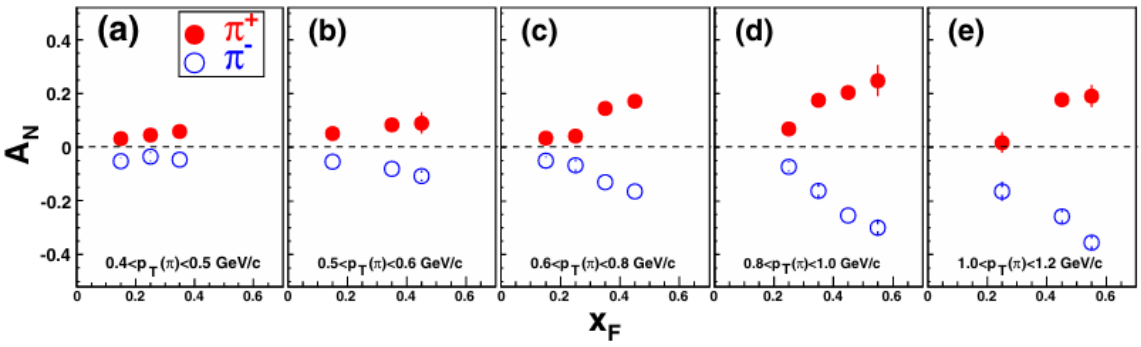

Figure 1.2: The TSSA as a function of x_F for the production of π^+(red circles) and π^-(blue circles) at fixed p_T values: (a) 0.4< p_T <0.5, (b) 0.5< p_T <0.6, (c) 0.6< p_T <0.8, (d) 0.8< p_T <1.0, and (e) 1.0< p_T <1.2 GeV/c [6].

of TSSA is important because it reflects the interplay between the intrinsic spin and orbital motion of quarks and gluons inside a hadron. It is sensitive to the partonic structure, especially the spin-orbit correlations and the transverse momentum distribution of quarks, which are not fully described by simple collinear parton distribution functions (PDFs). Instead, TSSA is a probe of more sophisticated and less understood distributions, such as the transverse momentum-dependent parton distribution functions (TMD PDFs), which account for both the momentum and spin structure of the partons inside a hadron.

Theoretical frameworks, including models of hadron dynamics and QCD, are actively being developed to explain and predict the magnitude and patterns of transverse single spin asymmetries. These studies are critical for advancing our understanding of hadron structure and spin physics, and they offer insight into the mechanisms of QCD at a fundamental level.

Chapter 2

Soft Collinear Effective Theory

2.1 Introduction

The soft-collinear effective Theory (SCET) is an effective field description of QCD that is particularly suitable for dealing with interactions where soft and collinear degrees of freedom are the most relevant. SCET provides a systematic way to describe the behavior of high-energy particles, such as those found in jet processes or hadronic scattering, by separating the contributions from large and small momentum scales.

The core idea behind SCET is the decoupling of soft and collinear degrees of freedom. Collinear momenta correspond to particles moving nearly parallel to the direction of the high-energy particle's motion, while soft momenta correspond to low-energy particles with small momentum components in all directions. By organizing the theory to focus on these two distinct momentum regimes, SCET simplifies the calculation of cross-sections and hadronic processes in scenarios like heavy-ion collisions or hadron colliders, where soft and collinear modes dominate.

SCET is particularly useful in calculating jet observables, factorization theorems, and resummation techniques, enabling precise predictions for experiments like those at the Large Hadron Collider (LHC). Its framework has also been extended to incorporate various high-

energy phenomena, such as the study of the form factors, parton distribution functions, and the calculation of hard scattering amplitudes in QCD.

2.2 SCET modes

The natural description of soft and collinear particles usually adopts the use of light cone coordinates system where two light-like vectors n_i^μ and $\bar{n}_i^\mu$ which are assigned to each collinear sector i satisfy the following properties

$$n_i^2 = 0, \qquad \bar{n}_i^2 = 0, \qquad n_i.\bar{n}_i = 2, \tag{2.1}$$

such that the momentum of each n_i-collinear particle is aligned to $\mathbf{n}_i$. Such light-like vectors are can be expressed as

$$n_i^\mu = (1, \mathbf{n}_i), \qquad \bar{n}_i^\mu = (1, -\mathbf{n}_i). \tag{2.2}$$

In this light cone coordinate system, a given four-vector p^μ can be expressed as

$$p^\mu = (\bar{n}_i.p)\frac{n_i^\mu}{2} + (n_i.p)\frac{\bar{n}_i^\mu}{2} + p_\perp^\mu = (p^+, p^-, \mathbf{p}_T)_i, \tag{2.3}$$

where

$$p^+ = n_i.p, \qquad p^- = \bar{n}_i.p, \qquad \mathbf{p}_T^2 = p^+p^- - p^2 = -p_\perp^2. \tag{2.4}$$

To determine the momentum of particles within the effective theory, one analyzes an energy jet Q traveling in the direction of $\mathbf{n}_i$. This jet comprises collimated particles with transverse momentum $p_\perp$ that satisfies $p_\perp \sim \Delta \ll Q$. As a result, this produces the following momentum scaling

$$p_c^\mu = (p^+, p^-, \mathbf{p}_T) \sim (\Delta^2/Q, Q, \Delta) = Q(\lambda^2, 1, \lambda), \tag{2.5}$$

where the scaling parameter is defined as $\lambda \sim \Delta/Q$. furthermore, the scaling $p^+ \sim Q\lambda^2$ is obtaining by imposing the condition $p^2 = 0$, therefore, $p^+ \sim p_\perp^2/p^-$. Alongside collinear modes, there are also low-energy modes that exhibit isotropic scaling

$$p_s^\mu \sim Q(\lambda, \lambda, \lambda), \qquad p_{us}^\mu(\lambda^2, \lambda^2, \lambda^2), \tag{2.6}$$

where the subscripts s, us denote soft and ultrasoft modes respectively. These modes lead to different effective theories, known as SCET_1, and SCET_2. In SCET, the hyperbolas represent the virtuality of modes, the principal difference between these two theories is that collinear and ultrasoft modes in SCET_1 are located on different hyperbolas, whereas collinear and soft modes in SCET_2 are located on the same hyperbola.

The SCET Lagrangian is obtained by expanding the QCD Lagrangian in terms of the counting parameter λ. In this section, one focuses on SCET_1, the effective theory for collinear and ultrasoft modes. In order to obtain the SCET Lagrangian, one can start by constructing two projection operators in spinor spaces

$$P_n = \frac{\not{n}\bar{\not{n}}}{4} = \frac{1}{2}\begin{pmatrix} \mathbb{I} & \sigma_3 \\ \sigma_3 & \mathbb{I} \end{pmatrix}, \qquad P_{\bar{n}} = \frac{\bar{\not{n}}\not{n}}{4} = \frac{1}{2}\begin{pmatrix} \mathbb{I} & -\sigma_3 \\ -\sigma_3 & \mathbb{I} \end{pmatrix}, \tag{2.7}$$

where $P_n + P_{\bar{n}} = 1$. The quark field ψ can be expressed in terms of projectors P_n and $P_{\bar{n}}$ as follows

$$\psi = P_n\psi + P_{\bar{n}}\psi = \hat{\xi}_n + \varphi_{\bar{n}}, \tag{2.8}$$

where $P_n\psi = \hat{\xi}_n$ and $P_{\bar{n}}\varphi_{\bar{n}} = \varphi_{\bar{n}}$. Thus, if on considers massless fermions, the QCD La-

grangian can be expressed as

$$\begin{aligned}\mathcal{L}_{QCD} =&\bar{\psi} i \not{D} \psi \\ =&(\bar{\hat{\xi}}_n + \bar{\varphi}_{\bar{n}})\left(\frac{\not{\bar{n}}}{2} \mathrm{i} n.D + \frac{\not{n}}{2} \mathrm{i}\bar{n}.D + \mathrm{i}\not{D}_\perp\right)(\hat{\xi}_n + \varphi_{\bar{n}}) \\ =&\bar{\hat{\xi}}_n \frac{\not{\bar{n}}}{2} \mathrm{i} n.D \hat{\xi}_n + \bar{\varphi}_{\bar{n}} \mathrm{i}\not{D}_\perp \hat{\xi}_n + \bar{\hat{\xi}}_n \mathrm{i}\not{D}_\perp \varphi_{\bar{n}} + \bar{\varphi}_{\bar{n}} \frac{\not{n}}{2} \mathrm{i}\bar{n}.D \varphi_{\bar{n}},\end{aligned} \tag{2.9}$$

where the expressions for various covariant derivatives are

$$\begin{aligned} \mathrm{i} n.D &= \mathrm{i} n.\partial + g n.\mathcal{A}_n + g n \mathcal{A}_{us}, \\ \mathrm{i}\bar{n}.D_n &= \mathrm{i}\bar{n}.\mathcal{P} + g\bar{n}.\mathcal{A}_n, \\ \mathrm{i}\not{D}_{n\perp} &= i\not{\mathcal{P}}_\perp + g\mathcal{A}_{n,\perp}, \end{aligned} \tag{2.10}$$

where $\mathcal{A}_n$, $\mathcal{A}_{us}$ are the collinear gluon and ultrasoft gluon fields respectively.

Since the $\bar{n}$ component of φ_n is relevant only at a subleading power of λ, it can be eliminated. By applying the equation of motion, we can express the leading power Lagrangian for collinear modes as follows.

$$\mathcal{L}^{(0)}_{\hat{\xi}_n} = \bar{\hat{\xi}}_n \left(\mathrm{i} n.D + \mathrm{i}\not{D}_{n\perp} \frac{1}{\mathrm{i}\bar{n}.D} \mathrm{i}\not{D}_{n\perp}\right) \frac{\not{\bar{n}}}{2} \hat{\xi}_n. \tag{2.11}$$

One can expresses the collinear momenta p_c^μ as the sum of pure $\mathcal{O}(\lambda)$, and $\mathcal{O}(\lambda^2)$ terms, and hence the collinear quark field $\hat{\xi}$ can be written as

$$\begin{aligned}\hat{\xi}_n(x) =& \int \frac{d^4p}{(2\pi)^4} e^{-ip.x} \tilde{\xi}_n(p) \\ =& \sum_{p_l \neq 0} \int \frac{d^4p_r}{(2\pi)^4} e^{-ip_l.x} e^{-ip_r.x} \tilde{\xi}_{n,p_l}(p_r) = \sum_{p_l \neq 0} e^{-ip_l.x} \xi_{n,p_l}(x),\end{aligned} \tag{2.12}$$

where $p_c^\mu = p_l^\mu + p_r^\mu$. The quantity p_l^μ scales as $p_l^\mu \sim (0, 1, \lambda)$, and the quantity $p_r^\mu \sim (\lambda^2, \lambda^2, \lambda^2)$.

The expression for $\xi_{n,p_l}(x)$ is given by

$$\xi_{n,p_l}(x) = \int \frac{d^4p_r}{(2\pi)^4} e^{-ip_r.x} \tilde{\xi}_{n,p_l}(p_r). \tag{2.13}$$

The dependence on x is associated with a purely ultrasoft momentum, leading to the following scaling $x^\mu \sim \lambda^{-2}$. The Taylor expansion in λ of the QCD Lagrangian gives the following SCET Lagrangian at leading order $\mathcal{O}(\lambda^0)$,

$$\mathcal{L}^{(0)} = \mathcal{L}^{(0)}_{n\xi} + \mathcal{L}^{(0)}_{ng} + \mathcal{L}^{(0)}_{us}, \tag{2.14}$$

where $\mathcal{L}^{(0)}_{n\xi}$ is the Lagrangian for collinear quarks, $\mathcal{L}^{(0)}_{ng}$ is the Lagrangian for collinear gluons, and $\mathcal{L}^{(0)}_{us}$ is the Lagrangian for ultrasoft fields

$$\begin{aligned}
\mathcal{L}^{(0)}_{n\xi} =& \bar{\xi}_n \left(\mathrm{i}n.D + \mathrm{i}\not{D}_{n\perp} \frac{1}{\mathrm{i}\bar{n}.D_n} \mathrm{i}\not{D}_{n\perp} \right) \frac{\not{\bar{n}}}{2} \xi_n, \\
\mathcal{L}^{(0)}_{ng} =& \frac{1}{2g^2} \mathrm{Tr}\left\{ \left[\mathrm{i}\mathcal{D}^\mu, \mathrm{i}\mathcal{D}^\nu \right]^2 \right\} + \tau \mathrm{Tr}\left\{ \left[\mathrm{i}\mathcal{D}^\mu_{\mathrm{us}}, \mathcal{A}_{\mathrm{n}\mu} \right]^2 \right\} + 2\mathrm{Tr}\left\{ \bar{\mathrm{c}}_{\mathrm{n}} \left[\mathrm{i}\mathcal{D}^{\mathrm{us}}_\mu, \left[\mathrm{i}\mathcal{D}^\mu, \mathrm{c}_{\mathrm{n}} \right] \right] \right\}, \\
\mathcal{L}^{(0)}_{us} =& \bar{q}_{us} \mathrm{i}\mathcal{D}_{us} q_{us} - \frac{1}{2} \mathrm{Tr}\left\{ \mathrm{G}^{\mu\nu}_{\mathrm{us}} \mathrm{G}^{\mathrm{us}}_{\mu\nu} \right\} + \lambda_{\mathrm{us}} \mathrm{Tr}\left\{ \left(\mathrm{i}\partial_\mu . \mathcal{A}^\mu_{\mathrm{us}} \right)^2 \right\} + 2\mathrm{Tr}\left\{ \bar{\mathrm{c}}_{\mathrm{us}} \mathrm{i}\partial_\mu \mathrm{i}\mathcal{D}^\mu_{\mathrm{us}} \mathrm{c}_{\mathrm{us}} \right\}.
\end{aligned} \tag{2.15}$$

where g is the gauge coupling. In the Lagrangian $\mathcal{L}^{(0)}_{ng}$, the quantities λ, and λ_{us} are collinear and ultrasoft gauge fixing parameters, and c_n and c_{us} are the associated ghost fields. The covariant derivatives in the Lagrangian $\mathcal{L}^{(0)}_{ng}$ are defined as

$$\begin{aligned}
\mathrm{i}\mathcal{D}^\mu =& \frac{n^\mu}{2} (\bar{\mathcal{P}} + g\bar{n}.\mathcal{A}_n) + (\mathcal{P}^\mu_\perp + g\mathcal{A}^\mu_{n\perp}) + \frac{\bar{n}}{2} + (\mathrm{i}n.\partial + gn.\mathcal{A}_n + gn.\mathcal{A}_{us}), \\
\mathrm{i}\mathcal{D}^\mu_{us} =& \frac{n^\mu}{2} \bar{\mathcal{P}} + \mathcal{P}^\mu_\perp + \frac{\bar{n}^\mu}{2} \mathrm{i}n.\partial + \frac{\bar{n}}{2} gn.\mathcal{A}_{us}.
\end{aligned} \tag{2.16}$$

The ultrasoft Lagrangian $\mathcal{L}^{(0)}_{us}$ is the same as the full QCD Lagrangian because ultrasoft fields have isotropic scaling, $\mathcal{A}^\mu_{us} \sim (\lambda^2, \lambda^2, \lambda^2)$, assuming that fields and covariant derivatives in the full QCD Lagrangian satisfy ultrasoft scaling.

One of the most important properties that should be preserved in the formulation of SCET is gauge invariance. In SCET there are two types of gauge transformations because gluon fields are split into collinear and ultrasoft fields. These two types of gauge transformations can be expressed as follows

$$U_n(x) = \exp\{i\alpha_n^A(x)T^A\}, \qquad U_{us}(x) = \exp\{i\alpha_{us}^A(x)T^A\}. \tag{2.17}$$

The gauge transformations of Eq.(2.17) should satisfy collinear and ultrasoft scaling respectively as follows

$$i\partial^\mu U_n(x) \sim Q(\lambda^2, 1, \lambda)U_n(x), \qquad i\partial^\mu U_{us}(x) \sim Q(\lambda^2, \lambda^2, \lambda^2)U_{us}(x). \tag{2.18}$$

Since ultrasoft fields have longer wavelengths than collinear fields, they act like a background for collinear fields. Hence, ultrasoft fields do not transform under collinear gauge transformations

$$q_{us}(x) \to q_{us}, \qquad \mathcal{A}_{us}^\mu(x) \to \mathcal{A}_{us}^\mu(x), \tag{2.19}$$

where q_{us} are ultrasoft quark fields, and $\mathcal{A}_{us}^\mu$ are ultrasoft gluon fields. However, collinear fields transform under ultrasoft gauge transformations while ultrasoft fields satisfy the standard QCD transformations

$$\begin{aligned} &\xi_n(x) \to U_{us}(x)\xi_n(x), \qquad q_{us}(x) \to U_{us}(x)q_{us}(x), \\ &\mathcal{A}_n^\mu(x) \to U_{us}(x)\mathcal{A}_n^\mu(x)U_{us}^\dagger(x), \qquad \mathcal{A}_{us}^\mu(x) \to U_{us}(x)\left(\mathcal{A}_{us}^\mu(x) + \frac{i}{g}\partial^\mu\right)U_{us}^\dagger(x). \end{aligned} \tag{2.20}$$

Since the gauge transformations of non-local operators require Wilson lines, the SCET requires two distinct Wilson lines, one for each mode.

Chapter 3

Wilson lines

In gauge theories, the Wilson line is a crucial mathematical construct used to describe the effect of gauge fields along a specified path in spacetime. The Wilson line captures how the gauge connection affects the phase of a quantum state as it is transported from one point to another. Formally, it is defined as a path-ordered exponential of the gauge field, which encodes the information about the field's configuration along the path. Wilson lines play a key role in various physical contexts, including confinement in quantum chromodynamics (QCD) and the study of topological features in gauge theories. They are also instrumental in understanding the non-perturbative aspects of these theories, providing insights into phenomena such as string tension and the behavior of gauge theories in strong coupling regimes.

3.1 Smooth Wilson lines

A Wilson line along a path is a path-ordered exponential of a line integral of a gauge field along a path $\mathcal{C}$

$$\mathcal{U}^{\mathcal{C}} = \mathcal{P} \exp\left\{ ig \int_{\mathcal{C}} dz^{\mu} A_{\mu}(z) \right\}, \tag{3.1}$$

where $A_\mu(z)$ is a gauge field, and g is a gauge coupling. The Taylor expansion of the Wilson line $\mathcal{U}^{\mathcal{C}}$ can be expressed as

$$\mathcal{U}^{\mathcal{C}} = \sum_{n=0}^{\infty} \frac{1}{n!}(ig)^n \mathcal{P} \int_{\mathcal{C}} dz_n^{\mu_n} \cdots dz_1^{\mu_1} A_{\mu_n}(z_n) \cdots A_{\mu_1}(z_1). \tag{3.2}$$

Physically, the n-th order expansion is thought as the radiation of n gauge fields. The presence of $\mathcal{P}$ which stands for path ordering ensures that radiated gauge fields are ordered along the path $\mathcal{C}$. The path ordering requirement for fields can be expressed as

$$\mathcal{P} A_{\mu_1}(z_1) \cdots A_{\mu_n}(z_n) = \sum_{\sigma(\zeta_1 \cdots \zeta_n)} \left(\prod_{i=1}^{n-1} \theta(\zeta_{i+1} - \zeta_i) \right) A_{\mu_1}(\zeta_1) \cdots A_{\mu_n}(\zeta_n), \tag{3.3}$$

where the sum runs over all possible permutations of ζ_i. For abelian gauge fields the path ordering has no effect because fields commute

$$\mathcal{P} A_{\mu_1}(z_1) \cdots A_{\mu_n}(z_n) = A_{\mu_1}(z_1) \cdots A_{\mu_n}(z_n). \tag{3.4}$$

Since each term in the expansion represents a power of the same integral, a Wilson line for abelian gauge fields is expressed as

$$\mathcal{U}_a^{\mathcal{C}} = \sum_{n=0}^{\infty} \frac{1}{n!}(ig)^n \left(\int_{\mathcal{C}} dz^\mu A_\mu(z) \right)^n. \tag{3.5}$$

Obviously, a Wilson line has both a path and field content. The Fourier transform can be utilized to separate one content from another. The path content is given by the integrals

$$\mathcal{I}_n = \frac{1}{n!}(ig)^n \mathcal{P} \int d\zeta_1 \cdots d\zeta_n (z_1^{\mu_1})' \cdots (z_n^{\mu_n})' \exp\left\{ i \prod^{n} k_i . z_i \right\}, \tag{3.6}$$

where ζ is a path parameter and k_i is a momentum. The n-th order term of the Wilson line expansion is expressed as

$$\mathcal{U}_n = \int \frac{d^w k_n}{(2\pi)^w} \cdots \frac{d^w k_1}{(2\pi)^w} A_{\mu_n}(-k_n) \cdots A_{\mu_1}(-k_1) \mathcal{I}_n. \tag{3.7}$$

3.2 Piece-wise Wilson lines

A Wilson line path $\mathcal{C}$ can have cusps rather than being smooth [31]. At these points, the path is continuous, but its derivative is discontinuous. Hence, the evaluation of such a Wilson line follows a piece-wise scheme. Since cusps are not natural, they can just appear as a result of interaction with an external force on a smooth path. To evaluate a Wilson line on a piece-wise path $\mathcal{C}$ with N smooth segments, we first define the following piece-wise function

$$p(\zeta) = \begin{cases} p^1(\zeta) & \text{if } \zeta = a_1 \cdots a_2, \\ p^2(\zeta) & \text{if } \zeta = a_2 \cdots a_3, \\ \vdots & \vdots \\ p^N(\zeta) & \text{if } \zeta = a_N \cdots a_{N'}. \end{cases} \tag{3.8}$$

Even though the path $\mathcal{C}$ is not entirely smooth because of the presence of cusps, each path of a segment is smooth, thus p^J is a smooth function. The first-order integral over the J-th segment involves only the J-th part of $p(\zeta)$

$$S_1^J = \int_{a_J}^{a_J+1} d\zeta p(\zeta) = \int_{a_J}^{a_J+1} d\zeta p^J(\zeta). \tag{3.9}$$

The first-order integral is

$$\mathcal{I}_1 = \sum_{J=1}^{N} \int_{a_J}^{a_J+1} d\zeta p^J(\zeta). \tag{3.10}$$

The second-order integral is more complex than the first-order integral, and one of complications is that the portion of the integral is a piece-wise function

$$\bar{S}^1_{\zeta_1}(i+1) = \begin{cases} \bar{S}^1_{\zeta_1}(i+1) & \text{if } \zeta_1 = a_1 \cdots a_2, \\ S^1(i+1) + \bar{S}^2_{\zeta_1}(i+1) & \text{if } \zeta_1 = a_2 \cdots a_3, \\ \vdots & \vdots \\ \tilde{S}^J(i+1) + \bar{S}^N_{\zeta_1}(i+1) & \text{if } \zeta_1 = a_N \cdots a_{N'}, \end{cases} \tag{3.11}$$

where $\bar{S}^J_{\zeta_1}$, and $\tilde{S}^J$ are given by

$$\bar{S}^J_{\zeta_1}(i+1) = \int_{a_J}^{\zeta_1} d\zeta_2 p_{i+1}(\zeta_2), \qquad \tilde{S}^J(i+1) = \sum_{J=1}^{N-1} S^J(i+1). \tag{3.12}$$

At this point it is important to clarify the presence of i in the above expressions which are related to the second-order integral. Obviously, the value of i equals 1, but the presence i instead of its value is beneficial because it allows to easily establish general expressions. The second-order integral is defined by

$$\begin{aligned} \mathcal{I}_2 &= \left\{ \int_{a_1}^{a_{N+1}} d\zeta_1 p_i(\zeta_1) \right\} \left\{ \int_{a_1}^{\zeta_1} d\zeta_2 p_{i+1}(\zeta_2) \right\} \\ &= \int_{a_1}^{a_2} d\zeta_1 p_i(\zeta_1) \int_{a_1}^{\zeta_1} d\zeta_2 p_{i+1}(\zeta_2) + \int_{a_2}^{a_3} d\zeta_1 p_i(\zeta_1) \left\{ (S^1(i+1) + \int_{a_2}^{\zeta_1} d\zeta_2 p_{i+1}(\zeta_2) \right\} + \cdots \\ &+ \int_{a_N}^{a_{N+1}} d\zeta_1 p_i(\zeta_1) \left\{ \sum_{J=1}^{N-1} S^J(i+1) + \int_{a_N}^{\zeta_1} d\zeta_2 p_{i+1}(\zeta_2) \right\}. \end{aligned} \tag{3.13}$$

The second-order segment integral is defined by

$$S^J_2(i) = \int_{a_J}^{a_{J+1}} d\zeta_1 \int_{a_J}^{\zeta_1} d\zeta_2 p^J_i(\zeta_1) p^J_{i+1}(\zeta_2). \tag{3.14}$$

Substituting Eq.(3.9), and Eq.(3.14) into Eq.(3.13), the expression of $\mathcal{I}_2$ becomes [31]

$$\mathcal{I}_2 = \sum_{J=1}^{N} S_2^J(1) + \sum_{J=2}^{N} \sum_{K=1}^{J-1} S_1^J(1) S_1^K(2). \tag{3.15}$$

The remaining task is to find the expression for the full path integral over separate segments. We first observe that S_2 relies solely on the J-th segment, with no mixing between segments. We expect this to hold for all orders. Also, for successive segment integrals, there is an increment in the argument, and this is expected to be true for all orders

$$S_{n_1}^{J_1}(i) S_{n_2}^{J_2}(i+1) \cdots S_{n_k}^{J_k}(i+k-1). \tag{3.16}$$

Thus, it is simple to obtain the expression for the n-th order integral. We simply need to create all potential combinations of S_i's that result in n internal p's, ensuring we also include the appropriate number of summation symbols while maintaining the order. The n-th order integral is expressed as

$$\mathcal{I}_n = \sum_{i=1}^{n} \left[\left(\prod_{j=1}^{i} \sum_{J_j=1-j+1}^{J_{j-1}-1} \right)_{J_0-1=N} \left(\begin{array}{c} \text{all terms of the form } \sum_{j=1}^{i} S_{l_j}^{J_j} \\ \text{such that } \sum_{j=1}^{i} l_j = n \end{array} \right) \right]. \tag{3.17}$$

The corresponding recursion relation is given by

$$\mathcal{I}_n = \sum_{J=1}^{N} S_n^J + \sum_{J=2}^{N} \sum_{i=1}^{n-1} S_i^J \mathcal{I}_{n-1}(J-1). \tag{3.18}$$

The expression for the Wilson line can be obtained by replacing every S with $\mathcal{U}$ in the last two equations. For example, replacing S with $\mathcal{U}$ in the recursion relation, one obtains the expression for the Wilson line

$$\mathcal{U}_n = \sum_{J=1}^{N} \mathcal{U}_n^J + \sum_{J=2}^{N} \sum_{i=1}^{n-1} \mathcal{U}_i^J \mathcal{U}_{n-1}(J-1), \tag{3.19}$$

where $\mathcal{U}_n^J$ is defined by

$$\mathcal{U}_n^J = \left(\frac{ig}{16\pi^4}\right)^n \int d^4k_1 \cdots d^4k_n A_{\mu_1}(k_1) \cdots A_{\mu_n}(k_n) S_n^J. \tag{3.20}$$

The ordering of $\mathcal{U}_n^J$ is necessary because the gauge fields $A_\mu(k)$ are non-commutative due to the color generators.

3.3 Infinite Wilson lines

The Wilson line path can be composed of linear segments [31]. In this case, a segment can have one or more infinite end-points, one end of a segment can extend to infinity, or both end-points can extend to infinity connecting $-\infty$ and $+\infty$. We consider a path that starts from a point a_μ to infinity along a direction n_μ, so that $z^\mu = a^\mu + n^\mu \zeta$, where ζ is a parameter, $\zeta = 0, \cdots, \infty$. Then, using the path-ordering Eq. (3.6) can be rewritten as

$$\mathcal{I}_n = (ig)^n n^{\mu_1} \cdots n^{\mu_n} \exp\left(ia \sum_j k_j\right) \int_0^\infty \int_{\zeta_1}^\infty \int_{\zeta_{n-1}}^\infty d\zeta_1 \cdots d\zeta_n \exp\left(i \sum_j (n.k_j + i\eta)\right) \zeta_j. \tag{3.21}$$

Furthermore, we can simplify the expression for $\mathcal{I}_n$ by evaluating the integrals. First, we realize that the general integral is just the Fourier transform of a Heaviside θ-function, hence we can simply write

$$\int_{\zeta_{n-1}}^\infty d\zeta_n \exp\left\{i(n.k_n + i\eta)\zeta_n\right\} = \frac{i}{n.k_n + i\eta} \exp\left\{i(n.k_n + i\eta)\zeta_{n-1}\right\}. \tag{3.22}$$

The result of the above integral has a factor of $1/(n.k_n)$ and the result of the next integral has a factor of $1/(n.k_n + n.k_{n-1})$. The appearance of similar terms allows to write in the compact form the expression for $\mathcal{I}_n$. After evaluating all integrals, the quantity $\mathcal{I}_n$ can be

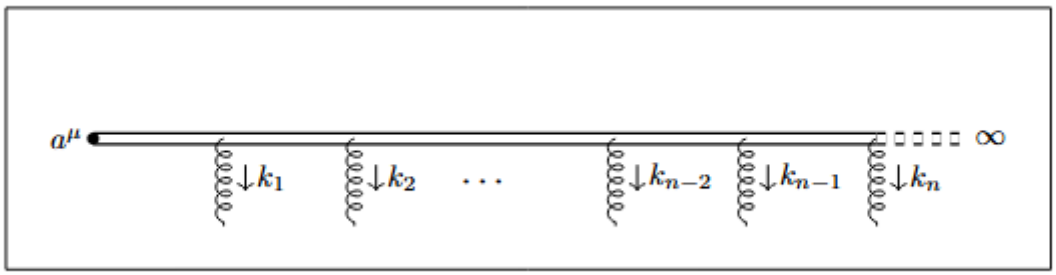

Figure 3.1: The diagram for n-gluon radiation for a Wilson line going from a^μ to $+\infty$. The Wilson line path is parametrized with $\zeta = 0,\cdots,\infty$.

expressed as

$$\mathcal{I}_n = (ig)^n n^{\mu_1}\cdots n^{\mu_n} \exp\left\{ia\sum_j k_j\right\}\prod_{j=1}^{n}\frac{i}{n.\sum_{l=j}^{n} k_l + i\eta}. \tag{3.23}$$

The result of the above equation can be easily obtained by applying the Feynman rules for Wilson lines. These Feynman rules are for momenta that point outward from the Wilson line. The resulting n-th order diagram is shown in Figure (3.1). For inward momenta, the prescription $k_i \to -k_i$ is utilized to obtain the appropriate Feynman rules.

The path of Wilson line can be put into a reversal direction. The action of reversing the path of a Wilson line $\mathcal{U}_{(a,b)}$ can be represented by

$$\mathcal{U}_{(a,b)} = \mathcal{P}\exp\left(ig\int_a^b dz^\mu A_\mu\right) \to \bar{\mathcal{P}}\exp\left(-ig\int_a^b dz^\mu A_\mu\right), \tag{3.24}$$

where $\bar{\mathcal{P}}$ is the anti-path ordering which ensures that fields are ordered in reverse. This shows that reversing the path of a Wilson line is directly equivalent to taking a Hermitian conjugate, thus we can simply write

$$\mathcal{U}_{(a,b)} = \mathcal{U}^\dagger_{(b,a)}. \tag{3.25}$$

However, in the standard path ordering, the final result should require to perform the substitution, $k \to -k$ since the field $A_\mu(k)$ transforms as $A^\dagger_\mu(k) = A_\mu(-k)$. We can also study

how an infinite Wilson line transforms under the action of the path reversal. In this case, we consider a Wilson line from $-\infty$ to b^μ.

$$\begin{aligned}
\mathcal{U}^\dagger_{b,-\infty} &= \Bigg[\underbrace{\sum_{n=0}^{\infty}(ig)^n\int\frac{d^\omega k_n}{(2\pi)^\omega}n.A(-k_n)\cdots n.A(-k_1)\exp\left\{ib.\sum_j^n k_j\right\}\prod_{j=1}^n\frac{-i}{n.\sum_{l=1}^j k_l-i\eta}}_{=\mathcal{U}_{(b,-\infty)}}\Bigg]^\dagger, \\
&= \sum_{n=0}^{\infty}(-ig)^n\int\frac{d^\omega k_n}{(2\pi)^\omega}n.A^\dagger(k_1)\cdots n.A^\dagger(k_n)\exp\left\{-ib.\sum_j^n k_j\right\}\prod_{j=1}^n\frac{i}{n.\sum_{l=1}^n k_j+i\eta} \\
&= \sum_{n=0}^{\infty}(-ig)^n\int\frac{d^\omega k_n}{(2\pi)^\omega}n.A(-k_1)\cdots n.A(-k_n)\exp\left\{ib.\sum_j^n k_j\right\}\prod_{j=1}^n\frac{-i}{n.\sum_{l=1}^n k_j-i\eta} \\
&= \sum_{n=0}^{\infty}(-ig)^n\int\frac{d^\omega k_n}{(2\pi)^\omega}n.A(-k_n)\cdots n.A(-k_1)\exp\left\{ib.\sum_j^n k_j\right\}\prod_{j=1}^n\frac{-i}{n.\sum_{l=1}^n k_j-i\eta},
\end{aligned} \tag{3.26}$$

where we have relabeled the fields according to the prescription, $1\to n, 2\to n-1,\cdots,n\to 1$ in the last line of Eq. (3.26). To elucidate the ramifications of the Hermitian conjugate, we reformulate the final expression in terms of the n-th integrals as follows

$$\mathcal{U}^\dagger_{(b,-\infty)} = \sum_{n=0}^{\infty}\int\frac{d^\omega k_n}{(2\pi)^\omega}\cdots\frac{d^\omega k_1}{(2\pi)^\omega}A_{\mu_n}(-k_n)\cdots A_{\mu_1}(-k_1)\mathcal{I}^\dagger_n, \tag{3.27}$$

where

$$\mathcal{I}^\dagger_n = (ig)^n(-n^{\mu_1})\cdots(-n^{\mu_n})\exp\left\{ib.\sum_j^n k_j\right\}\prod_{j=1}^n\frac{i}{-n.\sum_{l=j}^n k_j+i\eta}. \tag{3.28}$$

The expression for the n-integrals shows that under the prescription $n^{\mu_j}\to -n^{\mu_j}$, the Hermitian conjugate of a Wilson line from b^μ to $-\infty$ is equivalent to a Wilson line from b^μ to $+\infty$. Similarly, the Hermitian conjugate of a Wilson line from b^μ to $+\infty$ is equivalent to a Wilson

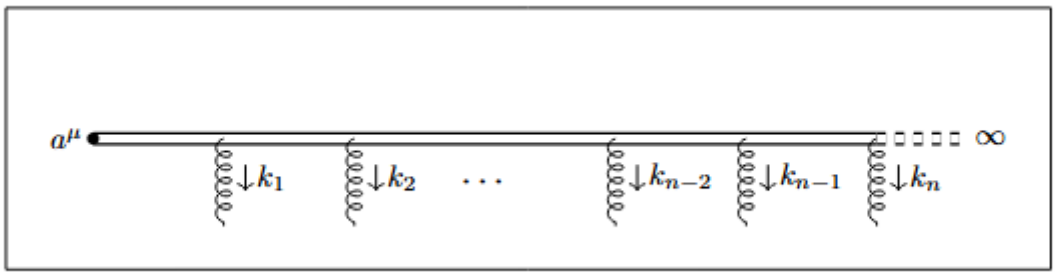

Figure 3.2: Changing the path direction of the Wilson line $\mathcal{U}_{(b,-\infty)}$ is equivalent to taking the Hermitian conjugate $\mathcal{U}^\dagger_{(b,-\infty)}$. However, the representation with the standard path ordering requires the prescription, $n^{\mu_j} \to -n^{\mu_j}$, and the new path direction that goes from b^μ to $+\infty$.

line from b^μ to $-\infty$ under the same prescription

$$\begin{aligned} \mathcal{U}^\dagger_{(b,-\infty)} &= \mathcal{U}_{(+\infty,b)}\big|_{n^{\mu_j}\to -n^{\mu_j}}, \\ \mathcal{U}^\dagger_{(+\infty,b)} &= \mathcal{U}_{(b,-\infty)}\big|_{n^{\mu_j}\to -n^{\mu_j}}. \end{aligned} \tag{3.29}$$

The path flow from left to right implies the presence of n^{μ_j} whereas the path flow from right to left implies the presence of $-n^{\mu_j}$ in the n-integrals. Figure (3.2) shows the reversed Wilson line of $\mathcal{U}_{(b,-\infty)}$, the arrow on the Wilson line indicates the direction of the path flow. Now, we consider a finite Wilson line of path $\mathcal{C}$ from a point a^μ to a point b^μ. In terms of the parameter ζ we define the variable

$$z^\mu = a^\mu + n^\mu \zeta, \qquad \lambda = 0, \cdots, \|b-a\| = (a^\mu - b^\mu)/n^\mu \tag{3.30}$$

Assume that there exist two paths $\mathcal{C}_1$ and $\mathcal{C}_2$ such that $\mathcal{C} = \mathcal{C}_1 + \mathcal{C}_2$. Then, we can express the Wilson line $\mathcal{U}$ of a path $\mathcal{C}$ as

$$\mathcal{U}_{(b,a)} = \mathcal{U}_{(b,+\infty)}\mathcal{U}_{(+\infty,a)} = \mathcal{U}_{(b,-\infty)}\mathcal{U}_{(-\infty,a)}. \tag{3.31}$$

The corresponding n-th segment integral is expressed as

$$\mathcal{I}_n = (ig)^n n^{\mu_1}\cdots n^{\mu_n} \exp\left\{ia.\sum_j k_j\right\} \int_0^{\|b-a\|} \int_0^{\zeta_n} \cdots \int_0^{\zeta_2} d\zeta_n \cdots d\zeta_1 \exp\left\{in.\sum_j^n k_j\zeta_j\right\}. \tag{3.32}$$

For the moment, we can disregard the factors in front of the integrals without loss of generality. The result of the first-order integral is expressed as

$$\mathcal{I}_1(k_1) = \int_0^{\|b-a\|} d\zeta_1 \exp\left\{in.k_1\zeta_1\right\} = \frac{-i}{n.k_1}\Big(\exp\{i(b-a).k_1 - 1\}\Big). \tag{3.33}$$

The derivation of the recursive relation can be done without much effort. The expression for the n-th order term is given by

$$\mathcal{I}_n = \sum_{m=0}^{n-1}\left(\exp\left\{i.(b-a).\sum_{m+1}^{n} k_j\right\} - 1\right)\left(\prod_{j=1}^{m}\frac{i}{n.\sum_{l=j}^{m} k_l}\right)\left(\prod_{j=m+1}^{n}\frac{-i}{n.\sum_{l=m+1}^{n} k_l}\right). \tag{3.34}$$

As expected, we realize that the n-th order term vanishes in the limit, $a \to b$. There are exactly n term without exponential, thus the eikonal identity can be obtained if we add to the sum of these n terms another term $m = n$

$$\sum_{m=0}^{n}\left(\prod_{j=1}^{m}\frac{i}{n.\sum_{l=j}^{m} k_l}\right)\left(\prod_{j=m+1}^{n}\frac{-i}{n.\sum_{l=m+1}^{n} k_l}\right) = 0. \tag{3.35}$$

The above expression represents the eikonal identity and is useful in the abelian limit of QCD. The eikonal identity allows to write the equality

$$\left(\prod_{j=1}^{m}\frac{i}{n.\sum_{l=j}^{m} k_l}\right)\left(\prod_{j=m+1}^{n}\frac{-i}{n.\sum_{l=m+1}^{n} k_l}\right) = -\prod_{j=1}^{n}\frac{i}{n.\sum_{l=j}^{m} k_j}. \tag{3.36}$$

The substitution of the above equality into the expression for the n-order term leads to the following expression

$$\begin{aligned}\mathcal{I}_n &= \sum_{m=0}^{n-1} \exp\left\{i(b-a).\sum_{m+1}^{n} k_j\right\}\left(\prod_{j=1}^{m}\frac{i}{n.\sum_{l=j}^{m} k_l}\right)\left(\prod_{j=m+1}^{n}\frac{-i}{n.\sum_{l=m+1}^{n} k_l}\right)+\prod_{j=1}^{n}\frac{i}{n.\sum_{l=j}^{n} k_j}\\ &= \sum_{m=0}^{n} \exp\left\{i(b-a).\sum_{m+1}^{n} k_j\right\}\left(\prod_{j=1}^{m}\frac{i}{n.\sum_{l=j}^{m} k_l}\right)\left(\prod_{j=m+1}^{n}\frac{-i}{n.\sum_{l=m+1}^{n} k_l}\right).\end{aligned} \tag{3.37}$$

Incorporating the factors in front of Eq. (3.32) into Eq. (3.37) and simplifying the overall first factor, the resulting path content can be expressed as

$$\mathcal{I}_n = \sum_{m=0}^{n}\left(\prod_{j=1}^{m}(ig)n^{\mu_j}\frac{i}{n.\sum_{j}^{m} k_j}\exp\left(ia.k_j\right)\right)\left(\prod_{j=m+1}^{n}(ig)n^{\mu_j}\frac{-i}{n.\sum_{l=m+1}^{j} k_l}\exp\left(ib.k_j\right)\right). \tag{3.38}$$

Also, we can sum over n from zero to infinity and add the same convergence terms in the fractions to obtain a product of two half-infinite Wilson lines. Hence, the path content of a product of two half-infinite Wilson lines can be expressed as

$$\tilde{\mathcal{I}}_n = \left(\sum_{n=0}^{\infty}(\prod_{j=1}^{n}(ig)n^{\mu_j}\frac{i}{n.\sum_{j}^{n} k_j \pm i\eta}\exp\left(ia.k_j\right)\right)\left(\sum_{n=0}^{\infty}\prod_{j=1}^{n}(ig)n^{\mu_j}\frac{-i}{n.\sum_{l=1}^{j} k_l \pm i\eta}\exp\left(ib.k_j\right)\right). \tag{3.39}$$

Here, + and − in $\pm i\eta$ indicate that the path content corresponds to two lower bound and two upper bound Wilson lines respectively.

A Wilson line can have an infinite linear segment from $-\infty$ to $+\infty$. If the path of direction

n^μ contains a point r^μ, for a parameter ζ, we define the following variable

$$z^\mu = r^\mu + n^\mu \zeta, \qquad \zeta = -\infty, \cdots, +\infty. \tag{3.40}$$

In this case, the path content is expressed as

$$\mathcal{I} = (ig)^n n^{\mu_1} \cdots n^{\mu_n} \exp\left\{ ir. \sum_j k_j \right\} \int_{-\infty}^{+\infty} \cdots \int_{-\infty}^{\zeta_2} d\zeta_n \cdots d\zeta_1 \exp\left\{ in. \sum_j^n k_j \zeta_j \right\}. \tag{3.41}$$

We can compute each integral to obtain the final expression for $\mathcal{I}$. Using the usual method of the Fourier transform of a Heaviside θ-function to find the result of each integral, we realize that the integral from $-\infty$ to $+\infty$ is divergent when other integrals are each finite and, vice versa. The solution to resolve the issue would be to regulate the path [32]. The parametrization for the regularized path is defined as

$$z^\mu_\xi = r^\mu + \frac{2}{\xi} \tanh\left(\frac{\xi}{2}\zeta\right) n^\mu, \qquad \xi > 0, \qquad \zeta = -\infty, \cdots, +\infty. \tag{3.42}$$

The result for the first-order integral is expressed as

$$\begin{aligned} \mathcal{I}_1 &= \int_{-\infty}^{\zeta_2} d\zeta_1 \mathrm{sech}^2\left(\frac{\xi}{2}\zeta_1\right) \exp\left\{ i\frac{2}{\xi}(n.k_1 - i\eta) \tanh\left(\frac{\xi}{2}\zeta_1\right) \right\} \\ &= \frac{-i}{n.k_1 - i\eta} \left[\exp\left\{ i\frac{2}{\xi}(n.k_1 - i\eta) \tanh\left(\frac{\xi}{2}\zeta_2\right) \right\} - \exp\left\{ -i\frac{2}{\xi}(n.k_1 - i\eta) \right\} \right]. \end{aligned} \tag{3.43}$$

Using the recursion relation, we find that the n-th term is defined by

$$\begin{aligned} \mathcal{I}_n =& 2i \sum_{m=0}^{n-1} \exp\left\{ -i\frac{2}{\xi}\left(n. \sum_l^m k_j - i\eta \right) \right\} \sin\left[\frac{2}{\xi}\left(n. \sum_{m+1}^n k_j - i\eta \right) \right] \\ &\times \prod_l^m \frac{i}{n. \sum_j^m k_l - i\eta} \prod_{m+1}^n \frac{-i}{n. \sum_{m+1}^j k_j - i\eta}. \end{aligned} \tag{3.44}$$

The n-th term for the original path can be obtained by taking the limit, $\xi \to 0$. By incorpo-

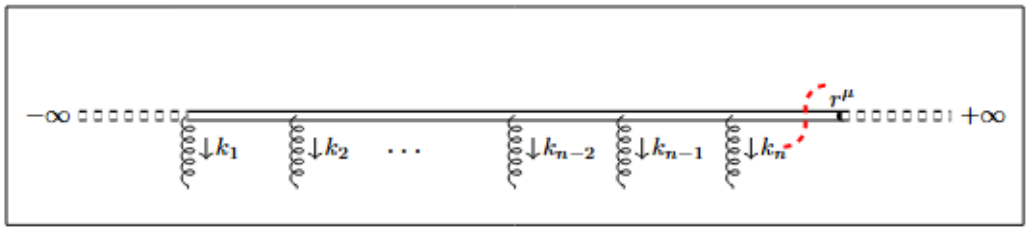

Figure 3.3: The diagram for n-gluon radiation from a Wilson line going from $-\infty$ to $+\infty$. The red line belongs to the cut propagator. The Wilson line path is parametrized with $\zeta =$ -∞,$\cdots$,+∞ .

rating the factors in front the n-th term path for the original path is expressed as

$$\mathcal{I}_n = (ig)^n n^{\mu_1}\cdots n^{\mu_n}\left(\prod_1^{n-1}\frac{-i}{n.\sum_1^j k_l - i\eta}\right)2\pi\delta\Big(n.\sum_1^n k_j - i\eta\Big), \tag{3.45}$$

where δ is the nascent delta function with the weak limit, $\lim_{\xi\overset{>}{\to}0}\delta_\xi(x) = \delta(x)$, for an infinitesimal parameter $\xi > 0$, which relates δ_ξ and δ through the shifting property.

One proper method to represent an infinite Wilson line is to position all emitted gluons on one side of the point r^μ as shown in Figure (3.3). The diagram shows that there are n gluons and k_n is the momentum of the n-th momentum. In this case, the contribution for the cut propagator is $\delta(n.k + i\eta)$.

Chapter 4

Transverse Momentum Dependent (TMD) Physics

4.1 Introduction

This section presents an introduction to transverse momentum dependent distributions, commonly known as TMDs. These distributions encapsulate the quantum correlations between hadron polarization and the motion and polarization of quarks and gluons within it. We will include a detailed examination of the fundamental and universally applicable TMDs, along with their defining characteristics. We will explore TMD factorization formalisms, which allow the alignment of these quantum distributions with physical observables observed in high-energy scattering experiments. Additionally, we will delve into various phenomenological methodologies for extracting these distributions from meticulously gathered experimental data. The subsequent portion of this section will offer an intuitive overview of the TMDs and their significance in elucidating the internal structure of hadrons.

4.1.1 Twist-2 TMD functions

Cross sections of DIS processes can be expressed in terms of a leptonic tensor and a hadronic tensor. In the Bjorken limit, it is possible to write the hadronic part in terms of the hard part and the soft part, containing the information on the parton distribution inside a hadron. This soft part is just a correlation function of quark fields between hadronic states. In one-particle inclusive processes, two types of correlation functions are necessary, one that characterizes the distributions of quarks and another that describes the hadronization of quarks into observable hadrons. At leading order in $1/Q$ (twist-2), where Q represents the hard scale of collision, the primary correlation functions of interest are the quark-quark correlation functions. The quark-quark correlation functions can be expressed as

$$\Phi^q_{ij}(k,P,S|n) = \int \frac{d\xi^-}{2\pi} e^{ik.\xi^-} \langle P,S|\bar{\psi}^q_j(0)\mathcal{W}_0(0,\xi^-)|n)\psi^q_i(\xi^-)|P,S\rangle, \tag{4.1}$$

$$\begin{aligned}\Delta^{h/q}_{i,j}(p,P_h,S_h|\bar{n}) = \sum\!\!\!\!\!\!\int_X \int \frac{d^4\xi}{(2\pi)^4} e^{ip.\xi}\langle 0|\mathcal{W}_1(\infty,\xi|\bar{n})\psi^q_i(\xi)|P_h,S_h,X\rangle \\ \times \langle P_h,S_h,X|\bar{\psi}^q_j(0)\mathcal{W}_2(0,\infty)|\bar{n})|0\rangle,\end{aligned} \tag{4.2}$$

where $\sum\!\!\!\!\!\!\int_X \equiv \sum_X \int d^3\mathbf{P}_X/(2\pi)^3 2P^0_X$. The quark q emerging from the target proton has a momentum k, and the quark q decaying into a hadron has a momentum p. The Wilson line is denoted by $\mathcal{W}_a$. The quantity $P(P_h)$ is the momentum of the proton(outgoing hadron) of spin $S(S_h)$, and $n(\bar{n})$ is the lightlike vector conjugate to the momentum $P(P_h)$. If the hadron in the final state has a small but nonzero transverse momentum, $\Lambda_{QCD} \lesssim P_{h\perp} \ll Q$, that is likely to originate from the transverse motion of quarks inside a hadron, one can apply the TMD formalism. Thus, the correlation functions can be expressed as

$$\begin{aligned}\Phi^q_{ij}(x,\mathbf{k}_\perp,P,S|n) &= \int dk^- \Phi^q_{ij}(k,P,S|n) \\ &= \int \frac{d\xi^- d^2\xi_\perp}{(2\pi)^3} e^{ik.\xi} \left[\langle P,S|\bar{\Phi}^q_j(0)\mathcal{W}_0(0,\xi)|n)\Phi^q_i(\xi)|P,S\rangle\right]_{\xi^+=0},\end{aligned} \tag{4.3}$$

$$\Delta_{ij}^{h/q}(z,\mathbf{p}_\perp,P_h,S_h|\bar{n}) = \int dp^+ \Delta_{ij}^{q}(p,P_h,S_h|\bar{n})$$
$$= \sum\!\!\!\!\!\!\int_X \int \frac{d\xi^+ d^2\xi_\perp}{(2\pi)^3} e^{ip.\xi}[\langle 0|\mathcal{W}_1(\infty,\xi|\bar{n})\psi_i^q(\xi)|P_h,S_h,X\rangle \tag{4.4}$$
$$\times \langle P_h,S_h,X|\bar{\psi}_j^q(0)|\mathcal{W}_2(0,\infty)|\bar{n})|0\rangle]_{\xi^-=0}.$$

The leading twist contributions are obtained by performing the Sudakov decomposition of Lorentz structures. Starting from the correlation function for PDF, we define a new $\mathbf{k}_\perp$-dependent correlation function in terms of Dirac traces as follows

$$\Phi^{q\Gamma}(x,\mathbf{k}_\perp,P,S|n) = \frac{1}{2}\mathrm{Tr}\left[\Phi^q(x,\mathbf{k}_\perp,P,S|n)\Gamma\right]. \tag{4.5}$$

These traces allow to express the correlation function $\Phi^{q\Gamma}(x,\mathbf{k}_\perp,P,S|n)$ in terms of eight twist-2 TMD PDFs as follows [33, 34]

$$\begin{aligned}
\Phi^{q[\gamma^+]} =& f_1^q(x,\mathbf{k}_1^2) - \frac{\epsilon_\perp^{ij}k_\perp^i S_\perp^j}{M} f_{1T}^{\perp q}(x,\mathbf{k}_\perp^2),\\
\Phi^{q[\gamma^+\gamma_5]} =& \lambda g_{1T}^q(x,\mathbf{k}_\perp^2) + \frac{\mathbf{k}_\perp.\mathbf{S}_\perp}{M} g_{1T}^q(x,\mathbf{k}_\perp^2),\\
\Phi^{q[i\sigma^{i+}\gamma_5]} =& S_\perp^i h_{1T}^q(x,\mathbf{k}_\perp^2) + \frac{\epsilon_\perp^{ij}k_\perp^j}{M} h_1^{\perp q}(x,\mathbf{k}_\perp^2) + \frac{k_\perp^i}{M}\left[\lambda h_{1L}^{\perp q}(x,\mathbf{k}_\perp^2) + \frac{\mathbf{k}_\perp.\mathbf{S}_\perp}{M} h_{1T}^{\perp q}(x,\mathbf{k}_\perp^2)\right],
\end{aligned} \tag{4.6}$$

where M represents the mass of the nucleon (e.g., proton) in the initial state. We adopt the definitions, $\epsilon_\perp^{ij} = \epsilon^{-+ij}$ with $\epsilon_\perp^{12} = 1$, and $2\sigma^{\mu\nu} = i[\gamma^\mu,\gamma^\nu]$. The collinear counterparts

	U	**L**	**T**
U	f_1		$h_1^\perp$
L		g_{1L}	$h_{1L}^\perp$
T	$f_{1T}^\perp$	g_{1T}	$h_1, h_{1T}^\perp$

Table 4.1: Illustration of eight twist-2 TMD-PDFs. The notations U, L, T correspond to unpolarized, longitudinally or transversely polarized quarks (columns) and nucleons (rows) respectively.

are obtained by integrating over the transverse momentum $\mathbf{k}_\perp$, for instance the collinear

unpolarized PDF is given by

$$f_1^q(x) = \int d^2\mathbf{k}_\perp f_1^q(x,\mathbf{k}_1^2) = \int d^2\mathbf{k}_\perp \Phi^{q[\gamma^+]}. \tag{4.7}$$

There is no contribution from $f_{1T}^{\perp q}$ to the collinear PDF because not all twist-2 functions possess counterparts upon integration over $\mathbf{k}_\perp$, the only functions that possess counterparts are shown in blue in Table (4.1). The functions which change sign under time-reversal are shown in red, while those that do not change sign under time-reversal are shown in black in Table (4.1). Similarly, starting from the correlation function for FF, we define a new $\mathbf{p}_\perp$-dependent correlation in terms of Dirac traces as follows

$$\Delta^{h/q[\Gamma]}(z,\mathbf{p}_\perp,P_h,S_h|\bar{n}) = \frac{1}{4z}\mathrm{Tr}\left[\Delta^{h/q}(z,\mathbf{p}_\perp,P_h,S_h|\bar{n})\Gamma\right]. \tag{4.8}$$

The traces provide various forms of correlation function $\Delta^{h/q[\Gamma]}(z,\mathbf{p}_\perp,P_h,S_h|\bar{n})$ which are expressed in terms of eight twist-2 TMD FFs as follows [35]

$$\begin{aligned}
\Delta^{h/q[\gamma^-]} &= D_1^{h/q}(z,z^2\mathbf{p}_\perp^2) + \frac{\epsilon^{ij}P_\perp^i S_{h\perp}^j}{M_h} D_{1T}^{\perp h/q}(z,z^2\mathbf{p}_\perp^2),\\
\Delta^{h/q[\gamma^-\gamma_5]} &= \lambda_h G_{1L}^{h/q}(z,z^2\mathbf{p}_\perp^2) + \frac{\mathbf{p}_\perp.\mathbf{S}_{h\perp}}{M_h} G_{1T}^{h/q},(z,z^2\mathbf{p}_\perp^2),\\
\Delta^{h/q[i\sigma^{i^-}\gamma_5]} &= S_{h\perp}^i H_{1T}^{h/q}(z,z^2\mathbf{p}_\perp^2) - \frac{\epsilon_\perp^{ij}p_\perp^j}{M_h} H_1^{\perp h/q}(z,z^2\mathbf{p}_\perp^2)\\
&\quad\times \frac{p_\perp^i}{M_h}\left[\lambda_h H_{1T}^{\perp h/q}(z,z^2\mathbf{p}_\perp^2) + \frac{\mathbf{p}_\perp.\mathbf{S}_{h\perp}}{M_h} H_{1T}^{\perp h/q}(z,z^2\mathbf{p}_\perp^2)\right],
\end{aligned} \tag{4.9}$$

where M_h is the mass of the outgoing hadron. The collinear counterparts are obtained by integrating over the transverse momentum of the outgoing hadron $P_{h\perp}$. Table (4.2) shows the eight twist-2 TMD FFs. The fragmentation functions that possess the counterparts are shown in blue in Table (4.2). The functions that change sign under time-reversal in shown in red in Table (4.2). The function $D_{1T}^\perp$ is the polarizing fragmentation function and can thus be regarded as the analog of the Sivers function for FFs. Sometimes quantities such

	U	L	T
U	D_1		$H_1^\perp$
L		G_{1L}	$H_{1L}^\perp$
T	$D_{1T}^\perp$	G_{1T}	$H_1, H_{1T}^\perp$

Table 4.2: Illustration of eight twist-2 TMD-FFs. The notations U, L, T correspond to unpolarized, longitudinally or transversely polarized quarks (columns) and nucleons (rows) respectively.

as structures functions can be easily expressed in terms of the $k_\perp(p_\perp)$-moments of TMD distributions. The general expressions for these $k_\perp(p_\perp)$-moments are

$$f^{(n)}(x) = \int d^2\mathbf{k}_\perp \left(\frac{k_\perp^2}{2M^2}\right)^n f(x, k_\perp^2), \quad D^{(n)}(z) = z^2 \int d^2\mathbf{p}_\perp \left(\frac{p_\perp^2}{2M_h^2}\right)^n D(z, z^2 p_\perp^2), \tag{4.10}$$

Hence, one can obtain an expression of the n-th moment for each TMD function. For instance, the first moments for the Sivers function $f_{1T}^\perp$ and the Collins fragmentation function $H_1^\perp$ are given by

$$f_{1T}^{\perp(1)}(x) = \int d^2\mathbf{k}_\perp \left(\frac{k_\perp^2}{2M^2}\right) f_{1T}^\perp(x, k_\perp^2), \quad H_1^{\perp(1)}(z) = z^2 \int d^2\mathbf{p}_\perp \left(\frac{p_\perp^2}{2M_h^2}\right) H_1^\perp(z, z^2 p_\perp^2). \tag{4.11}$$

The above moments are related to collinear twist-3 functions. The first moment of the Sivers function is related to the Qiu-Sterman function, and the first moment of the Collins function is related to the twist-3 fragmentation function.

4.1.2 Twist-3 TMD functions

Twist-3 correlation functions are key objects in the study of hadronic structure, particularly in the context of non-perturbative QCD effects. Unlike twist-2 functions, which describe the leading behavior at high energies, twist-3 functions, on the other hand, describe subleading effects and provide additional information about the hadronic structure, including contri-

butions from quark-gluon correlations and higher-order QCD effects. These functions arise in the description of phenomena like higher-twist contributions to deep inelastic scattering (DIS), as well as in the study of hadronic transverse momentum distributions, the transverse spin structure, and the analysis of certain asymmetries. Mathematically, twist-3 correlators typically involve higher derivatives or more intricate tensor structures compared to twist-2, and they play a crucial role in understanding the dynamics of partons inside hadrons at a more detailed level, particularly in the presence of non-perturbative effects that cannot be captured by leading-order approximations. In the twist-3 case, we can consider the following quark-quark and quark-gluon-quark correlation functions [36]

$$\Phi^q_{ij}(x,P,S_\perp) = \int \frac{d\xi^-}{2\pi} e^{ixP^+\xi^-} \langle P,S_\perp|\bar{\psi}^q_j(0)\psi^q_i(\xi^-)|P,S_\perp\rangle, \tag{4.12}$$

$$\Phi^{q,\mu}_{\partial_\perp,ij}(x,P,S_\perp) = \int \frac{d\xi^-}{2\pi} e^{ixP^+\xi^-} \langle P,S_\perp|\bar{\psi}^q_j(0)\partial^\mu_\perp\psi^q_i(\xi^-)|P,S_\perp\rangle, \tag{4.13}$$

$$\Phi^{q,\mu}_{A,ij}(x,x_1,P,S_\perp) = \int \frac{d\xi^-}{2\pi}\frac{d\zeta^-}{2\pi} e^{ix_1P^+\xi^-} e^{i(x-x_1)P^+\zeta^-} \langle P,S_\perp|\bar{\psi}^q_j(0)A^\mu_\perp(\zeta^-)\psi^q_i(\xi^-)|P,S_\perp\rangle. \tag{4.14}$$

Here, we emphasize that Wilson lines have been suppressed in the above correlators. It is worth to mention that Wilson lines are reduced to unity in the light-cone gauge. For gauge invariance, the gluon field $A_\perp$ in Eq. (4.14) for the quark-gluon-quark correlator can be replaced either with the covariant derivative $iD^\rho_\perp = i\partial^\rho + gA^\rho_\perp$ or the field strength tensor $F^{+\rho}_\perp$ in the light-cone gauge ($A^+ = 0$). The expansion allows the quark-gluon-quark correlator to be expressed in terms of twist-3 correlation functions [37]

$$\Phi^{q,\mu}_{D,ij}(x,x_1,P,S_T) = \frac{1}{2}M\left[F^q_{DT}(x,x_1)i\epsilon^{\mu\nu}_\perp S_{\perp\nu}\gamma^- + G^q_{DT}(x,x_1)S^\mu_\perp\gamma_5\gamma^-\right]_{(ij)}, \tag{4.15}$$

$$\Phi^{q,\mu}_{F,ij}(x,x_1,P,S_T) = \frac{1}{2}M'\left[F^q_{FT}(x,x_1)\epsilon^{\mu\nu}_\perp S_{\perp\nu}\gamma^- - G^q_{FT}(x,x_1)iS^\mu_\perp\gamma_5\gamma^-\right]_{(ij)}, \tag{4.16}$$

where $M' = M/P^+$. The field $A_\perp$ in Eq. (4.14) has been replaced by $iD^\rho_\perp$ and $F^{+\rho}_\perp$ to obtain Eq. (4.15) and Eq. (4.16) respectively. The parity and time reversal implies the following

relations

$$F^q_{DT}(x,x_1) = -F^q_{DT}(x_1,x), \qquad G^q_{DT}(x,x_1) = G^q_{DT}(x_1,x), \tag{4.17}$$

$$F^q_{FT}(x,x_1) = F^q_{FT}(x_1,x), \qquad G^q_{FT}(x,x_1) = -G^q_{FT}(x_1,x). \tag{4.18}$$

The above expressions form the following relations

$$\begin{aligned} F^q_{DT}(x,x_1) =& \mathcal{P}_V \frac{1}{x-x_1} F^q_{FT}(x,x_1), \\ G^q_{DT}(x,x_1) =& \mathcal{P}_V \frac{1}{x-x_1} G^q_{FT}(x,x_1) + \delta(x-x_1)\tilde{g}^q(x). \end{aligned} \tag{4.19}$$

Here, $\mathcal{P}_V$ is the principal value, and $\tilde{g}$ is the additional twist-3 function which is defined as the first $k_\perp$-moment of g^q_{1T} [36]. The quark-quark correlator of Eq. (4.12) leads to a contribution from the twist-3 g^g_T as follows

$$\mathrm{Tr}\left[\Phi^q(x,P,S_\perp)\right] = \frac{2M}{P^+} S^\mu_\perp g^q_\perp(x). \tag{4.20}$$

Hence, we have already identified six twist-3 PDFs. In the twist-3 FF case, we can consider the following correlation functions

$$\Delta^{h/q}_{ij}(z,P_h) = \sum\!\!\!\!\!\!\int_X z \int \frac{d\xi^+}{2\pi} e^{iP_h^-\xi^+/z} \langle 0|\psi^q_i(\xi^+)|P_h,X\rangle\langle P_h,X|\bar{\psi}^q_i(0)|0\rangle, \tag{4.21}$$

$$\Delta^{h/q,\mu}_{\partial_\perp,ij}(z,P_h) = \sum\!\!\!\!\!\!\int_X z \int \frac{d\xi^+}{2\pi} e^{iP_h\xi^+/z} \langle 0|\partial^\mu_\perp\psi^q_i(\xi^+)|P_h,X\rangle\langle P_h,X|\bar{\psi}^q_j(0)|0\rangle, \tag{4.22}$$

$$\begin{aligned} \Delta^{h/q,\mu}_{A,ij}(z,z_1,P_h) = \sum\!\!\!\!\!\!\int_X \frac{1}{z} \int \frac{d\xi^+}{2\pi}\frac{d\zeta^+}{2\pi} e^{iP_h^-\xi^+/z_1} e^{i(z_1-z)P_h^-\zeta^+/z_1 z} \langle 0|A^\mu_\perp(\zeta^+)\psi^q_i(\xi^+)|P_h,X\rangle \\ \times \langle P_h,X|\bar{\psi}^q_j(0)|0\rangle. \end{aligned} \tag{4.23}$$

Similar to twist-3 distribution correlators, the Wilson lines are suppressed and will not contribute in the light-cone gauge ($A^+ = 0$). Similar to twist-3 distribution correlators, the gluon field $A_\perp$ in Eq. (4.23) can be replaced by the covariant derivative iD^ρ or the field

strength tensor $F_\perp^{+\rho}$ which lead to the following twist-3 FFs

$$\Delta^{h/q,\mu}_{F,ij}(z,z_1,P_h) = -M_h\left[i\epsilon_\perp^{\mu\nu}\sigma_\nu^+\gamma_5\hat{H}^{h/q}_{\rm FU}(z,z_1)\right]_{(ij)}, \tag{4.24}$$

$$\Delta^{h/q,\mu}_{D,ij}(z,z_1,P_h) = -\frac{M_h}{P_h^-}\left[\epsilon_\perp^{\mu\nu}\sigma_\nu^+\gamma_5\hat{H}^{h/q}_{\rm DU}(z,z_1)\right]_{(ij)}, \tag{4.25}$$

where $\hat{H}^{h/q}_{FU}(z,z_1)$ and $\hat{H}^{h/q}_{DU}(z,z_1)$ are twist-3 complex functions. In terms of the principle value $\mathcal{P}_\mathcal{V}$, and the twist-3 function $\hat{H}^{h/q}(z)$, they can be expressed as

$$\hat{H}^{h/q}_{DU}(z,z_1) = \mathcal{P}_\mathcal{V}\frac{1}{\not{z}}\hat{H}^{h/q}_{FU}(z,z_1) - \frac{i}{z^2}\hat{H}^{h/q}(z)\delta(\not{z}), \tag{4.26}$$

where $\not{z} = (z_1 - z)/zz_1$. The function $\bar{H}^{h/q}(z)$ can be obtained from the Collins function $H_1^{\perp h/q}(z, z^2\mathbf{p}_\perp^2)$ by double-integrating over $\mathbf{p}_\perp$, thus $\hat{H}^{h/q}(z)$ is similar to the function $H_1^{\perp h/q(1)}(z)$ which is the first $\mathbf{p}_\perp$-moment of the Collins function. The quark-quark correlation function $\Delta^{h/q}_{ij}(z,P_h)$ leads to the following expressions [33]

$$\mathrm{Tr}\left[\Delta^{h/q}(z,P_h)i\sigma^{\mu\nu}\gamma_5\right] = \frac{4M_h}{P_h^-}\epsilon_\perp^{\mu\nu}H^{h/q}(z), \qquad \mathrm{Tr}\left[\Delta^{h/q}(z,P_h).\mathbb{1}\right] = \frac{4M_h}{P_h}E^{h/q}(z), \tag{4.27}$$

where $H^{h/q}(z)$ and $E^{h/q}(z)$ are the twist-3 functions. These twist-3 functions also can be expressed in terms of the z_1-integration of imaginary part of $\hat{H}^{h/q}_{DU}(z,z_1)$ and the real part of $\hat{H}^{h/q}_{FU}(z,z_1)$ respectively. Eq. (4.26) contains three twist-3 FFs and Eq. (4.27) contains two twist-3 FFs; thus, we obtain five twist-3 FFs.

4.2 TMD factorization theorems

This section presents a fundamental overview of the TMD factorization theorems pertaining to the Drell-Yan process, $pp \to \gamma^*/Z \to l^+l^-$, involving unpolarized protons. This serves the purpose of establishing fundamental notations and concepts essential to elucidate TMD factorization. To explore hard scattering processes effectively, employing light-cone coordi-

nates proves advantageous. This choice is driven by the fact that the dynamics of hadrons are predominantly examined along the collision axis, involving partons whose behavior is characterized by fluctuations near the light-cone. The momenta P_A, and P_B of the incoming protons in Drell-Yan process are defined as

$$P_A^\mu = P_A^+(1, e^{-2Y_A}, \mathbf{0}_T), \qquad P_B^\mu = P_B^-(e^{+2Y_B}, 1, \mathbf{0}_T), \tag{4.28}$$

where the components have the form, $p^\mu = (p^+, p^-, \mathbf{p}_T)$ and the proton rapidities are defined as

$$Y_A = \frac{1}{2}\ln\frac{P_A^+}{P_A^-} = \frac{1}{2}\ln\frac{2(P_A^+)^2}{m_p^2}, \qquad Y_B = \frac{1}{2}\ln\frac{P_B^+}{P_B^-} = \frac{1}{2}\ln\frac{m_p^2}{2(P_B^-)^2}, \tag{4.29}$$

where m_p is the proton mass. The massless limit, $m_p \to 0$, leads to $Y_{A,B} \to \pm\infty$, and then the protons are exactly aligned along the light-cone directions. For a lepton pair l^+l^- of total momentum q^μ and invariant mass $Q^2 = q^2$, the lepton pair rapidity Y and transverse momentum q_T are defined as

$$Y = \frac{1}{2}\ln\frac{q^+}{q^-}, \qquad q_T^\mu = (0, q_T^x, q_T^y, 0). \tag{4.30}$$

Here, q_T^μ is defined with respect to the Minkowski space-time (t, x, y, z). The Euclidean transverse momentum is denoted by $\mathbf{q}_T$. Assuming that $Q^2 \gg \Lambda^2_{\rm QCD}$, the cross section is decomposed as

$$\frac{d\sigma}{dQdYd^2\mathbf{q}_T} = \left(\frac{d\sigma^W}{dQdYd^2\mathbf{q}_T} + \frac{d\sigma^Y}{dQdYd^2\mathbf{q}_T}\right)\left[1 + \mathcal{O}\left(\frac{\Lambda^2_{\rm QCD}}{Q^2}\right)\right], \tag{4.31}$$

where $d\sigma^W$ represents the portion of the cross section that predominates at small q_T values and is commonly referred to as the W term. This part of the cross section includes all terms that are proportional to $1/q_T^2$ as q_T approaches zero at any order of expansion in the strong coupling α_s. The remaining portion $d\sigma^Y$, usually referred as the Y term [38, 39, 40], is

suppressed by $\mathcal{O}(q_T^2/Q^2)$ with respect to $d\sigma^W$. The TMD factorization was first put forward by Collins, Soper and Sterman (CSS) and in their original formulation, the σ^W is expressed as

$$\begin{aligned}\frac{d\sigma^W}{dQdYd^2\mathbf{q}_T} = \sum_j \mathcal{H}_{j,\bar{j}}(Q^2,\mu,\rho)\int d^2\mathbf{b}_T e^{i\mathbf{b}_T\cdot\mathbf{q}_T}\tilde{f}_{j/p}(x_a,\mathbf{b}_T,\mu,\tilde{\zeta}_a,\rho)\\ \times\tilde{f}_{\bar{j}/p}(x_b,\mathbf{b}_T,\mu,\tilde{\zeta}_b,\rho),\end{aligned} \tag{4.32}$$

where $\tilde{\zeta}$ and ρ are rapidity regulator parameters, and $\mathbf{b}_T$ is the two-dimensional variable which is conjugate to the transverse momentum $\mathbf{q}_T$. The hard function $\mathcal{H}_{q\bar{q}}$ stands for corrections to the hard process, $q\bar{q}\to\gamma^*/Z\to l^+l^-$. In the modern formulation proposed by Collins [41], which results in a factorization theorem analogous to several definitions in soft-collinear effective theories (SCET) [42, 43, 44, 45, 46, 47, 48] the cross section $d\sigma^W$ is expressed as

$$\begin{aligned}\frac{d\sigma^W}{dQdYd^2\mathbf{q}_T} &= \sum_j \mathcal{H}_{j,\bar{j}}(Q^2,\mu)\int d^2\mathbf{b}_T e^{i\mathbf{b}_T\cdot\mathbf{q}_T}\tilde{f}_{j/p}(x_a,\mathbf{b}_T,\mu,\zeta_a)\tilde{f}_{\bar{j}/p}(x_b,\mathbf{b}_T,\mu,\zeta_b)\\ &= \sum_j \mathcal{H}_{j,\bar{j}}(Q^2,\mu)\int d^2\mathbf{b}_T e^{i\mathbf{b}_T\cdot\mathbf{q}_T}\tilde{\mathcal{B}}_{j/p}(x_a,\mathbf{b}_T,\mu,\zeta_a/\nu^2)\\ &\quad\times\tilde{\mathcal{B}}_{\bar{j}/p}(x_b,\mathbf{b}_T,\mu,\zeta_b/\nu^2)\tilde{\mathcal{S}}(b_T,\mu,\nu),\end{aligned} \tag{4.33}$$

where $\tilde{\mathcal{S}}$ is the soft function which encodes soft exchange between partons $(j,\bar{j})$, and ν is the rapidity renormalization scale. The function $\tilde{f}$ is the unpolarized TMD parton distribution function (PDF), and the function $\tilde{\mathcal{B}}$ is the TMD beam function(BF). This function describes the collinear radiation close to the proton. For a quark flavor q, the simple relation between these two functions can be expressed as

$$\tilde{f}_{q/p}(x,\mathbf{b}_T,\mu,\zeta) = \tilde{\mathcal{B}}_{q/p}(x,\mathbf{b}_T,\mu,\zeta/\nu^2)\sqrt{\tilde{\mathcal{S}}(b_T,\mu,\nu)}. \tag{4.34}$$

The dependence of the TMD PDFs on both μ and ζ are governed by evolution equations which allow to evolve from initial scales μ_0 and ζ_0 to final scales μ and ζ. The final Collins-

Soper scales $\zeta_{a,b}$ are defined as

$$\zeta_a = 2(x_a P_A^+)^2 e^{-2y} = x_a^2 m_p^2 e^{2(Y_A - y)}, \qquad \zeta_b = 2(x_b P_A^+)^2 e^{-2y} = x_b^2 m_p^2 e^{2(Y_B - y)}, \tag{4.35}$$

where Y_A and Y_B are the rapidities of protons A and B respectively. In the center of momentum frame, $Y_A = Y_B$. The variable y represents the rapidity which govern an additional scheme dependence that cancels between the two TMD PDFs. The combination of ζ_a and ζ_b is directly related to the hard scale Q as follows

$$\zeta_a \zeta_b = (2 x_a x_b P_A^+ P_B^-)^2 = Q^4. \tag{4.36}$$

The quantity, $2P_A^+ P_B^- = (P_A^+ + P_B^-)^2$ is just the center of mass energy s of the proton-proton (pp) collision. Since y does not have other great benefit than allowing to obtain evolution equations with respect to $\zeta_{a,b}$ the frequently adopted choice is $y = 0$. The main difference between Eq. (4.32) and Eq. (4.33) is the nature of the scheme which is utilized for the hard function $\mathcal{H}_{j,\bar{j}}$ that directly defines the scheme for the remaining functions because the cross section σ^W is scheme-independent. The hard function $\mathcal{H}_{j,\bar{j}}$ described in Eq. (4.33) is established within the $\overline{\text{MS}}$ framework, therefore affected solely by the hard scale Q and the renormalization scale μ. The hard function $\mathcal{H}_{j,\bar{j}}$ in Eq. (4.33) can be obtained using $\overline{\text{MS}}$ subtractions of $1/\epsilon$ poles in dimensional regularization with $d = 4 - 2\epsilon$. However, The hard function $\mathcal{H}_{j,\bar{j}}$ in Eq. (4.32) depends on an additional scale ρ, and the TMD formalism uses different Collins-Soper scales.

4.3 TMD parton distribution functions

This section explores fundamental field theory definitions of transverse momentum dependent parton distribution functions(TMDPDFs). For more details, see Ref. [49]. In Drell-Yan

process, the definition for a TMDPDF can be expressed as

$$\tilde{f}_{i/p}(x,\mathbf{b}_T,\mu,\zeta) = \lim_{\substack{\epsilon\to 0\\ \tau\to 0}} Z^i_{uv}(\mu,\zeta,\epsilon)\frac{\tilde{f}^{0(u)}_{i/p}(x,\mathbf{b}_T,\epsilon,\tau,xP^+)}{\tilde{\mathcal{S}}^{(0)s}(b_T,\epsilon,\tau)}\sqrt{\tilde{\mathcal{S}}^{(0)}(b_T,\epsilon,\tau)}, \tag{4.37}$$

where expressions with the superscript ^{0} are bare quantities, for example, $\tilde{\mathcal{S}}^{(0)}$ is the bare soft function, and $\tilde{\mathcal{S}}^{(0)s}$ is the subtracted bare soft function. They experience both ultraviolet (UV) and rapidity divergences. The UV divergences can be regulated using dimensional regularization with $d = 4 - 2\epsilon$ dimensions, and rapidity divergences necessitate a regulator [50, 38, 51, 52, 42, 45, 53] which is indicated by τ in Eq. (4.37). The divergences in rapidity effectively nullify each other across different factors in Eq. (4.37) , such that the renormalization counterterm Z^i_{uv} in Eq. (4.37) only addresses divergences in ϵ. Typically, UV divergences lead to the introduction of the renormalization scale μ, which is established within the $\overline{\text{MS}}$ scheme. Similarly, the presence of rapidity divergences introduces sensitivity to the Collins-Soper scale ζ [39, 54], the precise definition of which relies on the chosen regulator ϵ. Since there are two protons in the process of interest, half of the soft function integrates into the TMDPDF $f_{i/p}$, while the other half integrates into the TMDPDF $f_{j/p}$ associated with the other proton. After the renormalization of both UV and rapidity divergences, the renormalized beam and soft functions in Eq. (4.33) are expressed as

$$\begin{aligned}
\tilde{\mathcal{B}}_{i/p}(x,\mathbf{b}_T,\mu,\zeta/\nu^2) &= \lim_{\substack{\epsilon\to 0\\ \tau\to 0}} Z^i_{uv(\mathcal{B})}(b_T,\mu,\nu,\epsilon,\tau,xP^+)\tilde{\mathcal{B}}^0_{i/p}(x,\mathbf{b}_T,\epsilon,\tau,xP^+),\\
\tilde{\mathcal{S}}(b_T,\mu,\nu) &= \lim_{\substack{\epsilon\to 0\\ \tau\to 0}} Z^i_{uv(\mathcal{S})}(b_T,\mu,\nu,\epsilon,\tau)\tilde{\mathcal{S}}^0(b_T,\epsilon,\tau).
\end{aligned} \tag{4.38}$$

The bare beam function $\tilde{\mathcal{B}}^0$ can be expressed in terms of the bare unsubtracted PDF $\tilde{f}^{0(u)}$ as

$$\tilde{\mathcal{B}}^0_{i/p}(x,\mathbf{b}_T,\epsilon,\tau,xP^+) = \frac{\tilde{f}^{0(u)}_{i/p}(x,\mathbf{b}_T,\epsilon,\tau,xP^+)}{\tilde{\mathcal{S}}^{(0)s}(b_T,\epsilon,\tau)}. \tag{4.39}$$

Here, ν is the rapidity renormalization scale which emerges because of the subtraction of poles in τ. Notice that Eq. (4.34) can easily be obtained from Eq. (4.38) and Eq. (4.39). The ν dependence in Eq. (4.34) cancels between beam and soft functions, and thus, in terms of rapidity, $\tilde{f}$ only depends on the Collins-Soper scale ζ.

To establish the gauge invariance, the bare unsubtracted TMD PDF (or equivalently the bare beam function) and the bare soft function should be expressed in terms of the Wilson lines $W_\sqsubset$ and $W_>$ as

$$\begin{aligned}\tilde{f}^{0(u)}(x,\mathbf{b}_T,\epsilon,\tau,xP^+) &= \int \frac{db^-}{2\pi} e^{-ib^-(xP^+)} \left\langle p(P)\left|\left[\overline{\psi}_i^0(b^\mu) W_\sqsubset(b^\mu,0)\frac{\gamma^+}{2}\psi_i^0(0)\right]_\tau\right|p(P)\right\rangle, \\ \tilde{S}^0(b_T,\epsilon,\tau) &= \frac{1}{N_c}\langle 0|\mathrm{Tr}[W_>(b_T)]_\tau|0\rangle,\end{aligned} \tag{4.40}$$

where the notation $[\cdots]_\tau$ means that operators inside depend on an additional rapidity

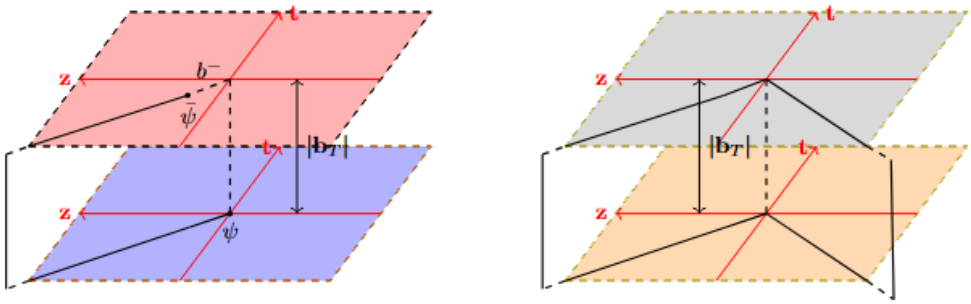

Figure 4.1: Illustration of the structure of the Wilson line $W_\sqsubset$ of the TMD parton distribution function (left) and that of the Wilson line $W_>$ of the soft function $\tilde{\mathcal{S}}$ (right).

regulator τ. The proton p is moving close to the light-cone direction $n_a^\mu = (1,0,\mathbf{0}_T)$ with a momentum $P^\mu = P^+(1,e^{-2y},\mathbf{0}_T)$. If the proton is moving along the direction $n_b^\mu = (0,1,\mathbf{0}_T)$, the corresponding expressions can be obtained from Eq. (4.40) by using the prescription $n_a \leftrightarrow n_b$. Due to Poincare invariance, the matrix element of the proton solely relies on the difference in position of the quark fields, denoted as $b^\mu - 0 = b^\mu$, with $b^\mu = (0,b^-,\mathbf{b}_T)$. The

Wilson lines $W_{\sqsubset}$ corresponding to $\tilde{f}$ is

$$W_{\sqsubset}(b^{\mu},0) = W_{n_b}(b^{\mu},-\infty,0)W_{\hat{b}_T}(-\infty n_b,0,b_T)W_{n_b}(0^{\mu},0,-\infty), \tag{4.41}$$

and for the soft function $\tilde{\mathcal{S}}$ the Wilson line $W_{>}$ is defined as

$$\begin{aligned} W_{>}(b_T) =& W_{n_a}(b_T,-\infty,0)W_{n_b}(b_T,-\infty,0)W_{\hat{b}_T}(-\infty n_b,0,b_T)W_{n_b}(0,0,-\infty) \\ &\times W_{n_a}(0,-\infty,0)W_{\hat{b}_T}(-\infty n_a,b_T,0), \end{aligned} \tag{4.42}$$

where $\hat{b}_T^{\mu} = b_T^{\mu}/b_T$. Here, the Wilson line along a general path γ is defined by the following the path-ordered exponential

$$W[\gamma] = \mathcal{P}\exp\left\{-ig_0\int_{\gamma} dx^{\mu}A_{\mu}^{c0}(x)t^{c}\right\}, \tag{4.43}$$

where t^c are the generators of SU(3) in the fundamental representation, g_0 denotes the bare strong coupling and A^{c0} stands for the bare gluon fields. The Wilson line of the form, $W(x,a,b)$ is defined as path-ordered exponential which links the point $x^{\mu}+an^{\mu}$ to $x^{\mu}+bn^{\mu}$ along the direction n

$$W_n(x^n,a,b) = \mathcal{P}\exp\left\{-ig_0\int_a^b dsn.A^{c0}(x^{\mu}+sn^{\mu})t^{c}\right\}, \tag{4.44}$$

where n is a four-vector. The symbol $\mathcal{P}$ employed in $W_n(x^n,a,b)$ indicates the path ordering utilized for the expanded exponential. In this ordering, the matrices t^c are arranged based on their respective values along a specific path, starting from the right and going to the left. The diagrams depicting the Wilson line structures present in the unsubtracted TMD PDF and soft functions are shown in Figure (4.1). The transverse Wilson lines W_{b_T} follow a straight line path in the transverse plane at the light-cone $-\infty$. The particular shape of the Wilson line $W_{\sqsubset}$ is dictated by the proof of factorization.

4.4 Rapidity regulator

The emergence of rapidity divergences stems from the derivation of TMD factorization, where the cross section is partitioned into distinct hard, collinear, and soft regions. Perturbatively, Feynman diagrams are dissected into these delineated sectors. Assume a full theory that contains the integrand $1/k$. The integral of $1/k$ can be expanded into collinear and soft regions as

$$\int_{q_T}^{Q} \frac{dk}{k} = \lim_{\tau\to 0}\int_{0}^{Q} \frac{dk}{k} R_c(k,\tau) + \lim_{\tau\to 0}\int_{q_T}^{\infty} \frac{dk}{k} R_s(k,\tau) = \ln\left(Q/q_T\right). \tag{4.45}$$

In the collinear region, the transverse momentum q_T which is much small compared to Q is expanded away, and in the soft region, the large momentum Q is expanded away. These expansions are inevitable because they are the cornerstone for the derivation of the factorization theorem. The divergence of collinear and soft integrals requires the introduction of respective regulating functions $R_c(k,\tau)$ and $R_s(k,\tau)$ where τ is a regulator. The final result is obtained by removing the regulator, $\tau \to 0$, in all sectors.

Here, we present a rapidity regulator that is used to regularize the rapidity divergence in our TMD formalisms. This is called the η-regulator in the literature. The η regulator changes the Wilson lines in the unsubtracted TMD PDF and soft functions [53]. This requires the introduction of factors $|k^+/\nu|^{-\eta}$ in the Wilson lines in $W_c(b^\mu, 0)$ and factors $|k^z/\nu|^{-\eta/2}$ in the soft function $\tilde{\mathcal{S}}$. Amplitudes undergo an expansion in the limit, $\eta \to 0$ and rapidity divergences arise as poles in η. This regulator is often used for the renormalization of either the unsubtracted TMD PDF or soft functions. The rapidity renormalization factor removes poles in η and this leads to an appearance of a rapidity ν. In this regulating scheme, the

expression for the renormalized TMD PDF is [53]

$$\begin{aligned}\tilde{f}_{i/p}(x,\mathbf{b}_T,\mu,\zeta) =& \lim_{\substack{\epsilon\to 0\\ \eta\to 0}} Z^i_{uv}(\mu,\zeta,\epsilon)\tilde{f}^{0(u)}_{i/p}(x,\mathbf{b}_T,\epsilon,\eta,xP^+)\sqrt{\tilde{S}^0(b_T,\epsilon,\eta)}\\ =& \tilde{B}_{i/p}(x,\mathbf{b}_T,\mu,\sqrt{\zeta}/\nu)\sqrt{\tilde{S}(b_T,\mu,\nu)},\end{aligned} \tag{4.46}$$

where the Collins-Soper kernel is given by $\zeta = 2(xP^+)^2$.

4.5 One-loop TMD parton distribution functions

This section introduces the perturbative study of the quark TMD PDF at one loop. For more details, see Ref. [49]. The purpose is to show the origin of rapidity divergences and different methods for their regularization. We focus on both unsubtracted quark TMD PDF and soft function, which can be combined into TMD PDF. Consider the following expression for the unsubtracted TMD PDF at next-to-leading order (NLO)

$$\tilde{f}^{0(u)}_{q/q'}(x,\mathbf{b}_T,\epsilon,\tau) = \int \frac{db^-}{2\pi} e^{-ib^-(xp^+)} \left\langle q'(p)\left|\left[\overline{\psi}^0_q(b^\mu) W_{\sqsubset}(b^\mu,0)\frac{\gamma^+}{2}\psi^0_q(0)\right]_\tau\right|q'(0)\right\rangle, \tag{4.47}$$

where the subscript on $f_{q'/q}$ means that the analysis is about the contribution from an external parton of flavor q' to the quark TMD PDF of flavor q. At one loop, $q = q'$, this means that quark flavors are identical, but for high-order loops, quark flavors can be different, $q \neq q'$. In addition, there can exist contributions from a mixture of quarks with gluons at one loop, which will not be the subject of investigation.

Thus, we require q to be a non-singlet combination of quark flavors. As illustrated in Fig. (4.2), there are no more than four Feynman diagrams and their mirror diagrams at one-loop level. Since we work in the Feynman gauge which a physical gauge transverse gauge links have no contributions. The nature of gluon exchange between the quarks and Wilson lines leads to different diagrams. The presence of Wilson lines in the diagrams requires the Feynman rules for the connection of a gluon to a Wilson line where k is the

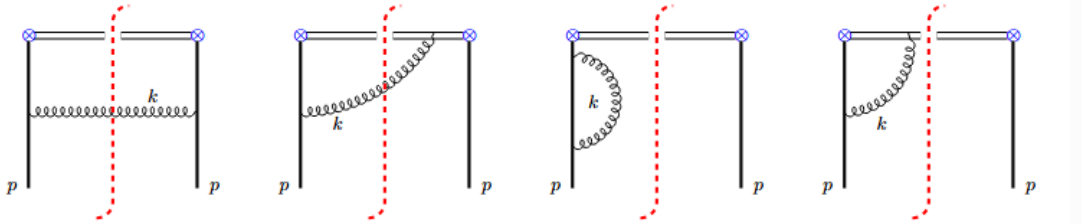

Figure 4.2: The diagrams for the one-loop contribution to the quark-TMD parton distribution function. The double lines and the dashed line represent the Wilson lines and the on-shell cut respectively. Since diagrams (c) and (d) are scaleless, only diagrams (a) and (b) contribute in the dimensional regularization.

incoming gluon momentum, a is the color index, and ϵ^μ is the polarization vector. There are no contributions from gluon exchange between the Wilson line portions since such gluon exchange is proportional to n_b^2 which is just equal to zero. The dimensional regularization with $d = 4-2\epsilon$ dimensions is chosen to regulate infrared (IR) and ultraviolet (UV) divergences. The application of Feynman rules for diagrams (4.2) leads to the following expressions

$$\mathcal{M}_a = -ig_0^2 C_F \int \frac{d^dk}{(2\pi)^d} \int \frac{db^-}{2\pi} e^{-ib^-(xP^+)} e^{i(p-k).b} \left\{ \frac{\overline{u}(p)\gamma^\mu(\not{p}-\not{k})\gamma^+(\not{p}-\not{k})\gamma_\mu u(p)}{2[(p-k)^2+i0]^2(k^2+i0)} \right\}, \quad (4.48)$$

$$\mathcal{M}_b = -2ig_0^2 C_F \int \frac{d^dk}{(2\pi)^d} \int \frac{db^-}{2\pi} e^{-ib^-(xP^+)} e^{i(p-k).b} \left\{ \frac{\overline{u}(p)\gamma^+(\not{p}-\not{k})\gamma^+ u(p)}{2(k^+ + i0)[(p-k)^2+i0]^2(k^2+i0)} \right\}, \quad (4.49)$$

where q^μ is the momentum flowing out the right vertex $\otimes$. There are no contributions from diagrams (c) and (d) in dimensional regularization because they depend on integrals which vanish in the dimensional regularization. The overall factor of 2 in $\mathcal{M}_b$ is due to the mirror diagram. The b^- integral in expressions for $\mathcal{M}_a$ and $\mathcal{M}_b$ can be evaluated in the following way

$$\begin{aligned} \int \frac{db^-}{2\pi} e^{-ib^-(xP^+)} e^{i(p-k).b} &= \int \frac{db^-}{2\pi} \exp\left\{-ib^-\left[(1-x)p^+ - k^+\right] + i\mathbf{b}_T.\mathbf{k}_T\right\} \\ &= \delta\left[(1-x)p^+ - k^+\right] \exp\left\{i\mathbf{b}_T.\mathbf{k}_T\right\}, \end{aligned} \quad (4.50)$$

where we have chosen $b^+ = p^- = 0$. Thus, the phase in final result depends solely on the transverse momentum. The b^- integral result indicates that the gluon is emitted with the

longitudinal momentum $k^+ = (1-x)p^+$ and the remaining momentum xp^+ is carried by the quark field. Now, the b^- integral result can be used in the evaluation of $\mathcal{M}_a$, and $\mathcal{M}_b$. After the Dirac algebra calculations, expressions for $\mathcal{M}_a$ and $\mathcal{M}_b$ become

$$\mathcal{M}_a = ig_0^2 C_F \int \frac{d^{d-2}\mathbf{k}_T}{(2\pi)^d} e^{i\mathbf{b}_T.\mathbf{k}_T} \int dk^- \frac{(2-d)(1-x)p^+}{[(p-k)^2+i0]\,(k^2+i0)}, \tag{4.51}$$

$$\mathcal{M}_b = ig_0^2 C_F \int \frac{d^{d-2}\mathbf{k}_T}{(2\pi)^d} e^{i\mathbf{b}_T.\mathbf{k}_T} \int dk^- \frac{-4x/(1-x)p^+}{[(p-k)^2+i0]\,(k^2+i0)}, \tag{4.52}$$

The residue theorem can be utilized to compute the k^- integral,

$$\begin{aligned}\int dk^- \frac{1}{[(p-k)^2+i0]\,(k^2+i0)} &= \int dk^- \frac{1}{(-2xp^+k^- - \mathbf{k}_T^2 + 0i)\,[2(1-x)p^+k^- - \mathbf{k}_T^2 + i0]} \\ &= \frac{i\pi}{p^+\mathbf{k}_T^2}\theta(x)\theta(1-x),\end{aligned} \tag{4.53}$$

If x and $1-x$ have opposite signs, the residues of k^- live in the same complex plane, and the deformation of the k^- contour can lead to a vanishing integral. The only values of x that provide physical contributions are $0 < x < 1$, and, surprisingly, these are expected values for the momentum fraction. The condition of the gluon on the shell is $k^2 = 0$, which is the same as choosing the residue at $k^- = \mathbf{k}_T^2/(2k^+) > 0$. The one-loop contribution to the bare unsubtracted quark TMD PDF is obtained by combining expressions for $\mathcal{M}_a$ and $\mathcal{M}_b$, and the resulting expression is

$$\mathcal{M}_a + \mathcal{M}_b = \frac{g_0^2 C_F}{2\pi}\left[\frac{1+x^2}{1-x} - \epsilon(1-x)\right]\int \frac{d^{d-2}\mathbf{k}_T}{(2\pi)^{d-2}} \frac{e^{i\mathbf{b}_T.\mathbf{k}_T}}{\mathbf{k}_T^2}, \tag{4.54}$$

The evaluation of the $\mathbf{k}_T$ integral requires making choice for $\mathbf{k}_T$ and $\mathbf{b}_T$ in $2-2\epsilon$ dimensions, the choice can be arbitrary because every choice yields the same TMD PDFs. The choice of $\mathbf{k}_T = (b_T, 0, \mathbf{0}_{-2\epsilon})$ and $\mathbf{k}_T = k_T(\cos\theta, \sin\theta, \mathbf{0}_{-2\epsilon})$ leads to the following result for the $\mathbf{k}_T$

integral

$$\int \frac{d^{d-2}\mathbf{k}_T}{(2\pi)^{d-2}} \frac{e^{i\mathbf{b}_T\cdot\mathbf{k}_T}}{\mathbf{k}_T^2} = \frac{\Omega_{-2\epsilon}}{(2\pi)^{2-2\epsilon}} \int dk_T k_T^{1-2\epsilon} \int_0^\pi d\theta \sin^{-2\epsilon}\theta \frac{e^{ib_T k_T \cos\theta}}{k_T^2} = \frac{\Gamma(-\epsilon)}{4\pi}(\pi \mathbf{b}_T^2)^\epsilon, \quad (4.55)$$

where Ω_n is defined as the area of a unit n-sphere. Using the $\mathbf{k}_T$ integral result, the sum of the matrix elements $\mathcal{M}_a$ and $\mathcal{M}_b$ becomes

$$\mathcal{M}_a + \mathcal{M}_b = \frac{\alpha_s(\mu) C_F}{2\pi}\left[\frac{1+x^2}{1-x} - \epsilon(1-x)\right]\Gamma(-\epsilon)\left(\frac{\mathbf{b}_T^2\mu^2}{4e^{-\gamma_E}}\right)^\epsilon. \quad (4.56)$$

The use of the $\overline{\text{MS}}$ scheme allowed to replace the bare coupling by renormalized coupling. In this scheme, the relation between the bare and renormalized coupling is

$$g_0 = Z_g \mu^\epsilon g(\mu)\left(\frac{e^{\gamma_E}}{4\pi}\right)^{\epsilon/2}, \quad \alpha_s(\mu) = \frac{g(\mu)^2}{4\pi}, \quad (4.57)$$

where $Z_q = 1 + \mathcal{O}(g^2)$ is the counterterm for the strong coupling. The presence of the factor $(e^{\gamma_E}/4\pi)^{\epsilon/2}$ indicates the use of the $\overline{\text{MS}}$ scheme. The expansion of Eq. (4.56) in $\epsilon \to 0$ leads to the desired bare result. However, there is an appearance of poles $1/\epsilon$ resulting from the regularization of the $k_T \to 0$ region in Eq. (4.55). In addition, there is a divergence in Eq. (4.56) in the limit all energy is transferred to the struck quark, $x \to 1$, which means that the emitted gluon would carry no energy, $k^+ \to 0$. This is the rapidity divergence and will only be canceled by the divergence, $k^\mu \to 0$, in the soft function. The proper inclusion of the soft function to cancel the rapidity divergence requires a regulator which can then be removed to obtain the finite result. The regulator that can be easily incorporated into Eq. (4.56) is the η regulator[1]

$$R_c(k,\tau) = \left|\frac{\sqrt{2}k^+}{\nu}\right|^{-\tau} = \left(\frac{(1-x)p^+}{\nu/\sqrt{2}}\right)^{-\tau}. \quad (4.58)$$

[1]The regularization is done using the η regulator, but it is denoted as τ. The factor of $\sqrt{2}$ is due to the use of different light-cone conventions.

This regulator allows to cancel divergence in Eq. (4.56) through the following identity

$$\frac{1+x^2}{1-x}(1-x)^{-\tau} = -\left(\frac{2}{\tau}+\frac{3}{2}\right)\delta(1-x)+\left[\frac{1+x^2}{1-x}\right]_+ +\mathcal{O}(\tau). \tag{4.59}$$

The application of Eq. (4.58) to Eq. (4.56), and the substitution of Eq. (4.59) lead to the following expression for the bare unsubtracted TMD PDF

$$\begin{aligned}\tilde{f}^{0(u)(1)}_{q/q}(x,\mathbf{b}_T,\epsilon,\tau) =& \frac{\alpha_s(\mu)C_F}{2\pi}\Bigg\{-\left(\frac{1}{\epsilon}+L_b\right)[P_{qq}(x)]_+ +(1-x)+\delta(1-x)\left(\frac{1}{\epsilon}+L_b\right)\\ &\times\left(\frac{3}{2}+\frac{2}{\tau}-2\ln\frac{xp^+}{\nu/\sqrt{2}}\right)+\mathcal{O}(\tau)+\mathcal{O}(\epsilon)\Bigg\},\end{aligned} \tag{4.60}$$

where

$$L_b = \ln\frac{\mathbf{b}_T^2\mu^2}{b_0^2}, \quad b_0 = 2e^{-\gamma_E}. \tag{4.61}$$

The exponent γ_E is the Euler's constant. The quark-quark one loop splitting function in Eq. (4.60) is expressed as

$$P_{qq}(x) = \frac{1+x^2}{1-x}. \tag{4.62}$$

The divergence as $x \to 0$ in Eq. (4.60) is regulated through $[P_{qq}(x)]_+$, and this causes the divergence to show up as a pole in $1/\tau$. In addition, there is a presence of a pole $1/\epsilon$ from the $k_T \to 0$ region of the integral in Eq. (4.55). The divergence which is proportional to $P_{qq}(x)$ in Eq. (4.60) is also present in the collinear PDF.

The diagrams for the one-loop calculation of the soft function are shown in Fig. (4.3) and previous methods of calculations for unsubtracted TMD PDF can be applied for evaluations of diagrams for the soft function. The matrix element for the soft function can be expressed

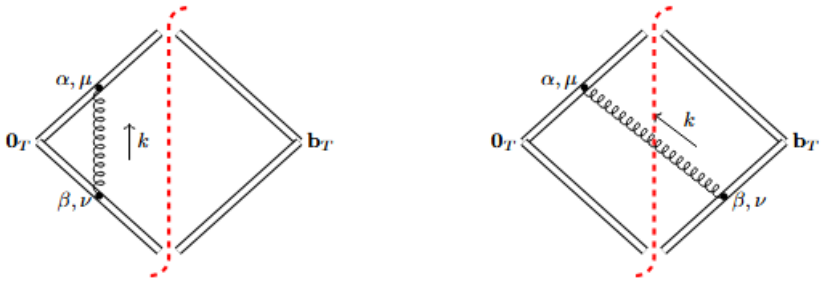

Figure 4.3: The diagrams for the one-loop contribution to the soft function $\tilde{\mathcal{S}}$. The double lines represent the Wilson lines and the dashed lines indicate the one-shell cut. Since the diagram (a) is scaleless, its contribution to $\tilde{\mathcal{S}}$ vanishes in dimensional regularization.

as

$$\begin{aligned}\mathcal{M}_S &= 2g_0^2 C_F \int \frac{d^dk}{(2\pi)^d} e^{i\mathbf{b}_T\cdot\mathbf{k}_T} \frac{-i}{(2k^+k^- - \mathbf{k}_T^2 + i0)} \frac{1}{(k^+ - i0)(-k^- + i0)} \\ &= 2g_0^2 C_F \int \frac{d^dk}{(2\pi)^d} e^{i\mathbf{b}_T\cdot\mathbf{k}_T} (2\pi)\delta_+(k^2) \frac{1}{k^+k^-} \\ &= \frac{g_0^2 C_F}{\pi} \int \frac{d^{2-2\epsilon}\mathbf{k}_T}{(2\pi)^{d-2}} \frac{e^{i\mathbf{b}_T\cdot\mathbf{k}_T}}{k_T^2} \int \frac{dk^-}{k^-}.\end{aligned} \tag{4.63}$$

Clearly, there are divergences in Eq. (4.63) when $k^- \to 0$ and $k^- \to \infty$. Since the rapidity is defined by, $y_k = (1/2)\ln(k_+/k_-)$, the limits $k^- \to 0$ or $k^+ \to \infty$ lead to $y_k \to \pm\infty$, in other words, the rapidity divergence. Using the methods used for the calculations of the unsubstrated TMD PDFs, the regulation of this rapidity divergence requires the following η regulator

$$R_s(k,\tau) = \left|\frac{k^+ - k^-}{\nu/\sqrt{2}}\right|^{-\tau} w^2(\tau,\nu), \tag{4.64}$$

where, $w(\tau,\nu)$ is the bookkeeping parameter of the rapidity divergence, and is related to a bare parameter by $w^0 = w(\tau,\nu)\nu^{\tau/2}$. Thus, the regulation with $R_s(k,\tau)$ leads to the following regulated integral

$$\int_0^\infty \frac{dk^-}{k^-} \to w^2\left(\frac{\nu}{\sqrt{2}}\right)^\tau \int_0^\infty \frac{dk^-}{k^-} \left|\frac{\mathbf{k}_\perp^2}{2k^-} - k^-\right|^{-\tau} = \frac{\nu^\tau k_\perp^{-\tau}}{2^\tau\sqrt{\pi}}\Gamma\left(\frac{1}{2} - \frac{\tau}{2}\right)\Gamma\left(\frac{1}{2}\right). \tag{4.65}$$

The substitution of Eq. (4.65) into Eq. (4.63) yields the following rapidity-regulated soft

function

$$\begin{aligned}\tilde{S}_q^{0(1)}(b_\perp,\epsilon,\tau) =& \frac{g_0^2 C_F}{\pi}\frac{\nu^\tau}{2^\tau\sqrt{\pi}}\Gamma\left(\frac{1}{2}-\frac{\tau}{2}\right)\Gamma\left(\frac{\tau}{2}\right)\int\frac{d^{2-2\epsilon}\mathbf{k}_\perp}{(2\pi)^{d-2}}\frac{e^{i\mathbf{b}_\perp\cdot\mathbf{k}_\perp}}{k_\perp^{2+\tau}}\\ =& \frac{g_0^2 C_F}{\pi}\frac{\nu^\tau}{2^\tau\sqrt{\pi}}\Gamma\left(\frac{1}{2}-\frac{\tau}{2}\right)\Gamma\left(\frac{\tau}{2}\right)\frac{\pi^\epsilon\Gamma(-\epsilon-\tau/2)}{4\pi 2^\tau\Gamma(1+\tau/2)}b_T^{2\epsilon+\tau},\end{aligned} \tag{4.66}$$

where the $\mathbf{k}_\perp$ integral is the same as the $\mathbf{k}_T$ integral of Eq. (4.55). After expanding in $\epsilon\to 0$ and $\tau\to 0$ and using Eq. (4.57) the bare rapidity-regulated soft function becomes

$$\tilde{S}_q^{0(1)}(b_\perp,\epsilon,\tau) = \frac{\alpha_s(\mu)C_F}{2\pi}\left[\frac{2}{\epsilon^2}+4\left(\frac{1}{\epsilon}+L_b\right)\left(-\frac{1}{\tau}+\ln\frac{\mu}{\nu}\right)-L_b^2-\frac{\pi^2}{6}\right]+\mathcal{O}(\tau)+\mathcal{O}(\epsilon). \tag{4.67}$$

Now, using the calculated unsubtracted TMD PDF and soft function the physical TMD PDF is

$$\tilde{f}_{i/H}(x,\mathbf{b}_T,\mu,\zeta) = \lim_{\substack{\epsilon\to 0\\ \tau\to 0}} Z^i_{uv}(\mu,\zeta,\epsilon)\tilde{f}^{0(u)}_{i/H}(x,\mathbf{b}_T,\epsilon,\tau,xP^+)\sqrt{\tilde{\mathcal{S}}^0(b_T,\epsilon,\tau)}. \tag{4.68}$$

The product of $\tilde{f}^{0(u)}_{q/q}\sqrt{\tilde{\mathcal{S}}^0}$ leads to the cancellation of poles in τ in Eq. (4.68) and the final bare result of the physical TMD PDF at the one-loop is

$$\begin{aligned}\tilde{f}^{0(1)}_{q/q}(x,\mathbf{b}_T,\epsilon,\zeta) =& \frac{\alpha_s(\mu)C_F}{2\pi}\left[-\left(\frac{1}{\epsilon}+L_b\right)[P_{qq}(x)]_+ + (1-x)\right]\\ &+\frac{\alpha_s C_F}{2\pi}\delta(1-x)\left[\frac{1}{\epsilon^2}-\frac{L_b^2}{2}+\left(\frac{1}{\epsilon}+b_b\right)\left(\frac{3}{2}+\ln\frac{\mu^2}{\zeta}\right)-\frac{\pi^2}{12}\right]+\mathcal{O}(\epsilon).\end{aligned} \tag{4.69}$$

There are an infrared (IR) $1/\epsilon$ pole and ultraviolet (UV) $1/\epsilon$ poles in the first and second lines of Eq. (4.69) respectively, these poles are removed by renormalization. The renormalized TMD PDF $f_{q/q}$ is obtained by canceling out all UV $1/\epsilon$ poles with the counterterm Z^q_{UV} which is defined in $\overline{\text{MS}}$ as follows

$$Z^q_{UV}(\mu,\zeta,\epsilon) = 1-\frac{\alpha_s(\mu)C_F}{2\pi}\left[\frac{1}{\epsilon^2}+\frac{1}{\epsilon}\left(\frac{3}{2}+\ln\frac{\mu^2}{\zeta}\right)\right]+\mathcal{O}(\alpha_s^2). \tag{4.70}$$

The substitution of Eq. (4.70) and other expressions into Eq. (4.37) lead to the quark-to-

quark contribution to the renormalized TMD PDF at one-loop as follows

$$\tilde{f}^{(1)}_{q/q}(x,\mathbf{b}_T,\mu,\zeta) = \frac{\alpha_s(\mu)C_F}{2\pi} \times\left[-\left(\frac{1}{\epsilon}+L_b\right)[P_{qq}(x)]_+ + (1-x) - \frac{L_b^2}{2} + L_b\left(\frac{3}{2}+\ln\frac{\mu^2}{\zeta}\right) - \frac{\pi^2}{12}\right]. \tag{4.71}$$

The remaining $1/\epsilon$ pole is just the IR pole. This collinear divergence is also present for the PDF and serves for matching the TMD PDF onto the PDF for perturbative b_T. There is no dependence of the chosen rapidity regulator in the results of Eqs. (4.69) and (4.71).

4.6 TMD fragmentation functions

This section provides a short introduction to the TMD fragmentation functions (FFs) which describe the final-state nonperturbative process of a quark that is produced in hard interaction and then fragments into a detected hadron. To better introduce TMD FFs and compare with with TMD PDFs, one may start with DY process. The factorization theorem in the DY process, $p(P_A) + p(P_B) \to \ell^+(l) + \ell^-(l') + X$, is appropriate when measuring $q = l + l'$ of $\ell^+\ell^-$ final state at small q_T, thus the cross section can be expressed as

$$\frac{d\sigma^W}{dQdY\,d^2\mathbf{q}_\perp} \sim \int d^2\mathbf{b}_T e^{i\mathbf{b}_T\cdot\mathbf{q}_T}\tilde{f}_{i/p}(x_a,\mathbf{b}_T,\mu,\zeta_a)\tilde{f}_{\bar{i}/p}(x_b,\mathbf{b}_T,\mu,\zeta_b), \tag{4.72}$$

where $\tilde{f}_{i/p}$ denotes the TMD PDF that characterizes the process of extracting a parton of flavor i from the hadron p at low transverse momentum. The SIDIS process, $e^-(l) + p(P) \to e^-(l') + h(P_h) + X$, can be obtained from the DY process by exchanging the incoming hadron with outgoing hadron, thus $q = l - l'$. For a small transverse momentum $P_{h\perp}$ of the produced hadron, the factorization is appropriate, thus the cross section can be expressed as

$$\frac{d\sigma^W}{dxdydz_h d^2\mathbf{P}_{hT}} \sim \int d^2\mathbf{b}_T e^{i\mathbf{b}_T\cdot\mathbf{P}_{hT}/z_h}\tilde{f}_{i/p}(x,\mathbf{b}_T,\mu,\zeta_a)\tilde{D}_{h/i}(z_h,\mathbf{b}_T,\mu,\zeta_b). \tag{4.73}$$

The TMD PDF $\tilde{f}_{i/p}$ in Eq. (4.73) is similar to that in the DY process as it plays the identical role of extracting a parton from a hadron, however the second TMD PDF was replaced by the TMD FF $\tilde{D}_{h/i}$ which describes the fragmentation of the parton of flavor i into the hadron h that carries a longitudinal momentum fraction z_h.

The bare unsubtracted TMD FF for a parton of flavor i inside a hadron h is expressed as

$$\tilde{\Delta}^{0(u)}_{h/i}(z_h, \mathbf{b}_T, \epsilon, \tau, P^+/z_h) = \frac{1}{4N_c z_h}\mathrm{Tr}\int \frac{\mathrm{db}^-}{2\pi}\sum_X \mathrm{e}^{\mathrm{ib}^-(\mathrm{P}^+/\mathrm{z_h})}\gamma^+_{\alpha\alpha'} \times \left\langle 0\middle|[(W_{\lrcorner}\psi^{0\alpha}_i)(b)]_\tau\middle|h(P), X\right\rangle\left\langle h(P), X\middle|[(\bar{\psi}^{0\alpha'}_i W_{\urcorner})(0)]_\tau\middle|0\right\rangle, \tag{4.74}$$

where P denotes the hadron momentum, $b^\mu = (0, b^-, \mathbf{b}_T)$, and τ is a rapidity regulator. The quantity, $1/N_c z_h$, is the normalization factor where N_c is the number of colors. The Wilson lines $W_{\lrcorner}$ and $W_{\urcorner}$ each represent half of the Wilson line $W_{\sqsupset}$. The trace runs over color and spin indices α, α'. The hadron state is just an out-state in the matrix element as indicated in Eq. (4.74). Since P in Eq. (4.74) has no transverse component, the TMD FF in the momentum space is defined with respect to the transverse momentum $\mathbf{p}'_T$ of the quark field ψ as

$$\tilde{\Delta}^{0(u)}_{h/i}(z_h, \mathbf{b}_T, \epsilon, \tau, P^+/z_h) = \int d^2\mathbf{p}'_T e^{i\mathbf{p}'_T\cdot\mathbf{b}_T}\Delta^{0(u)}_{h/i}(z_h, -z_h\mathbf{p}'_T, \epsilon, \tau, P^+/z_h). \tag{4.75}$$

Finally, the TMD FF can be expressed in terms of Eq. (4.75) by incorporating the soft function and the UV renormalization factor as follows

$$\tilde{\Delta}_{h/i}(z, \mathbf{b}_T, \mu, \zeta) = \lim_{\substack{\epsilon\to 0\\ \tau\to 0}} Z^i_{uv}(\mu, \zeta, \epsilon)\frac{\tilde{\Delta}^{0(u)}_{h/i}(z, \mathbf{b}_\perp, \epsilon, \tau, P^+/z)}{\tilde{S}^{0(s)}(\mathbf{b}_T, \epsilon, \tau)}\sqrt{\tilde{S}^0(\mathbf{b}_T, \epsilon, \tau)}, \tag{4.76}$$

where ζ depends on the rapidity cutoff parameter $\tilde{\eta}$. Hence, the Fourier transform of Eq. (4.76) can yield the TMD FF in the momentum space.

Chapter 5

TMD Evolution

5.1 Importance of resummation

The renormalization group equation (RGE) of a function $\mathcal{G}(q,\mu)$ which contains $\ln(q/\mu)$ can be expressed as

$$\mu\frac{d\mathcal{G}(q,\mu)}{d\mu} = -\alpha_s\mathcal{G}(q,\mu), \tag{5.1}$$

where the anomalous dimension $\gamma_{\mathcal{G}}$ is replaced by $-\alpha_s$. Assuming that the μ dependence of α_s is negligible, then the solution to the RGE equation is

$$\mathcal{G}(q,\mu) = \mathcal{G}(q,\mu_0)\tilde{\mathcal{G}}(\mu_0,\mu),\ \tilde{\mathcal{G}}(\mu_0,\mu) = \exp\left(\alpha_s\ln\left(\mu_0/\mu\right)\right), \tag{5.2}$$

where μ_0 is an arbitrary reference scale and $\tilde{\mathcal{G}}(\mu_0,\mu)$ is the evolution kernel with $\tilde{\mathcal{G}}(\mu_0,\mu_0) = 1$. The boundary condition is defined by $\mathcal{G}$ at the reference scale μ_0, namely, $\mathcal{G}(q,\mu_0)$. The exponential in $\tilde{\mathcal{G}}(\mu_0,\mu)$ allows the resummation of the logarithms $\ln(\mu_0/\mu)$. In perturbation theory, if q is a scalar quantity then the boundary term $\mathcal{G}(q,\mu_0)$ can have a logarithmic structure

$$\mathcal{G}(q,\mu_0) = 1 + \alpha_s\ln\frac{q}{\mu_0} + \frac{1}{2}\alpha_s^2\ln^2\frac{q}{\mu_0} + \cdots. \tag{5.3}$$

The choice on the reference scale, $\mu_0 = q$, eliminates all large logarithms in the boundary function $\mathcal{G}$. Thus under this particular choice, the boundary function $\mathcal{G}$ becomes finite, $\mathcal{G}(q, \mu_0 = q) = 1 + \cdots$, then the function $\mathcal{G}(q, \mu)$ can be expressed as

$$\begin{aligned}\mathcal{G}(q,\mu) =& (1+\cdots)\tilde{\mathcal{G}}(\mu_0 = q, \mu) \\ =& 1 + \alpha_s \ln\frac{q}{\mu_0} + \frac{1}{2}\alpha_s^2 \ln^2\frac{q}{\mu_0} + \cdots,\end{aligned} \tag{5.4}$$

in this particular choice, the evolution kernel $\tilde{\mathcal{G}}$ is capable of predicting and resumming all large logarithms in $\mathcal{G}(q, \mu)$ to all orders in α_s. However, this depends on the nature of the boundary term $\mathcal{G}(q, \mu_0)$ and is usually possible whenever $\mathcal{G}(q, \mu_0)$ is a regular function.

5.2 Resummation through RG evolution

The resummation through RG evolution incorporates naturally a classification of the order of accuracy

$$\begin{aligned}\mu\frac{d\mathcal{G}(q,\mu)}{d\mu} =& \gamma_{\mathcal{G}}(q,\mu)\mathcal{G}(q,\mu), \\ \gamma_{\mathcal{G}}(q,\mu) =& -2\Gamma_{\text{cusp}}(\alpha_s(\mu))\ln\frac{q}{\mu} - \gamma_{\mathcal{G}}(\alpha_s(\mu)),\end{aligned} \tag{5.5}$$

where $\Gamma_{\text{cusp}}(\alpha_s)$, and $\gamma_{\mathcal{G}}(\alpha_s)$ are cusp and non-cusp anomalous dimensions respectively. For $\mu_0 = q$, the solution to Eq. (5.5) is expressed as

$$\begin{aligned}\mathcal{G}(q,\mu) =& \mathcal{G}(q,q)\exp\left(\int_q^\mu \frac{d\mu'}{\mu'}\gamma_{\mathcal{G}}(k,\mu')\right) \\ =& \mathcal{G}(q,q)\exp\left(-2\int_q^\mu \frac{d\mu'}{\mu'}\Gamma_{\text{cusp}}(\alpha_s(\mu'))\ln\frac{q}{\mu'} - \int_q^\mu \frac{d\mu'}{\mu'}\ln(\alpha_s(\mu'))\right) \\ =& \mathcal{G}(q,q)\exp\left(\Gamma_{\text{cusp}}(\alpha_s(\mu))\ln^2\frac{q}{\mu} + \gamma_{\mathcal{G}}(\alpha_s(\mu))\ln\frac{q}{\mu} + \cdots\right),\end{aligned} \tag{5.6}$$

where (...) stands for higher-order expansion terms in α_s. In certain situations, for instance $L = \ln(q/\mu) \sim 1/\alpha_s$, the perturbative expansion in α_s of the exponential factor in $\mathcal{G}(q, \mu)$ becomes divergent. Then the resummation method plays an important role to resum the

large logarithms. For the case of $L = \ln(q/\mu) \sim 1/\alpha_s$, the expansion of $\mathcal{G}(q,\mu)$ can be expressed in the single-logarithmic resummation scheme as

$$\begin{aligned}\mathcal{G}(q,\mu) = \mathcal{G}(q,q)\exp\Bigg\{&\Gamma_0\left(\frac{\alpha_s}{4\pi}\right)L^2 - \frac{2}{3}\Gamma_0\beta_0\left(\frac{\alpha_s}{4\pi}\right)^2 L^3 + \mathcal{O}(\alpha_s^n L^{n+1}) \\ &+ \Gamma_1\left(\frac{\alpha_s}{4\pi}\right)^2 L^2 + \gamma_0\frac{\alpha_s}{4\pi}L - \frac{2}{3}\Gamma_0\beta_1\left(\frac{\alpha_s}{4\pi}\right)^3 L^3 + \mathcal{O}(\alpha_s^n L^n) \\ &+ \Gamma_2\left(\frac{\alpha_s}{4\pi}\right)^3 L^2 + \gamma_1\left(\frac{\alpha_s}{4\pi}\right)^2 L - \frac{2}{3}\Gamma_0\beta_2\left(\frac{\alpha_s}{4\pi}\right)^4 L^3 + \mathcal{O}(\alpha_s^n L^{n-1})\Bigg\},\end{aligned} \tag{5.7}$$

where β_n are the coefficients of the *beta* function. Each line in Eq. (5.7) corresponds to a particular order in α_s. Using the scaling parameter $L \sim 1/\alpha_s$, it is obvious that the first line corresponds to α_s^{-1} , the second line corresponds to α_s^0, and the third line corresponds to α_s^1.

The expansion up to $\mathcal{O}(\alpha_s^n L^{n+1})$ corresponds to a leading-logarithmic (LL) accuracy, the expansion up to $\mathcal{O}(\alpha_s^n L^n)$ corresponds to a next-to-leading logarithmic (NLL) accuracy, and the expansion up to $\mathcal{O}(\alpha_s^n L^{n-1})$ corresponds to a next-to-next-to-leading logarithmic (NNLL) accuracy. In addition, the boundary term $\mathcal{G}(q,q)$ that possesses an expansion in terms of α_s, can be consistently incorporated in the expansion.

The QCD factorization requires two scales q and Q and is only relevant up to power corrections $\mathcal{O}(q/Q)$ where q is the resolution scale and Q is the hard scale of the collision. However, if $q \sim Q$ the singular logarithms $\ln(q/Q)$ are small, thus the resummation is not necessary and should be turned off for better results. To prove that one can start with the cross section as follows

$$\begin{aligned}\frac{d\sigma}{dq} \sim& 1 + \alpha_s \ln\frac{q/Q}{1+q/Q} + \cdots \\ =& 1 + \alpha_s \ln\frac{Q}{q} - \alpha_s \underbrace{\ln\left(1+\frac{Q}{q}\right)}_{=\mathcal{O}(q/Q)} + \cdots,\end{aligned} \tag{5.8}$$

where $(\cdots)$ stands for additional terms. The logarithms $\ln(q/Q)$ can be resummed at all orders in α_s and the logarithm $\ln(1+q/Q)$ is only included as fixed order. Both logarithmic terms are of similar magnitude if $q \sim Q$, and for $q/Q \gg 1$, there is a cancellation among

these two logarithmic terms and with the naive resummation, the cross section of Eq. (5.8) is expressed as

$$\begin{aligned}\frac{d\sigma}{dq} \sim & \exp\left(\alpha_s \ln\frac{Q}{q}\right) - \alpha_s \ln\left(1+\frac{Q}{q}\right) + \cdots \\ = & 1 + \alpha_s \ln\frac{q/Q}{1+q/Q} + \frac{1}{2}\alpha_s^2 \ln^2\frac{Q}{q} + \cdots.\end{aligned} \tag{5.9}$$

However, there is a cancellation only at $\mathcal{O}(\alpha_s)$ and hence the resummation should be turned off at this order of expansion to avoid the inclusion of unnecessary high-order terms. To achieve that, the reference scale μ_0 can be chosen as $\mu_0(q)$ so that the expression for the cross section becomes

$$\begin{aligned}\frac{d\sigma}{dq} \sim & \exp\left(\alpha_s \ln\frac{Q}{\mu_0(q)}\right) - \alpha_s \ln\left(1+\frac{Q}{q}\right) + \cdots \\ = & 1 + \alpha_s \ln\frac{\mu_0(q)/Q}{1+q/Q} + \frac{1}{2}\alpha_s^2 \ln^2\frac{Q}{\mu_0(q)} + \cdots.\end{aligned} \tag{5.10}$$

The scale $\mu_0(q)$ should satisfy the following relations

$$\begin{aligned}\mu_0(q) &\sim q, \quad q \ll Q, \\ \mu_0(q) &\sim Q, \quad q \geq Q.\end{aligned} \tag{5.11}$$

This method allows the resummation of all logarithms in the limit, $q \ll Q$, but the resummation is turned off at $q \sim Q$ to avoid the inclusion of unnecessary terms, in order words, the $\mathcal{O}(\alpha^2)$ terms.

5.3 TMD evolution equations

This section provides on overview of the derivation of the TMD evolution equations for the rapidity and renormalization scales, ζ and μ, respectively. In the CSS scheme [38, 55, 41], the evolution equations for the TMD PDFs of flavor q are expressed as

$$\frac{\partial \ln \tilde{f}_{i/p}(x, \mathbf{b}_T, \mu, \zeta)}{\partial \ln \sqrt{\zeta}} = \tilde{K}(b_T, \mu), \tag{5.12}$$

$$\frac{d \ln \tilde{f}_{i/p}(x, \mathbf{b}_T, \mu, \zeta)}{d \ln \mu} = \gamma_q(\alpha_s(\mu), \zeta/\mu^2), \tag{5.13}$$

$$\frac{d\tilde{K}(b_T, \mu)}{d \ln \mu} = -\gamma_K(\alpha_s(\mu)), \tag{5.14}$$

where $\tilde{K}$ is the Collins-Soper (CS) kernel, and γ_q and γ_K are anomalous dimensions. The first equation is the rapidity evolution equation for the Collins-Soper scale ζ originating from regulating rapidity divergences. The last two equations are the usual RG evolution equations for the renormalization scale μ originating from the UV renormalization. Using the evolution equations, the relation between the anomalous dimensions γ_q and γ_K can be expressed as

$$\frac{\partial \gamma_q(\alpha_s(\mu), \zeta/\mu^2)}{\partial \ln(\sqrt{\zeta})} = -\gamma_K(\alpha_s(\mu)). \tag{5.15}$$

The direct integration of Eq. (5.15) with respect to ζ ,where $\zeta_0 \sim \mu^2$, yields the following expression solution

$$\gamma_q(\alpha_s(\mu), \zeta/\mu^2) = -\frac{1}{2}\gamma_K(\alpha_s(\mu)) \ln \frac{\zeta}{\mu^2} + \gamma_q(\alpha_s(\mu), 1), \tag{5.16}$$

where γ_K is the anomalous dimension in the differential equation of the SC kernel. Furthermore, the expression of the Collins-Soper kernel, $\tilde{K}$, can be obtained by the integration of Eq. (5.14) with respect to μ as follows

$$\tilde{K}(b_T, \mu) = -\int_{1/\bar{b}_T}^{\mu} \frac{d\mu'}{\mu'} \gamma_K(\alpha_s(\mu')) + \tilde{K}(b_T, 1/\bar{b}_T), \tag{5.17}$$

where $\bar{b}_T = b_T/b_0$, $b_0 = 2e^{-\gamma_E}$. The first term directly depends on the SC equation, but the remaining term arises due to the boundary condition, therefore such term cannot be

predicted by the SC evolution equation. The solutions of the TMD evolution equations for TMD PDFs can generically expressed as

$$\tilde{f}_{i/p}(x, \mathbf{b}_T, \mu, \zeta) = \tilde{f}_{i/p}(x, \mathbf{b}_T, \mu_0, \zeta_0) U_{\mathrm{RG}}(\mu_0, \mu, \zeta_0) V_{\mathrm{RRG}}(\zeta_0, \zeta, \mathbf{b}_T, \mu), \tag{5.18}$$

where U_{RG} is the contribution of the evolution from a scale μ_0 to another scale μ, and V_{RRG} is the contribution of the evolution from a rapidity scale ζ_0 to another scale ζ. Since U_{RG} is the solution obtained by integrating Eq. (5.13) over the renormalization scale μ', and V_{RRG} is the solution obtained by integrating Eq. (5.12) over the rapidity scale ζ', then the evolved TMD PDFs can be expressed as follows

$$\begin{aligned}\tilde{f}_{i/p}(x, \mathbf{b}_T, \mu, \zeta) &= \tilde{f}_{i/p}(x, \mathbf{b}_T, \mu_0, \zeta_0) \\ &\times \exp\left\{ \int_{\mu_0}^{\mu} \frac{d\mu'}{\mu'} \gamma_q(\alpha_s(\mu'), \zeta_0/\mu'^2) \right\} \exp\left\{ \tilde{K}(b_T, \mu) \ln \sqrt{\frac{\zeta}{\zeta_0}} \right\},\end{aligned} \tag{5.19}$$

where γ_q controls the RG evolution between μ_0 and μ scales, and $\tilde{K}$ controls the rapidity evolution between ζ_0 and ζ scales. Since the full description of the TMD PDFs requires the Fourier integration over $\mathbf{b}_T$ to involve all values of b_T, which demands the consideration of both perturbative and non-perturbative domains of b_T, and the existence of large logarithms from higher order terms in the fixed order perturbation expansion of the CS kernel $\tilde{K}(b_T, \mu)$, then the standard perturbation approach is not applicable. To deal with this issue, the CSS formalism utilizes the b_*-prescription function to connect smoothly both perturbative and non-perturbative domains.

$$\mathbf{b}_* = \mathbf{b}_*(\mathbf{b}_T) = \frac{\mathbf{b}_T}{\sqrt{1 + b_T^2/b_{MAX}^2}}, \tag{5.20}$$

where b_{MAX} is the cutoff. The prescription clearly shows that for large b_T, the value of b_* is b_{MAX}. The value of b_{MAX} is chosen to be ~ 1 GeV^{-1}. The implementation of the b_*

prescription allows to express the evolved TMD PDFs as follows

$$\tilde{f}_{i/p}(x,\mathbf{b}_T,\mu,\zeta) = \tilde{f}_{i/p}(x,\mathbf{b}_*,\mu,\zeta)\frac{\tilde{f}_{i/p}(x,\mathbf{b}_T,\mu,\zeta)}{\tilde{f}_{i/p}(x,\mathbf{b}_*,\mu,\zeta)}. \tag{5.21}$$

For large $\mathbf{b}_T$ the mismatch between $\tilde{f}_{i/p}(x,\mathbf{b}_T,\mu,\zeta)$ and $\tilde{f}_{i/p}(x,\mathbf{b}_*,\mu,\zeta)$ can be expressed in terms of functions $g_{j/p}(x,b_T,b_M)$ and $g_k(b_T,b_M)$ as follows

$$\begin{aligned}\frac{\tilde{f}_{i/p}(x,\mathbf{b}_T,\mu,\zeta)}{\tilde{f}_{i/p}(x,\mathbf{b}_*,\mu,\zeta)} &= \frac{\tilde{f}_{i/p}(x,\mathbf{b}_T,\mu_0,\zeta_0')}{\tilde{f}_{i/p}(x,\mathbf{b}_*,\mu_0,\zeta_0')}\exp\left\{\ln\sqrt{\frac{\zeta}{\zeta_0'}}\left(\tilde{K}(b_T,\mu)-\tilde{K}(b_*,\mu)\right)\right\}\\ &= \exp\left\{-g_{i/p}(x,b_T)\right\}\exp\left\{-\ln\sqrt{\frac{\zeta}{\zeta_0'}}g_k(b_T,b_{MAX})\right\}.\end{aligned} \tag{5.22}$$

Here, the quantities $g_{j/p}(x,b_T,b_{MAX})$ and $g_k(b_T,b_{MAX})$ are the nonperturbative universal functions which do not depend on scales. The nonperturbative part of the Collins-Soper kernel $g_k(b_T,b_{MAX})$ is defined as

$$g_k(b_T,b_{MAX}) = \tilde{K}(b_*,\mu_0) - \tilde{K}(b_T,\mu_0). \tag{5.23}$$

And the function $g_{i/p}(x,b_T)$ is related to the intrinsic transverse momentum distribution. The functions, $g_{j/p}(x,b_T,b_{MAX})$ and $g_k(b_T,b_{MAX})$ are independent of ζ and μ scales and they tend to vanish in the limit, $b_T \to 0$. The substitution of Eq. (5.22) and Eq. (5.23) into Eq. (5.19) allows the evolved TMD PDF can be written as

$$\begin{aligned}\tilde{f}_{i/p}(x,\mathbf{b}_T,\mu,\zeta) =& \tilde{f}_{i/p}(x,\mathbf{b}_*,\mu_0,\zeta_0)\\ &\times\exp\left[\ln\sqrt{\frac{\zeta}{\zeta_0}}\tilde{K}(b_*,\mu_0)+\int_{\mu_0}^{\mu}\frac{d\mu'}{\mu'}\left(\gamma_q(\alpha_s(\mu'),1)-\ln\frac{\sqrt{\zeta}}{\mu'}\gamma_K(\alpha_s(\mu'))\right)\right]\\ &\times\exp\left[-g_{i/p}(x,b_T)-\ln\left(\sqrt{\frac{\zeta}{\zeta_0'}}g_k(b_T,b_{MAX})\right)\right].\end{aligned} \tag{5.24}$$

Perturbative calculations of $\tilde{K}$ and $\tilde{f}$ require the application of the respective RG and RRG transformations, $\mu_0 \to 1/b_*$, $\zeta_0 \to 1/b_*^2$, thus Eq. (5.27) can be expressed as

$$\begin{aligned}\tilde{f}_{i/p}(x, \mathbf{b}_T, \mu, \zeta) =& \tilde{f}_{i/p}(x, \mathbf{b}_*, \mu_{b_*}, \mu_{b_*}^2) \\ &\times \exp\left[\ln \sqrt{\frac{\zeta}{\mu_{b_*}^2}} \tilde{K}(b_*, \mu_{b_*}) + \int_{\mu_{b_*}}^{\mu} \frac{d\mu'}{\mu'} \left(\gamma_q(\alpha_s(\mu'), 1) - \ln \frac{\sqrt{\zeta}}{\mu'} \gamma_K(\alpha_s(\mu')) \right) \right] \\ &\times \exp\left[- g_{i/p}(x, b_T) - \ln\left(\sqrt{\frac{\zeta}{\zeta_0'}} g_k(b_T, b_{MAX}) \right) \right],\end{aligned} \tag{5.25}$$

where $\mu_{b*} = C_1/b_*$ is the hard scale which is usually utilized to perform perturbative calculations of b_*-dependent quantities, and C_1 is a constant whose value is selected to avoid large logarithms in perturbative methods [41, 56]. For small $\mathbf{b}_T$, the TMD PDFs can be expressed in terms of collinear PDFs using operator product expansion (OPE) as follows

$$\tilde{f}_{i/p}(x, \mathbf{b}_*, \mu_{b_*}, \mu_{b_*}^2) = \sum_j \int_x^1 \frac{d\hat{x}}{\hat{x}} \tilde{C}_{i/j}\left(\frac{x}{\hat{x}}, b_T, \mu_{b_*}, \mu_{b_*}^2, \alpha_s(\mu_{b_*}) \right) f_{j/p}(\hat{x}, \mu_{b_*}) + \mathcal{O}((m b_*(b_T))^p), \tag{5.26}$$

where the sum is taken over all flavors $j = q, g$. The substitution of Eq. (5.26) into Eq. (5.27) leads to the following expression for the evolved TMD PDF

$$\begin{aligned}\tilde{f}_{i/p}(x, \mathbf{b}_T, \mu, \zeta) =& \sum_j \int_x^1 \frac{d\hat{x}}{\hat{x}} \tilde{C}_{ij}\left(\frac{x}{\hat{x}}, b_T, \mu_{b_*}, \mu_{b_*}^2, \alpha_s(\mu_{b_*}) \right) f_{j/p}(\hat{x}, \mu_{b_*}) \\ &\times \exp\left[\ln \sqrt{\frac{\zeta}{\mu_{b_*}^2}} \tilde{K}(b_*, \mu_{b_*}) + \int_{\mu_{b_*}}^{\mu} \frac{d\mu'}{\mu'} \left(\gamma_q(\alpha_s(\mu'), 1) - \ln \frac{\sqrt{\zeta}}{\mu'} \gamma_K(\alpha_s(\mu')) \right) \right] \\ &\times \exp\left[- g_{i/p}(x, b_T) - \ln\left(\sqrt{\frac{\zeta}{\zeta_0'}} \right) g_k(b_T, b_{MAX}) \right],\end{aligned} \tag{5.27}$$

where μ_{b_*} is the renormalization scale for the collinear PDF $f_{j/p}$. In the CS scheme, the rapidity divergence is regulated by tilting a space-like gauge link away from the light-cone. A similar method of tilting is used in the Ji-Ma-Yuan (JMY) scheme, where a time-like gauge link is tilted away from the light-front direction to regulate the rapidity divergence.

The off-light-front direction ν of the gauge link introduces a rapidity regulator $\zeta^2 = (\nu.P)/\nu^2$.

5.4 Evolution in Soft Collinear Effective Theory

This section provides the TMD PDF evolution equations which are obtained in terms of RG evolution and rapidity RG evolution equations of beam and soft functions for collinear and soft modes in the context of SCET. Without loss of generality, we will consider in this section the DY process.

5.4.1 Evolution equations in SCET

The differential cross section in terms of beam function and soft function for the DY process can be expressed as

$$\frac{d\sigma^W}{dQdYd^2\mathbf{q}_T} = H(Q,\mu)\int d^2\mathbf{b}_T e^{i\mathbf{b}_T\cdot\mathbf{q}_T}\tilde{B}(x_a,\mathbf{b}_T,\mu,\zeta_a/\nu^2)\tilde{B}(x_b,\mathbf{b}_T,\mu,\zeta_b/\nu^2)\tilde{S}(b_T,\mu,\nu), \tag{5.28}$$

where H is the hard function, $\tilde{B}$ is the beam function, and $\tilde{S}$ is the soft function. Anomalous dimension for μ and ν evolution equations which are associated with the beam and soft functions are expressed as

$$\begin{aligned}
\gamma^B_\mu(\mu,\zeta/\nu^2) &= -(\tilde{Z}_B)^{-1}\mu\frac{d}{d\mu}\tilde{Z}_B(\mathbf{b}_T,\mu,\nu,xP), \qquad & \gamma^S_\mu(\mu,\mu/\nu) &= -(\tilde{Z}_S)^{-1}\mu\frac{q}{d\mu}\tilde{Z}_S(b_T,\mu,\nu),\\
\gamma^B_v(b_T,\mu) &= -(\tilde{Z}_B)^{-1}\nu\frac{d}{d\nu}\tilde{Z}_B(\mathbf{b}_T,\mu,\nu,xP), \qquad & \gamma^S_\nu(b_T,\mu) &= -(\tilde{Z}_S)^{-1}\nu\frac{d}{d\nu}\tilde{Z}_S(b_T,\mu,\nu),
\end{aligned} \tag{5.29}$$

where $\tilde{Z}_B$, and $\tilde{Z}_S$ are the counter-terms for the beam function and soft function respectively. The expression xP is either equal to $x_aP^+_a$ or $x_bP^-_b$ depending on whether the beam function depends on x_a or x_b. Since the hard function H does not depend on ν, the only one anomalous

evolution equation is for the scale μ

$$\gamma_\mu^H = -(Z_H)^{-1}\mu\frac{d}{d\mu}Z^H(Q,\mu), \tag{5.30}$$

where Z^H is the hard function counter-term. The RG and rapidity RG evolution equations for the beam and soft functions are expressed as

$$\mu\frac{d}{d\mu}\hat{B} = \gamma_\mu^{\hat{B}}(\mu,\zeta/\nu^2)\hat{B}, \qquad \nu\frac{d}{d\nu}\hat{B} = \gamma_\nu^{\hat{B}}(b_T,\mu)\hat{B}, \tag{5.31}$$

$$\mu\frac{d}{d\mu}\hat{S} = \gamma_\mu^{\hat{S}}(\mu,\mu/\nu)\hat{S}, \qquad \nu\frac{d}{d\nu}\hat{S} = \gamma_\nu^{\hat{S}}(b_T,\mu)\hat{S}, \tag{5.32}$$

where $\hat{B} \equiv \tilde{B}(x,\mathbf{b}_T,\mu,\zeta/\nu^2)$, and $\hat{S} \equiv \tilde{S}(b_T,\mu,\nu)$. And the RG evolution equation for the hard function H is expressed as

$$\mu\frac{d}{d\mu}H(Q,\mu) = \gamma_\mu^H(Q,\mu)H(Q,\mu), \tag{5.33}$$

Since the DY cross section is an observable, there is no dependence on the RG and rapidity RG scales μ,ν, hence such independence yields additional equations for anomalous dimensions

$$\begin{aligned} 0 &= \gamma_\mu^H(Q,\mu) + \gamma_\mu^S(\mu,\mu/\nu) + \gamma_\mu^B(\mu,\zeta_a/\nu^2) + \gamma_\mu^B(\mu,\zeta_b/\nu^2), \\ 0 &= \gamma_\nu^S(b_T,\mu) + 2\gamma_\nu^B(b_T,\mu). \end{aligned} \tag{5.34}$$

An additional significant equation arises due to the commuting properties between μ and ν derivatives, and can be expressed as

$$\mu\frac{d}{d\mu}\gamma_\nu = \nu\frac{d}{d\nu}\gamma_\mu^B = 2\Gamma_{\text{cusp}}^{(g,q)}. \tag{5.35}$$

The above equation establishes a strong restriction on the beam and soft anomalous dimensions, ensuring the equivalence between RG evolutions along two different paths. Thus, the

RG evolution becomes path-independent.

5.4.2 Solutions to evolution equations

The RG and RRG solutions are obtained by solving RG and RRG evolutions equations respectively. The solutions to RG and RRG evolution equations for the beam function B and the soft function S are expressed as

$$B = \mathcal{B}_H \mathcal{U}_B(\mu_L, \mu, \nu)\bar{\mathcal{U}}_B(\nu_H, \nu, \mu_L), \quad S = \mathcal{S}_L \mathcal{U}_S(\mu_L, \mu, \nu)\bar{\mathcal{U}}_S(\nu_L, \nu, \mu_L) \tag{5.36}$$

where $\mathcal{B}_H \equiv \tilde{B}(x, \mathbf{b}_T, \mu_L, \zeta/\nu_H^2)$ and $\mathcal{S}_L \equiv \tilde{S}(b_T, \mu_L, \nu_L)$. The functions B and S are derived from their natural scales, where the fixed-order logarithms in their expansions remain relatively small. The corresponding RG evolution kernels are defined by

$$\mathcal{U}_B(\mu_L, \mu, \nu) = \exp\left[\int_{\mu_L}^{\mu} \frac{d\mu'}{\mu'}\gamma_\mu^B(\mu', \not{B})\right], \quad \mathcal{U}_S(\mu_L, \mu, \nu) = \exp\left[\int_{\mu_L}^{\mu} \frac{d\mu'}{\mu'}\gamma_\mu^S(\mu', \not{S})\right], \tag{5.37}$$

where $\not{B} = \zeta/\nu^2$ and $\not{S} = \mu'/\nu$. The corresponding RRG evolution kernels are defined by

$$\bar{\mathcal{U}}_B(\nu_H, \nu, \mu) = \exp\left[\int_{\nu_H}^{\nu} \frac{d\nu'}{\nu'}\gamma_\nu^B(b_T, \mu)\right], \qquad \bar{\mathcal{U}}_S(\nu_L, \nu, \mu) = \exp\left[\int_{\nu_L}^{\nu} \frac{d\nu'}{\nu'}\gamma_\nu^S(b_T, \mu)\right]. \tag{5.38}$$

The natural scales of the function B are μ_L, ν_H, and the natural scales for the function S are μ_L, ν_L. While the beam and soft functions undergo both RG and RRG evolutions, the hard function undergoes RG evolution only.

Chapter 6

Simultaneous Extraction of Sivers function in TMD physics

6.1 Introduction

This chapter is partially based on the paper titled 'Simultaneous global analysis of the Sivers Asymmetry in SIDIS, Drell-Yan, and Jet Production', in preparation to submit to JHEP, authored by Zhong-Bo Kang, John Terry, and Fidele J. Twagirayezu.

Transverse momentum-dependent distribution functions (TMDs) are crucial ingredients for understanding the three-dimensional partonic structure of nucleons in momentum space. TMDs provide non-perturbative information, and thus they are obtained either through lattice calculations [57, 58] or by global fit of the spin asymmetry data within the framework of TMD factorization theorems [41, 59, 38, 45, 60, 61, 62]. Due to the intense ongoing effort to understand the partonic structure of matter, significant effort has been dedicated to extracting TMDs to enhance our understanding of the internal structure of nucleons [63, 64, 57, 65, 49, 41]. The correlation between the partonic transverse momentum and the nucleon's transverse spin is governed by the Sivers function [66, 67], which plays a key role in probing the contributions of quark and gluon orbital angular momentum (OAM) to the

nucleon spin [68]. The study of the Sivers function has greatly advanced our understanding of spin-momentum interactions and QCD factorization theorems [62, 69, 70, 41]. A key feature of the Sivers function is its process dependence, meaning it varies depending on the hard scattering process through which it is probed and extracted. This variation stems from the differences in the initial-state and final-state interactions between the active parton and the nucleon remnant [71, 72]. A well-known example is the sign flip of the quark Sivers function between the semi-inclusive deep-inelastic scattering (SIDIS) process to the Drell-Yan (DY) process. This arises because, in the SIDIS process, the outgoing quark undergoes "final-state" interactions with the nucleon remnant after the quark-photon interaction, while in the DY process, the incoming quark experiences "initial-state" interactions with the nucleon remnant before the quark-antiquark annihilation into a virtual photon [69, 62, 71, 73, 74, 75]. The extraction of the Sivers function presents several challenges. Firstly, experimental measurements of the Sivers asymmetry are normalized by the unpolarized cross section. Thus extraction of the Sivers function requires a careful extraction of the unpolarized TMDs. Modern extractions of the unpolarized TMDs have been performed in for instance [76, 77, 78, 79, 80] where the most precise extractions have utilized data from both SIDIS and DY production and resummation has been performed up to N^{4}LL accuracy with the exception of the complete 5 loop cusp anomalous dimension. In [81], a global extraction of the Sivers function from SIDIS and Drell-Yan data was performed at NLO and NNLL accuracy, while a NLL extraction was performed in [82]. In [83], a global extraction of the Sivers function from SIDIS, Drell-Yan lepton pair, and W/Z production processes was performed using resummation at N^{3}LL using the ζ-prescription. Despite the progress in the perturbative accuracy used for these extractions, additional experimental data is required to uncover the behavior of these functions at regions of large x. The second challenge in obtaining an extraction of the Sivers function is the relatively limited. The previous study for the first global analysis of the Sivers asymmetry took into consideration experimental data from SIDIS [13, 84, 9, 10, 11] and from DY collisions [85, 15]. In this study, it was shown that there

was tension between the STAR measurement and the remaining experimental measurements. A key requirement for resolving this tension was the introduction of additional experimental measurements that are sensitive to the Sivers function.

6.2 Sivers Formalism

This section we present the TMD factorization formalism for the Sivers asymmetry in semi-inclusive deep inelastic scattering (SIDIS), Drell-Yan(DY), W/Z productions and single jet production in pp collisions. The Sivers formalism in SIDIS is presented in (6.2.1), the Sivers formalism in DY is presented in (6.2.2), the Sivers formalism in W/Z productions is presented in (6.2.3), and the A_N formalism for single jet production in pp collisions is presented in (6.2.4) respectively.

6.2.1 Sivers Formalism in SIDIS process

The differential cross section for SIDIS, $e(\ell) + n(P, \mathbf{S}_\perp) \to e(\ell') + h(P_h) + X$ can be written in the following form [86, 87]

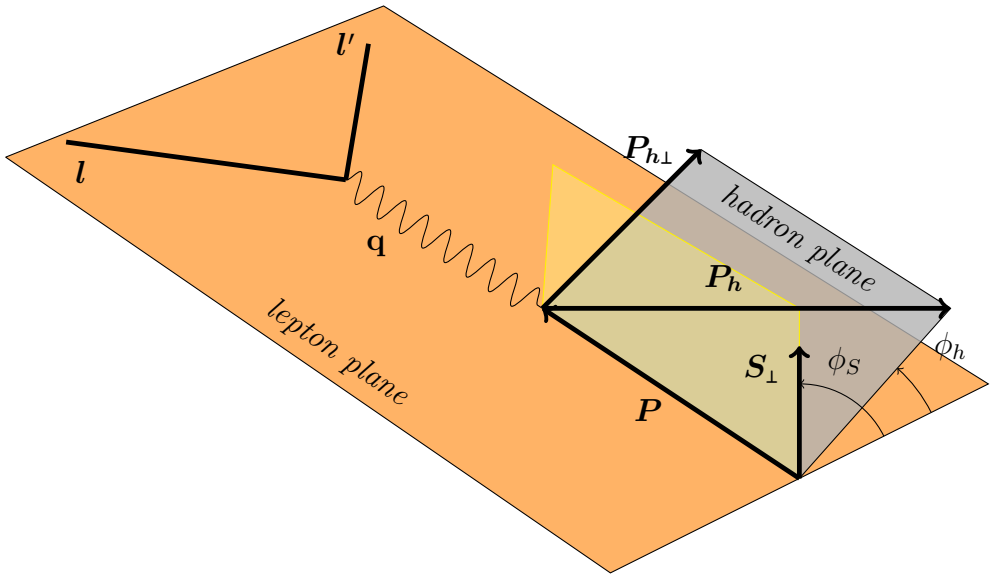

Figure 6.1: The kinematics for Semi-Inclusive DIS. The exchanged photon carries a momentum q. The quantity $\mathbf{S}_\perp$ is the transverse polarization of the proton, ϕ_S is the azimuthal angle between $\mathbf{S}_\perp$ and the lepton plane, and ϕ_h is the azimuthal angle between the hadron plane and the lepton plane. In this case, the modulation depends on the difference between azimuthal angles.

$$\frac{d\sigma}{d\mathcal{PS}} = \sigma_0^{\mathrm{DIS}} \left[F_{UU} + \sin(\phi_h - \phi_s) F_{UT}^{\sin(\phi_h - \phi_s)} \right], \tag{6.1}$$

where the phase space $d\mathcal{PS} = dx_B\, dQ^2\, dz_h\, d^2P_{h\perp}$, the electron-proton center-of-mass (CM) energy $S = (P + \ell)^2$ and the exchanged virtual photon momentum $q = \ell' - \ell$ with $Q^2 = -q^2$, and the usual SIDIS kinematic variables are defined as

$$x_B = \frac{Q^2}{2P \cdot q}, \qquad y = \frac{Q^2}{x_B S}, \qquad z_h = \frac{P \cdot P_h}{P \cdot q}. \tag{6.2}$$

The plane containing the initial and final lepton momentum vectors is termed the lepton plane, while the momentum vectors of the photon and final state hadron establish the hadron plane, see Fig. (6.1). The azimuthal angle of the hadron plane with respect to the lepton plane is designated as ϕ_h, while the azimuthal angle of the transversely polarized proton spin with

respect to the lepton plane is designed as ϕ_s. We utilize the *Trento* conventions [88] to define these azimuthal angles. In this expression, $\sigma_0^{\rm DIS}$ is the leading order (LO) electromagnetic scattering cross section given by

$$\sigma_0^{\rm DIS} = \frac{2\pi\alpha_{\rm EM}^2}{Q^4}\left[1+(1-y)^2\right] \tag{6.3}$$

where $\alpha_{\rm EM}$ is the electromagnetic fine structure constant.

The quantities F_{UU} and $F_{UT}^{\sin(\phi_h-\phi_s)}$ in (6.1) represent the spin-independent and spin-dependent structure functions, respectively. The experimentally measured quantity, the Sivers asymmetry, $A_{UT}^{\sin(\phi_h-\phi_s)}$, for this process is written in terms of the structure functions as follows

$$A_{UT}^{\sin(\phi_h-\phi_s)} = \frac{F_{UT}^{\sin(\phi_h-\phi_s)}}{F_{UU}} \tag{6.4}$$

The structure functions F_{UU} and $F_{UT}^{\sin(\phi_h-\phi_s)}$ in the momentum space are expressed as follows

$$\begin{aligned} F_{UU}(x_B,z_h,P_{h\perp},Q) &= H^{\rm DIS}(Q,\mu)\mathcal{C}^{\rm DIS}\left[fD\right], \\ F_{UT}^{\sin(\phi_h-\phi_s)}(x_B,z_h,P_{h\perp},Q) &= H^{\rm DIS}(Q,\mu)\mathcal{C}^{\rm DIS}\left[-\frac{\hat{\mathbf{h}}\cdot\mathbf{k}_\perp}{M}f_{1T}^\perp D\right] \end{aligned} \tag{6.5}$$

where the expression of the the hard factor, $H^{\rm DIS}(Q,\mu)$, is given in [89, 90] as follows

$$H^{\rm DIS}(Q,\mu) = 1+\frac{\alpha_s}{\pi}C_F\left[\frac{3}{2}\ln\left(\frac{Q^2}{\mu^2}\right)-\frac{1}{2}\ln^2\left(\frac{Q^2}{\mu^2}\right)-4+\frac{\pi^2}{12}\right] \tag{6.6}$$

The shorthand notation utilized in the expressions of structure functions is given by

$$\begin{aligned} \mathcal{C}^{\rm DIS}\left[wAB\right] = \sum_q e_q^2 \int d^2\mathbf{k}_\perp d^2\mathbf{p}_\perp \delta^2\left(z_h\mathbf{k}_\perp+\mathbf{p}_\perp-\mathbf{P}_{h\perp}\right) \\ \times w(\mathbf{k}_\perp,\mathbf{p}_\perp)A_{q/p}(x_B,k_\perp^2,\mu,\zeta_A)\,B_{h/q}(z_h,p_\perp^2,\mu,\zeta_B) \end{aligned} \tag{6.7}$$

for the convolution integrals. The factors, A and B represent the quark distribution function

and fragmentation function respectively, while e_q denotes the fractional electric charge for the quarks. $\mathbf{k}_\perp$ represents the transverse momentum of the quark relative to the nucleon, while $\mathbf{p}_\perp$ is the transverse momentum of the final-state hadron relative to the fragmenting quark. $\hat{\mathbf{h}} = \mathbf{P}_{h\perp}/P_{h\perp}$ is the unit vector that points in the direction of the transverse momentum of the final-state hadron and M is the mass of the struck nucleon. $f_{q/p}(x_B, k_\perp^2, \mu, \zeta)$ is the unpolarized TMDPDF, while $f_{1T,q/p}^\perp(x_B, k_\perp^2, \mu, \zeta)$ is the SIDIS Sivers function and $D_{h/q}(z_h, p_\perp^2, \mu, \zeta)$ is the unpolarized TMDFF. These functions are dependent of μ and ζ which are just the renormalization and rapidity (Collins-Soper) scales [41], they are utilized to regulate ultraviolet and rapidity divergences, respectively. Moreover, the rapidity scales obey the relation $\zeta_A \zeta_B = Q^4$ [90, 61, 45, 91] in the TMD region.

The expressions for the structure functions are simplified by going to the $b_\perp$-space, the Fourier conjugate space to the transverse momentum space. In the $b_\perp$-space, these expressions become

$$\begin{aligned} F_{UU}(x_B, z_h, P_{h\perp}, Q) =& H^{\mathrm{DIS}}(Q, \mu) \sum_q e_q^2 \int_0^\infty \frac{b_\perp \, db_\perp}{2\pi} \\ & \times J_0\left(\frac{b_\perp P_{h\perp}}{z_h}\right) f_{q/p}(x_B, b_\perp, \mu, \zeta_A) D_{h/q}(z_h, b_\perp, \mu, \zeta_B)\,, \end{aligned} \tag{6.8}$$

$$\begin{aligned} F_{UT}^{\sin(\phi_h - \phi_s)}(x_B, z_h, P_{h\perp}, Q) =& H^{\mathrm{DIS}}(Q, \mu) \sum_q e_q^2 \int_0^\infty \frac{b_\perp^2 \, db_\perp}{4\pi} \\ & \times J_1\left(\frac{b_\perp P_{h\perp}}{z_h}\right) f_{1T,q/p}(x_B, b_\perp, \mu, \zeta_A) D_{h/q}(z_h, b_\perp, \mu, \zeta_B). \end{aligned} \tag{6.9}$$

Here the $b_\perp$-space TMDs are defined as

$$f_{q/p}(x, b_\perp, \mu, \zeta) = \int d^2\mathbf{k}_\perp e^{-i\mathbf{k}_\perp \cdot \mathbf{b}_\perp} f_{q/p}(x, k_\perp^2, \mu, \zeta) \tag{6.10}$$

$$D_{h/q}(z, b_\perp, \mu, \zeta) = \int \frac{d^2\mathbf{p}_\perp}{z^2} e^{-i\mathbf{p}_\perp \cdot \mathbf{b}_\perp / z} D_{h/q}(z, p_\perp^2, \mu, \zeta)\,, \tag{6.11}$$

$$\begin{aligned} f_{1T,q/p}^{\perp\,\alpha\,\mathrm{SIDIS}}(x, b_\perp, \mu, \zeta) =& \frac{1}{M} \int d^2\mathbf{k}_\perp \, k_\perp^\alpha \, e^{-i\mathbf{k}_\perp \cdot \mathbf{b}_\perp} f_{1T,q/p}^{\perp\,\mathrm{SIDIS}}(x, k_\perp^2, \mu, \zeta) \\ \equiv & \left(\frac{i b_\perp^\alpha}{2}\right) f_{1T,q/p}^\perp(x, b_\perp, \mu, \zeta)\,. \end{aligned} \tag{6.12}$$

At small $b_\perp$ where $1/b_\perp \gg \Lambda_{\rm QCD}$, one can perform an operator product expansion (OPE) of these functions in terms of their collinear counterparts as follows

$$f_{q/p}(x, b_\perp, \mu, \zeta) = \Big[C_{q\leftarrow i} \otimes f_{i/p}\Big](x, b_\perp, \mu, \zeta) \,, \tag{6.13}$$

$$D_{h/q}(z, b_\perp, \mu, \zeta) = \frac{1}{z^2}\Big[\hat{C}_{i\leftarrow q} \otimes D_{h/i}\Big](z, b_\perp, \mu, \zeta) \,, \tag{6.14}$$

$$f^\perp_{1T,q/p}(x, b_\perp, \mu, \zeta) = \Big[\bar{C}_{q\leftarrow i} \otimes T_{F\,i/p}\Big](x, b_\perp, \mu, \zeta) \,, \tag{6.15}$$

where $f_{i/p}(x,\mu)$, $D_{h/i}(z,\mu)$ and $T_{F\,i/p}(x_1, x_2, \mu)$ are the collinear PDF, FF and the Qiu-Sterman function, respectively [37, 92, 93]. The operator $\otimes$ denotes the convolution over the parton momentum fractions and are given by

$$\Big[C_{q\leftarrow i} \otimes f_{i/p}\Big](x, b_\perp, \mu, \zeta) = \int_x^1 \frac{d\hat{x}}{\hat{x}} C_{q\leftarrow i}\left(\frac{x}{\hat{x}}, b_\perp, \mu, \zeta\right) f_{i/p}\left(\hat{x}, \mu\right) \,, \tag{6.16}$$

for $f_{i/p}$ and likewise for $D_{h/i}$. In these expressions, the sum over the index $i = (q, g)$ is implicit. The convolution in the case of the Sivers function is more complicated, since it involves two kinematic variables $\hat{x}_1$ and $\hat{x}_2$

$$\Big[\bar{C}_{q\leftarrow i} \otimes T_{F\,i/p}\Big](x, b_\perp, \mu, \zeta) = \int_x^1 \frac{d\hat{x}_1}{\hat{x}_1}\frac{d\hat{x}_2}{\hat{x}_2} \bar{C}_{q\leftarrow i}(x/\hat{x}_1, x/\hat{x}_2, b_\perp, \mu, \zeta)\, T_{F\,i/p}(\hat{x}_1, \hat{x}_2, \mu) \,. \tag{6.17}$$

The C functions in the above equations are the Wilson coefficient functions, and their expressions at NLO are in Appendix of Ref. [81].

A few remarks are necessary regarding the Sivers function case. At the outset, although the coefficient function exhibits complexity across various scales μ and ζ, it notably simplifies under the selection of canonical scales $\mu = \sqrt{\zeta} = \mu_b = c_0/b$, where $c_0 = 2e^{-\gamma_E}$ and γ_E denotes the Euler constant. Such scales are commonly known as the intrinsic scales of the TMDs. Additionally, there exist diverse conventions for the normalization of the Qiu-Sterman function. In our approach, we initially adhere to the *Trento* convention [88] for the quark Sivers

function, and subsequently, the convention for the Qiu-Sterman function ensures that the coefficient $\bar{C}$ function in Eq.(6.15) simplifies to a straightforward delta function at leading order. Our choice aligns with the concept of the first transverse moment of the Sivers function [71, 94].

$$f_{1T\,q/p}^{\perp\,(1)}(x,Q) = -\frac{1}{2M} T_{F\,q/p}(x,x,Q)\,. \tag{6.18}$$

where M is the nucleon mass. The operator $\otimes$ in the above equations represents the convolution over the parton momentum fractions and are given by

$$\Big[C_{q\leftarrow i}\otimes f_{i/p}\Big](x,b_\perp,\mu,\zeta) = \int_x^1 \frac{d\hat{x}}{\hat{x}} C_{q\leftarrow i}\left(\frac{x}{\hat{x}},b_\perp,\mu,\zeta\right) f_{i/p}\left(\hat{x},\mu\right)\,, \tag{6.19}$$

for $f_{i/p}$ and likewise for $D_{h/i}$ where $i=\{q,g\}$. The sum over the index i is implicit. For the Sivers function, the convolution is given by

$$\Big[\bar{C}_{q\leftarrow i}\otimes T_{F,i/p}\Big](x,b_\perp,\mu,\zeta) = \int_x^1 \frac{d\hat{x}_1}{\hat{x}_1}\frac{d\hat{x}_2}{\hat{x}_2} \bar{C}_{q\leftarrow i}(x/\hat{x}_1,x/\hat{x}_2,b_\perp,\mu,\zeta)\, T_{F,i/p}(\hat{x}_1,\hat{x}_2,\mu)\,. \tag{6.20}$$

It is important to realize that the C-function for the Sivers function is in general complex since it involves two momentum fractions x_1 and x_2. However, it reduces to a simple form at the nominal scales $\mu_i = \sqrt{\zeta_i} = \mu_b$, where the convolution reduces to a single convolution and one depends on the diagonal part of the ETQS function, $T_{F,q/p}(x,x,\mu_b)$, at the scale μ_b. The C-functions in the above equations are the Wilson coefficient functions, and their expressions at NLO are found in Ref. [81].

Finally, in the large $b_\perp$ region where $b_\perp \gtrsim 1/\Lambda_{\rm QCD}$, the TMD evolution extends into the non-perturbative domain. To take into account the non-perturbative contribution, we adopt the conventional b_*-prescription [40]

$$b_* = b_\perp/\sqrt{1+b_\perp^2/b_{MAX}^2}\,, \tag{6.21}$$

with $b_{MAX} = 1.5\ \text{GeV}^{-1}$. With the b_* prescription, the resulting expressions for the structure functions are written as follows

$$
\begin{aligned}
F_{UU}(x_B, z_h, P_{h\perp}, Q) =& H^{\text{DIS}}(Q,Q) \int_0^\infty \frac{db_\perp b_\perp}{2\pi} J_0\left(b_\perp q_\perp\right) \sum_q e_q^2 \qquad (6.22)\\
&\times \Big[C_{q\leftarrow i} \otimes f_{i/p}\Big]\left(x_B, b_*, \mu_{b_*}, \mu_{b_*}^2\right) \frac{1}{z_h^2}\Big[\hat{C}_{j\leftarrow q} \otimes D_{h/j}\Big]\left(z_h, b_*, \mu_{b_*}, \mu_{b_*}^2\right)\\
&\times \exp\Big[-2S_{\text{pert}}(b_*, \mu_{b_*}, \mu_{b_*}^2, Q, Q^2) - S_{\text{NP}}^f(x_B, b_\perp, Q_0, Q) - S_{\text{NP}}^D(z_h, b_\perp, Q_0, Q)\Big],\\
F_{UT}^{\sin(\phi_h-\phi_s)}(x_B, z_h, P_{h\perp}, Q) =& H^{\text{DIS}}(Q,Q) \int_0^\infty \frac{db_\perp\, b_\perp^2}{4\pi} J_1\left(b_\perp q_\perp\right) \sum_q e_q^2 \qquad (6.23)\\
&\times \Big[\bar{C}_{q\leftarrow i} \otimes T_{F,i/p}\Big](x_B, b_*, \mu_{b_*}, \mu_{b_*}^2) \frac{1}{z_h^2}\Big[\hat{C}_{j\leftarrow q} \otimes D_{h/j}\Big]\left(z_h, b_*, \mu_{b_*}, \mu_{b_*}^2\right)\\
&\times \exp\Big[-2S_{\text{pert}}(b_*, \mu_{b_*}, \mu_{b_*}^2, Q, Q^2) - S_{\text{NP}}^s(x_B, b_\perp, Q_0, Q) - S_{\text{NP}}^D(z_h, b_\perp, Q_0, Q)\Big],
\end{aligned}
$$

where $\mathbf{q}_\perp = -\mathbf{P}_{h\perp}/z_h$ with $q_\perp = |\mathbf{q}_\perp|$, μ_b has been substituted with $\mu_{b_*} = b_0/b_*$, and Q_0 denotes the reference scale of the TMDs. The functions S_{NP}^f, S_{NP}^D, and S_{NP}^s represent the respective non-perturbative Sudakov form factors for the unpolarized TMDPDF, TMDFF, and the Sivers function which will be elaborated upon in the subsequent section.

It is important to emphasize that the ETQS function, $T_{F,q/p}(x,x,\mu)$, is an important ingredient in the above TMD evolution formalism through the OPE procedure for the quark Sivers function, as encoded in the spin-dependent structure function $F_{UT}^{\sin(\phi_h-\phi_s)}$. Since the TSSA for single inclusive jet production in proton-proton collisions crucially depends on the ETQS function, this allows us to perform a combined fit of the TSSA for single jet production within the collinear factorization at twist-three level and the Sivers asymmetry within the TMD factorization.

6.2.2 Sivers Formalism in Drell-Yan process

For Drell-Yan lepton pair production in transversely polarized proton-proton collisions, $p(P_A, \mathbf{S}_\perp) + p(P_B) \to [\gamma^*(q) \to] \ell^+\ell^- + X$, the differential cross section with the relevant terms

is given in [95, 74, 96, 97] by the expression

$$\frac{d\sigma}{d\mathcal{PS}} = \sigma_0^{\mathrm{DY}} \left[W_{UU} + \sin(\phi_q - \phi_s) W_{UT}^{\sin(\phi_q - \phi_s)} + \cdots \right], \tag{6.24}$$

where $d\mathcal{PS} = dQ^2\, dy\, d^2q_\perp$, y stands for the rapidity of the lepton pair while $\mathbf{q}_\perp$ and Q represents the transverse momentum and invariant mass of the virtual photon, respectively.

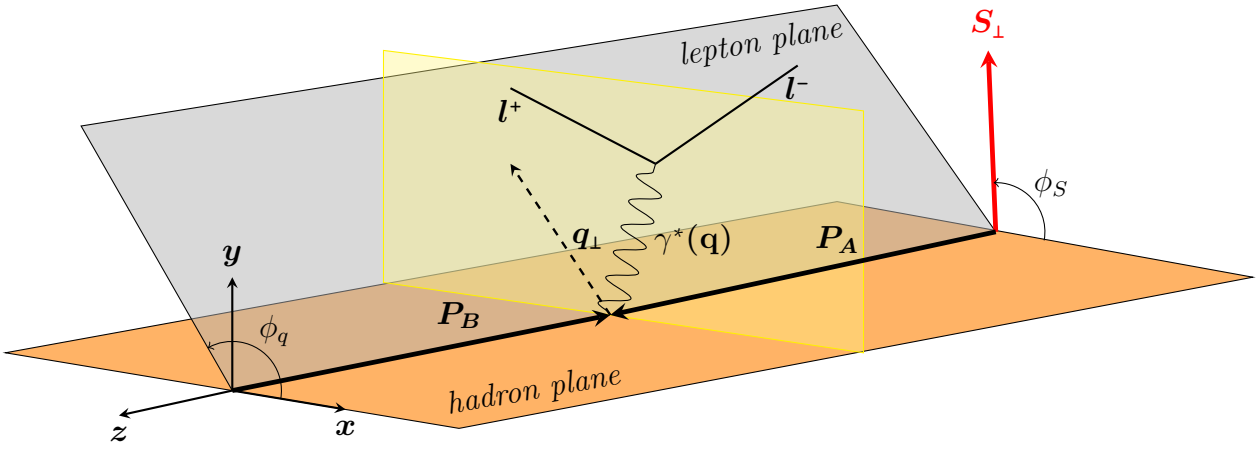

Figure 6.2: The diagram for the Drell-Yan vector boson production in collisions of hadrons A and B. The transversely polarized hadron A is moving in the +z-direction, while the unpolarized hadron B is along the -z-direction. The transverse momentum $q_\perp$ of the vector boson is represented by a dotted line

The expression for the leading-order electromagnetic scattering cross section is as follows

$$\sigma_0^{\mathrm{DY}} = \frac{4\pi\alpha_{\mathrm{EM}}^2}{3SQ^2N_C}, \tag{6.25}$$

where $S = (P_A + P_B)^2$ is the center of mass energy squared and $N_C = 3$ is the number of color. We study the Drell-Yan production in the center-of-mass frame of the incoming proton beams. The polarized proton moves along the $+z$ axis, while the transverse spin vector of the proton $\mathbf{S}_\perp$ and the transverse momentum of the virtual photon $\mathbf{q}_\perp$ have azimuthal angles ϕ_s and ϕ_q, respectively.

As usual, W_{UU} and $W_{UT}^{\sin(\phi_q - \phi_s)}$ represent the unpolarized and transversely polarized struc-

ture functions, respectively. The Sivers asymmetry in Drell-Yan processes can be formulated using the structure function as follows

$$A_{UT}^{\sin(\phi_q-\phi_s)} = \frac{W_{UT}^{\sin(\phi_q-\phi_s)}}{W_{UU}}. \tag{6.26}$$

In the TMD formalism, these structure functions are given by the following expressions

$$W_{UU}(x_a, x_b, q_\perp, Q) = H^{\rm DY}(Q,\mu)\mathcal{C}^{\rm DY}\left[f\ f\right], \tag{6.27}$$

$$W_{UT}^{\sin(\phi_q-\phi_s)}(x_a, x_b, q_\perp, Q) = H^{\rm DY}(Q,\mu)\mathcal{C}^{\rm DY}\left[\frac{\hat{\mathbf{q}}_\perp\cdot\mathbf{k}_{a\perp}}{M} f_{1T}^\perp\ f\right]. \tag{6.28}$$

For Drell-Yan process, the above convolution in the structure functions is expressed as follows

$$\begin{aligned}\mathcal{C}^{\rm DY}\left[wAB\right] = \sum_q e_q^2 \int d^2\mathbf{k}_{a\perp} d^2\mathbf{k}_{b\perp} \delta^2\left(\mathbf{k}_{a\perp}+\mathbf{k}_{b\perp}-\mathbf{q}_\perp\right) w(\mathbf{k_{a\perp}}, \mathbf{k_{b\perp}}) \\ \times A_{q/A}(x_a, k_{a\perp}^2, \mu, \zeta_A)\, B_{\bar{q}/B}(x_b, k_{b\perp}^2, \mu, \zeta_B)\,.\end{aligned} \tag{6.29}$$

Here, x_a and x_b represent the momentum fractions of the hadrons carried by the quarks, and they are given by

$$x_a = \frac{Q}{\sqrt{S}} e^y\,, \qquad x_b = \frac{Q}{\sqrt{S}} e^{-y}\,. \tag{6.30}$$

In this process, the standard Feynman-x can be expressed in terms of $x_{a,b}$ as $x_F = x_a - x_b$, a relation that will be referenced in the subsequent section. Additionally, $\mathbf{k}_{a\perp}$ and $\mathbf{k}_{b\perp}$ represent the transverse momenta of the partons relative to their respective nucleons. The expression of the hard function is provided in [45] by

$$H^{\rm DY}(Q,\mu) = 1 + \frac{\alpha_s}{\pi} C_F \left[\frac{3}{2}\ln\left(\frac{Q^2}{\mu^2}\right) - \frac{1}{2}\ln^2\left(\frac{Q^2}{\mu^2}\right) + \frac{7}{12}\pi^2 - 4\right]. \tag{6.31}$$

At this point, it is crucial to reiterate that there is a sign flip between the Sivers function

$f_{1T}^{\perp}$ for the Drell-Yan process and its counterpart in SIDIS:

$$f_{1T}^{\perp\,\mathrm{DY}}(x,k_\perp^2,\mu,\zeta) = -f_{1T}^{\perp\,\mathrm{SIDIS}}(x,k_\perp^2,\mu,\zeta)\,. \tag{6.32}$$

This will lead to slightly different definition for the Sivers function in the $b_\perp$-space

$$f_{1T,q/p}^{\perp\,\alpha\,\mathrm{DY}}(x,b_\perp,\mu,\zeta) = \frac{1}{M}\int d^2\mathbf{k}_\perp\, k_\perp^\alpha\, e^{-i\mathbf{k}_\perp\cdot\mathbf{b}_\perp} f_{1T,q/p}^{\perp\,\mathrm{DY}}(x,k_\perp^2,\mu,\zeta) \equiv \left(-\frac{ib_\perp^\alpha}{2}\right) f_{1T,q/p}^{\perp}(x,b_\perp,\mu,\zeta).$$

Including the Sudakov factor, we have the following expressions for the $b_\perp$-space structure functions

$$\begin{aligned} W_{UU}(x_a,x_b,q_\perp,Q) &= H^{\mathrm{DY}}(Q,Q)\int \frac{db_\perp\, b_\perp}{2\pi} J_0(b_\perp q_\perp)\sum_q e_q^2 \\ &\times \Big[C_{q\leftarrow i}\otimes f_{i/A}\Big]\big(x_a,b_*,\mu_{b_*},\mu_{b_*}^2\big)\Big[C_{\bar q\leftarrow j}\otimes f_{j/B}\Big]\big(x_b,b_*,\mu_{b_*},\mu_{b_*}^2\big) \\ &\times \exp\Big[-2S_{\mathrm{pert}}(b_*,\mu_{b_*},\mu_{b_*}^2,Q,Q^2) - S_{\mathrm{NP}}^f(x_a,b_\perp,Q_0,Q) - S_{\mathrm{NP}}^f(x_b,b_\perp,Q_0,Q)\Big], \end{aligned} \tag{6.33}$$

$$\begin{aligned} W_{UT}^{\sin(\phi_q-\phi_s)}(x_a,x_b,q_\perp,Q) &= H^{\mathrm{DY}}(Q,Q)\int \frac{db_\perp\, b_\perp^2}{4\pi} J_1(b_\perp q_\perp)\sum_q e_q^2 \\ &\times \Big[\bar C_{q\leftarrow i}\otimes T_{F,i/p}\Big](x_a,b_*,\mu_{b_*},\mu_{b_*}^2)\Big[C_{\bar q\leftarrow j}\otimes f_{j/B}\Big]\big(x_b,b_*,\mu_{b_*},\mu_{b_*}^2\big) \\ &\times \exp\Big[-2S_{\mathrm{pert}}(b_*,\mu_{b_*},\mu_{b_*}^2,Q,Q^2) - S_{\mathrm{NP}}^s(x_a,b_\perp,Q_0,Q) - S_{\mathrm{NP}}^f(x_b,b_\perp,Q_0,Q)\Big]. \end{aligned} \tag{6.34}$$

6.2.3 Sivers Formalism in W/Z production

The production of W/Z bosons in proton-proton collisions closely resembles that of virtual-photon production. Here, the hard scale Q is defined as the mass of the vector boson produced, denoted $Q = M_{W,Z}$. The differential cross-section expression for this process is provided as follows

$$\frac{d\sigma_V}{d\mathcal{PS}} = \sigma_0^{\mathrm{V}}\Big[W_{UU,V} + \sin(\phi_q-\phi_s)W_{UT,V}^{\sin(\phi_q-\phi_s)}\Big]\,, \tag{6.35}$$

where the phase space $d\mathcal{PS} = dy\, d^2q_\perp$ and $V = W, Z$. The leading-order scattering cross sections are given by

$$\sigma_0^W = \frac{\sqrt{2}\pi G_F M_W^2}{SN_C}\,, \tag{6.36}$$

$$\sigma_0^Z = \frac{\sqrt{2}\pi G_F M_Z^2}{SN_C}\,, \tag{6.37}$$

where G_F is the Fermi weak coupling constant. On the other hand, the structure functions are given by

$$\begin{aligned} W_{UU,V}(x_a, x_b, q_\perp, Q) &= H^{\rm DY}(Q,Q) \int \frac{db_\perp\, b_\perp}{2\pi} J_0(b_\perp q_\perp) \sum_{q,q'} e^2_{qq',V} \\ &\times \Big[C_{q\leftarrow i} \otimes f_{i/A}\Big]\big(x_a, b_*, \mu_{b_*}, \mu^2_{b_*}\big)\Big[C_{q'\leftarrow j} \otimes f_{j/B}\Big]\big(x_b, b_*, \mu_{b_*}, \mu^2_{b_*}\big) \\ &\times \exp\Big[-2S_{\rm pert}(b_*, \mu_{b_*}, \mu^2_{b_*}, Q, Q^2) - S^f_{\rm NP}(x_a, b_\perp, Q_0, Q) - S^f_{\rm NP}(x_b, b_\perp, Q_0, Q)\Big], \end{aligned} \tag{6.38}$$

$$\begin{aligned} W^{\sin(\phi_q-\phi_s)}_{UT,V}(x_a, x_b, q_\perp, Q) &= H^{\rm DY}(Q,Q) \int \frac{db_\perp\, b_\perp^2}{4\pi} J_1(b_\perp q_\perp) \sum_{q,q'} e^2_{qq',V} \\ &\times \Big[\bar{C}_{q\leftarrow i} \otimes T_{F,i/p}\Big](x_a, b_*, \mu_{b_*}, \mu^2_{b_*})\Big[C_{q'\leftarrow j} \otimes f_{j/B}\Big]\big(x_b, b_*, \mu_{b_*}, \mu^2_{b_*}\big) \\ &\times \exp\Big[-2S_{\rm pert}(b_*, \mu_{b_*}, \mu^2_{b_*}, Q, Q^2) - S^s_{\rm NP}(x_a, b_\perp, Q_0, Q) - S^f_{\rm NP}(x_b, b_\perp, Q_0, Q)\Big], \end{aligned} \tag{6.39}$$

where we have

$$e^2_{qq',W} = |V_{qq'}|^2\,, \qquad e^2_{qq',Z} = \big(V_q^2 + A_q^2\big)\,\delta_{qq'}\,. \tag{6.40}$$

In this context, $|V_{qq'}|^2$ represents the Cabibbo-Kobayashi-Maskawa (CKM) matrix, while V_q and A_q denote the vector and axial couplings of the Z boson to a flavor quark q. Similarly to Eq. (6.26) discussed in the preceding section, the asymmetry can be expressed as a ratio of these structure functions in an analogous way.

6.2.4 Sivers Formalism in A_N single jet production in pp collisions

Consider a single-inclusive jet production from transversely polarized proton-proton $p^{\uparrow}p$ collisions

$$p(P_1, \mathbf{S}_\perp) + p(P_2) \to \text{jet}(P_J) + X, \tag{6.41}$$

where the momentum of the incoming transversely polarized proton is denoted by P_1 with a transverse polarization vector given by $\mathbf{S}_\perp$. The momenta of the unpolarized proton and the final jet produced are denoted by P_2 and P_J, respectively. The energy of the center of mass is defined as $S = (P_1 + P_2)^2$. In the center-of-mass frame of the incoming proton beams where P_1 (P_2) moves along the $+z$ ($-z$) direction, we define ϕ_S and ϕ_J as azimuthal angles for the spin vector $\mathbf{S}_\perp$ and the transverse momentum of the jet $\mathbf{P}_\perp$, respectively. A convenient choice of frame is illustrated in Fig. (6.3), where we introduce the so-called the reaction plane, which is formed by the incoming proton momenta and the final state jet axis. In this frame, one has $\phi_J = 0$.

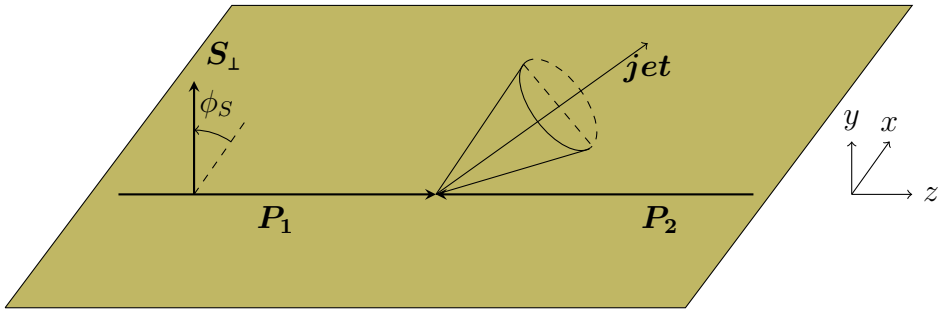

Figure 6.3: Illustration for single inclusive jet production in transversely polarized proton-proton collisions, $p(P_1, \mathbf{S}_\perp) + p(P_2) \to \text{jet}(P_J) + X$. The azimuthal angle of the transverse spin vector, $\mathbf{S}_\perp$, with respect to the reaction plane is denoted by ϕ_S.

The differential cross section for single-inclusive jet production for transversely polarized

$p^{\uparrow}\,p$ collisions is given by

$$E_J \frac{d\sigma(\mathbf{S}_\perp)}{d^3P_J} = E_J \frac{d\sigma}{d^3P_J} + \sin\left(\phi_S - \phi_J\right) E_J \frac{d\Delta\sigma}{d^3P_J}\,, \tag{6.42}$$

where the first term on the right hand side of this expression is the spin-averaged cross section, and the second term is a spin-dependent cross section. Within the collinear factorization formalism [98], the spin-averaged cross section at the leading order can be written as

$$E_J \frac{d\sigma}{d^3P_J} = \frac{\alpha_s^2}{S} \sum_{a,b} \int \frac{dx_a}{x_a} \frac{dx_b}{x_b} f_{a/p}(x_a,\mu) f_{b/p}(x_b,\mu) H^{\mathrm{U}}_{ab\to c}(\hat{s},\hat{t},\hat{u}) \delta(\hat{s}+\hat{t}+\hat{u})\,, \tag{6.43}$$

where $f_{a,b/p}$ are the collinear parton distribution functions (PDFs) with x_a and x_b the momentum fractions of the proton carried by the partons. On the other hand, $H^{\mathrm{U}}_{ab\to c}$ are the well-known leading-order (LO) hard functions for the unpolarized process, which are given, for example, in [99, 74]. The strong coupling constant is denoted by α_s, and $\hat{s}$, $\hat{t}$, $\hat{u}$ are the standard partonic Mandelstam variables.

On the other hand, the second term on the right-hand side of Eq. (6.42) is the spin-dependent contribution. Within the collinear factorization at twist-three level [100], the spin-dependent cross section can be written as

$$\begin{aligned} E_J \frac{d\Delta\sigma}{d^3P_J} = &- P_{J\perp} \frac{\alpha_s^2}{S} \sum_{a,b} \int \frac{dx_a}{x_a} \frac{dx_b}{x_b} f_{b/p}(x_b,\mu) \frac{1}{\hat{u}} H^{\mathrm{Sivers}}_{ab\to c}(\hat{s},\hat{t},\hat{u}) \delta(\hat{s}+\hat{t}+\hat{u}) \\ &\times \left[T_{F,a/p}(x_a,x_a,\mu) - x_a \frac{d}{dx_a} T_{F,a/p}(x_a,x_a,\mu) \right]. \end{aligned} \tag{6.44}$$

Here $T_{F,a/p}(x_a,x_a,\mu)$ is the ETQS function that is often referred to as the quark-gluon-quark correlator inside the proton. $H^{\mathrm{Sivers}}_{ab\to c}$ is the hard function for the polarized case, which takes into account the initial-state and final-state interactions, and they can be written as

follows [100, 101]

$$H^{\text{Sivers}}_{ab\to c}(\hat{s},\hat{t},\hat{u}) = H^{\text{I}}_{ab\to c}(\hat{s},\hat{t},\hat{u}) + H^{\text{F}}_{ab\to c}(\hat{s},\hat{t},\hat{u})\left(1+\frac{\hat{u}}{\hat{t}}\right), \tag{6.45}$$

where $H^{\text{I}}_{ab\to c}$ and $H^{\text{F}}_{ab\to c}$ incorporates the initial-state and final-state interactions, respectively.

Finally, the transverse single spin asymmetry A_N for the single inclusive jet production is defined as the ratio of the spin-dependent and spin-averaged cross sections

$$A_N = E_J\frac{d\Delta\sigma}{d^3P_J}\Big/ E_J\frac{d\sigma}{d^3P_J}. \tag{6.46}$$

Since $E_J d\sigma/d^3P_J = d\sigma/d\eta_{\text{jet}}d^2\mathbf{P}_\perp$, the jet asymmetry would be a function of rapidity η_{jet} and transverse momentum $P_\perp$. Another commonly used variable, $x_F = 2P_z/\sqrt{S}$, called the Feynman-x, is related to η_{jet} and $P_\perp$ as follows

$$x_F = \frac{P_\perp}{\sqrt{S}}\left(e^{\eta_{\text{jet}}} - e^{-\eta_{\text{jet}}}\right). \tag{6.47}$$

6.3 Results

In this section we present the results of the simultaneous global analysis of the Sivers asymmetries in SIDIS, DY lepton pair, and W/Z production, both with and without the inclusion of jet A_N data. We begin by detailing the non-perturbative parametrization used in our theoretical framework, followed by an explanation of our fitting procedure. Finally, we discuss the impact of jet A_N data on the Sivers asymmetries and the extracted Sivers functions.

6.3.1 Non-perturbative parametrization

The fitting is carried out at NLO+NNLL accuracy as described in Ref. [81], where we use the following non-perturbative parametrization for the unpolarized TMD PDFs and TMD

FFs

$$U^f_{\rm NP}(x,b_\perp,\zeta_0,\zeta) = \exp\left(-g_1^f b_\perp^2 - \frac{g_2}{4}\ln\frac{\zeta}{\zeta_0}\ln\frac{b_\perp}{b_*}\right),$$
$$U^D_{\rm NP}(z,b_\perp,\zeta_0,\zeta) = \exp\left(-g_1^D \frac{b_\perp^2}{z^2} - \frac{g_2}{4}\ln\frac{\zeta}{\zeta_0}\ln\frac{b_\perp}{b_*}\right), \tag{6.48}$$

with the values of g_1 and g_2 given by

$$g_1^f = 0.106\ \text{GeV}^2, \quad g_1^D = 0.042\ \text{GeV}^2, \quad g_2 = 0.84\,. \tag{6.49}$$

To describe the COMPASS Drell-Yan production in $\pi+p$ scattering, we use $g_1^f = 0.082\ \text{GeV}^2$ for the pion beam [102] and use collinear pion PDFs in [103]. For numerical calculations, the HERAPDF20_NLO_VAR parametrization [104] was utilized for the proton PDFs. The DSS14 parametrization [105] was utilized for the collinear pion FFs. In addition, the DSS17 parametrization [106] was utilized for the collinear kaon FFs. And for unidentified charged hadrons, the collinear FF could be viewed as the sum of the collinear pion FF and collinear kaon FF [77].

On the other hand, the non-perturbative parametrization of the Sivers function is

$$U^{f_{1T}^\perp}_{\rm NP}(z,b_\perp,\zeta_0,\zeta) = \exp\left(-g_1^T b_\perp^2 - \frac{g_2}{4}\ln\frac{\zeta}{\zeta_0}\ln\frac{b_\perp}{b_*}\right). \tag{6.50}$$

Note that the term written in terms of g_2 is universal. In this case, g_1^T gives the information about the width of the Sivers function, and it will be a fit parameter. The ETQS function $T_{F,q/p}(x,x,\mu_0)$ is parametrized in terms of the unpolarized collinear PDF at an initial scale μ_0 [47]

$$T_{F,q/p}(x,x,\mu_0) = N_q \frac{(\alpha_q+\beta_q)^{(\alpha_q+\beta_q)}}{\alpha_q^{\alpha_q}\beta_q^{\beta_q}} x^{\alpha_q}(1-x)^{\beta_q} f_{q/p}(x,\mu_0)\,. \tag{6.51}$$

To obtain the ETQS function at other scale μ, we use the diagonal piece as an approximation

in its evolution equation [74, 107, 108, 109, 110, 111, 112, 113, 114]

$$\frac{dT_{F,q/p}(x,x,\mu)}{d\ln\mu^2} = \frac{\alpha_s(\mu^2)}{2\pi}\left[P^T_{q\leftarrow q}\otimes T_{F,q/p}\right](x,\mu)\,, \tag{6.52}$$

where $P^T_{q\leftarrow q}$ is the quark to quark splitting (kernel) function

$$P^T_{q\leftarrow q}(x) = C_F\left[\frac{1+x^2}{(1-x)_+}+\frac{3}{2}\delta(1-x)\right]-\eta\,\delta(1-x)\,. \tag{6.53}$$

The fitting was performed with $\eta = 0$. Finally, the fit parameters are N_q, α_q, and β_q, where q stands for quark flavors, q=$\{u,d,s\}$. We choose N_u, N_d, N_s, $N_{\bar{u}}$, $N_{\bar{d}}$, $N_{\bar{s}}$, α_u, α_d, β_u, β_d, g_1^T, along with α_{sea} and β_{sea} for $\bar{u}$, $\bar{d}$, s, $\bar{s}$. In total, there are 13 fit parameters.

6.3.2 Fitting procedure

To proceed with the fit, we utilize the MINUIT package to minimize χ^2

$$\chi^2(\{a\}) = \sum_{i=1}^{N}\sum_{j=1}^{N_i}\frac{(T_j(\{a\})-E_j)^2}{(\Delta E_j)^2}\,, \tag{6.54}$$

for $i = 1,..N$ data sets each containing N_i data points. Experimental measurement of each point is E_j, and the experimental uncertainty is ΔE_j. The theoretical estimate T_j depends on a set of parameters $\{a\}$ which are just fit parameters. We take into account both statistical and systematic uncertainties in quadrature. The uncertainty band is generated by following the replica method [47, 115, 116]. We generate 200 replicas and perform the fit on both noisy and noise-free datasets, resulting in 201 sets of fit parameters. Using these 201 sets of parameters, we calculate the asymmetry for each data point and other observables. To determine the uncertainty band at each point, we select the central (middle) 68% of the 200 replicas.

6.3.3 Impact of jet data on the Sivers function

In this section, we present our global extraction of the Sivers and ETQS functions by fitting the Sivers asymmetry from various datasets, along with the jet A_N data. The datasets include SIDIS measurements from JLab on a neutron target [11], recent HERMES data [14] with three-dimensional kinematic binning for charged pion production on a proton target, and COMPASS data on both proton [9] and deuteron targets [10]. We also incorporate DY lepton pair data from the COMPASS collaboration [12] and W/Z boson production data from RHIC [15, 16]. The jet A_N data are provided by the STAR [7] and AnDY [8] collaborations at RHIC. Additionally, we include previous HERMES SIDIS data on π^0 production [13], as the three-dimensional binning is only available for charged pions. The datasets used in our fit are summarized in Table (6.1).

We apply the same kinematic cuts as described in Ref. [47]: $q_\perp/Q < 0.75$, $P_{h\perp} < 1$ GeV, and $z_h < 0.7$. The jet A_N data covers a wide range of x_F, providing additional constraints on the quark Sivers function in the large-x region. In the following, we analyze the impact of including the jet A_N data on the extraction of the Sivers function. To this end, we perform two separate fits: one without the jet A_N data, referred to as the 'SIDIS+DY' fit, which consists of Sivers asymmetry data from SIDIS, DY lepton pair production, and W/Z production; and another, the 'SIDIS+DY+jet' fit, which incorporates the jet A_N data from RHIC.

In Table. (6.1), we present the χ^2/dof for each of the sets as a well as the χ^2/dof of all sets of the SIDIS+DY+jet data. It can be seen that there is an excellent agreement between the theoretical model and the experiment with a global χ^2/dof = 1.145. Next, we will start detailing and interpreting our results.

Even though the global χ^2/dof is already very good, Table. (6.2) shows that a significantly improved global χ^2/dof= 1.047 is achieved if the AnDY jet data is not included in the fit. And the STAR 200 and STAR 500 jet data yield $\chi^2/N_{data} = 1.445$, and $\chi^2/N_{data} = 0.645$ respectively. Therefore, the theoretical model is more compatible with STAR jet data than

AnDY jet data.

Collab	Ref	Process	N_{data}	χ^2/N_{data}
JLAB	[11]	$lN \to l\pi^+X$	4	0.807
		$lN \to l\pi^-X$	4	1.446
HERMES	[14]	$lp \to lK^-X$	38	1.292
		$lp \to lK^+X$	40	0.992
		$lp \to l\pi^-X$	38	0.995
		$lp \to l\pi^+X$	40	1.186
	[13]	$lp \to l\pi^0X$	4	1.482
COMPASS	[10]	$ld \to lK^0X$	7	0.780
		$ld \to lK^-X$	11	1.389
		$ld \to lK^+X$	13	0.701
		$ld \to l\pi^-X$	11	0.788
		$ld \to l\pi^+X$	12	0.842
	[9]	$lp \to lh^-X$	41	1.058
		$lp \to lh^+X$	42	0.772
COMPASS (Drell-Yan)	[12]	$\pi^-p \to \gamma^*X$	15	0.588
RHIC (W/Z)	[15]	$pp \to W^+X$	8	2.135
		$pp \to W^-X$	8	1.102
		$pp \to Z^0X$	1	0.246
	[16]	$pp \to Z^0X$	1	0.862
RHIC (jet)	[7]	STAR 200: $pp \to \text{jet}X$	9	2.217
		STAR 500: $pp \to \text{jet}X$	9	0.716
	[8]	AnDY 500: $pp \to \text{jet}X$	5	4.885
Total			361	1.145

Table 6.1: The table presents the experimental data used in our 'SIDIS+DY+jet' fit, showing the χ^2/N_{data} for each dataset. The last number (at the bottom) in the right column is the global χ^2/dof. The total number of fitted data points after the kinematic cut is 361.

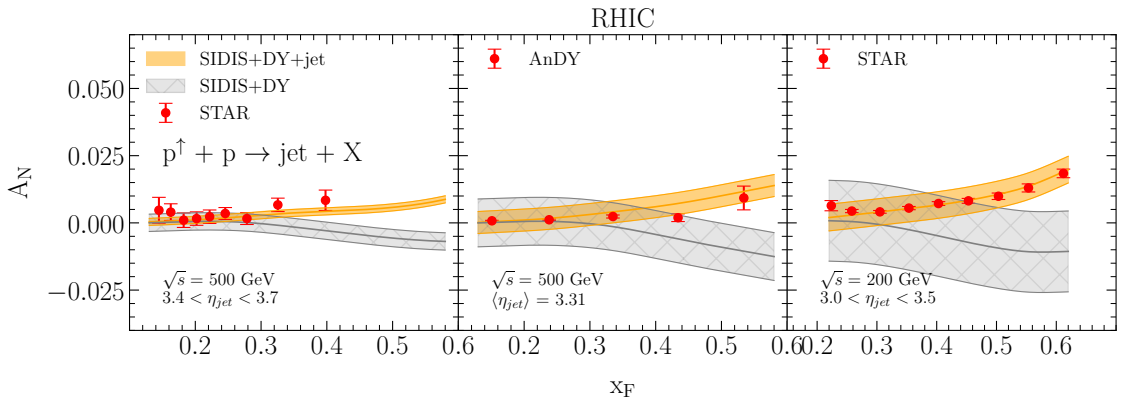

Figure 6.4: The result illustrates the impact of jet A_N data. The fit results with and without jet A_N data are compared to STAR measurements at $\sqrt{s} = 200$ GeV and $\sqrt{s} = 500$ GeV [7], as well as AnDY measurements at $\sqrt{s} = 500$ GeV [8]. For each case, the result is plotted as a function of x_F. The $\pi^- p \to \gamma^* X$ and $pp \to W/ZX$ processes are considered as DY process.

Collab	Ref	Process	N_{data}	χ^2/N_{data}
JLAB	[11]	$lN \to l\pi^+X$	4	0.711
		$lN \to l\pi^-X$	4	0.799
HERMES	[14]	$lp \to lK^-X$	38	1.264
		$lp \to lK^+X$	40	1.021
		$lp \to l\pi^-X$	38	0.951
		$lp \to l\pi^+X$	40	1.153
	[13]	$lp \to l\pi^0X$	4	1.635
COMPASS	[10]	$ld \to lK^0X$	7	0.619
		$ld \to lK^-X$	11	1.742
		$ld \to lK^+X$	13	1.230
		$ld \to l\pi^-X$	11	0.793
		$ld \to l\pi^+X$	12	0.856
	[9]	$lp \to lh^-X$	41	0.956
		$lp \to lh^+X$	42	0.786
COMPASS (Drell-Yan)	[12]	$\pi^-p \to \gamma^*X$	15	0.219
RHIC (W/Z)	[15]	$pp \to W^+X$	8	2.246
		$pp \to W^-X$	8	1.097
		$pp \to Z^0X$	1	0.208
	[16]	$pp \to Z^0X$	1	0.862
RHIC (jet)	[7]	STAR 200: $pp \to \text{jet}X$	9	1.445
		STAR 500: $pp \to \text{jet}X$	9	0.645
Total			356	1.074

Table 6.2: The table presents the experimental data used in our fit with jet $A_N^{(*)}$ data only, showing the χ^2/N_{data} for each dataset and the global χ^2/dof. The total number of fitted data points after the kinematic cut is 356. The symbol $^{(*)}$ indicates that the jet A_N data consists of STAR data only.

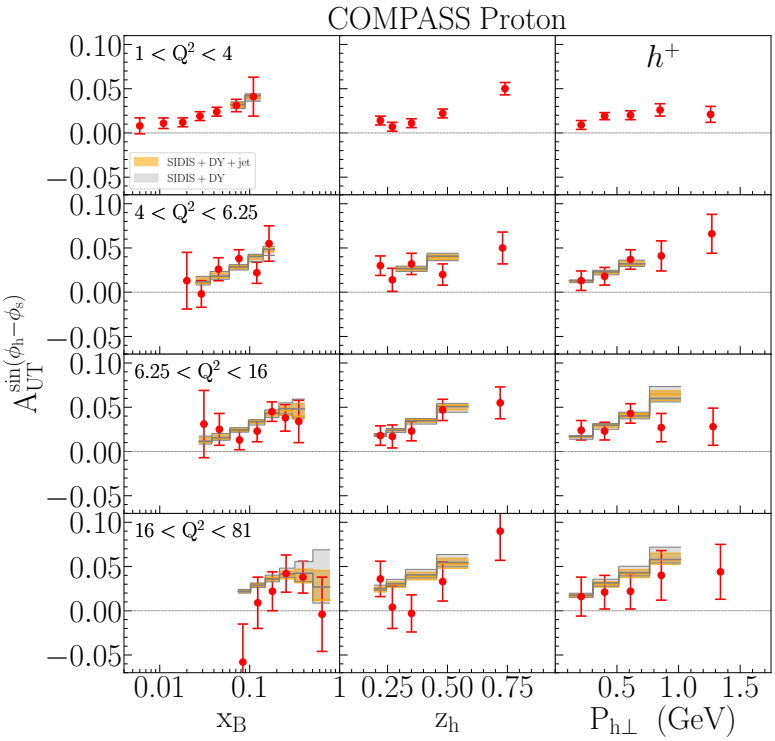

Figure 6.5: The comparison of the fit result without jet $A_N^{(*)}$ data with the fit result with jet $A_N^{(*)}$ data for SIDIS measurement for h^+ [9]. In both cases, the results are plotted for different hard scale intervals as a function of x_B, z_h, and $P_{h\perp}$. The symbol $^{(*)}$ indicates that the jet A_N data consists of STAR data only.

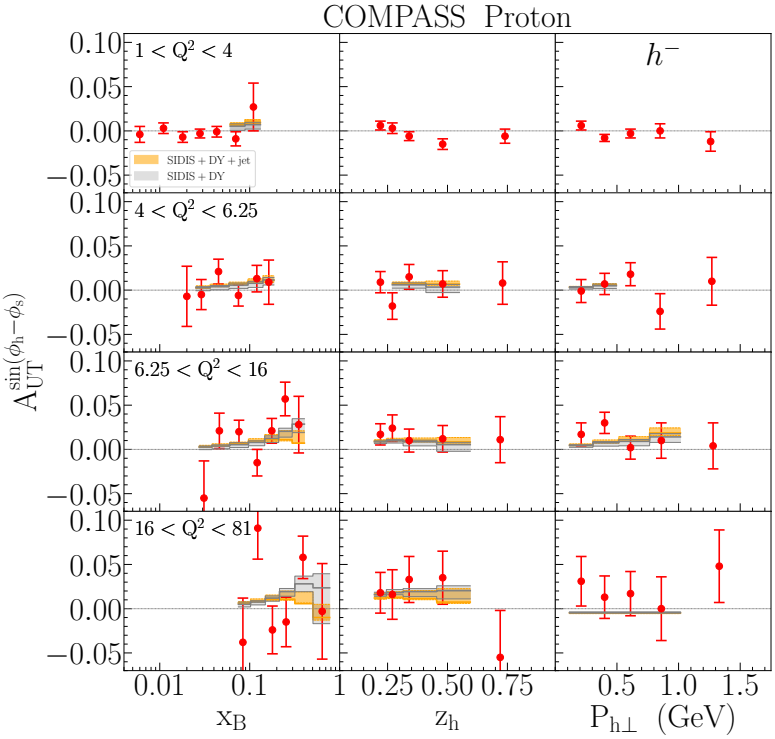

Figure 6.6: The comparison of the fit result without jet $A_N^{(*)}$ data and the fit result with jet $A_N^{(*)}$ data for SIDIS measurement for h^- [9]. In both cases, the results are shown for different hard scale intervals as a function of x_B, z_h, and $P_{h\perp}$. The symbol $^{(*)}$ indicates that the jet A_N data consists of STAR data only.

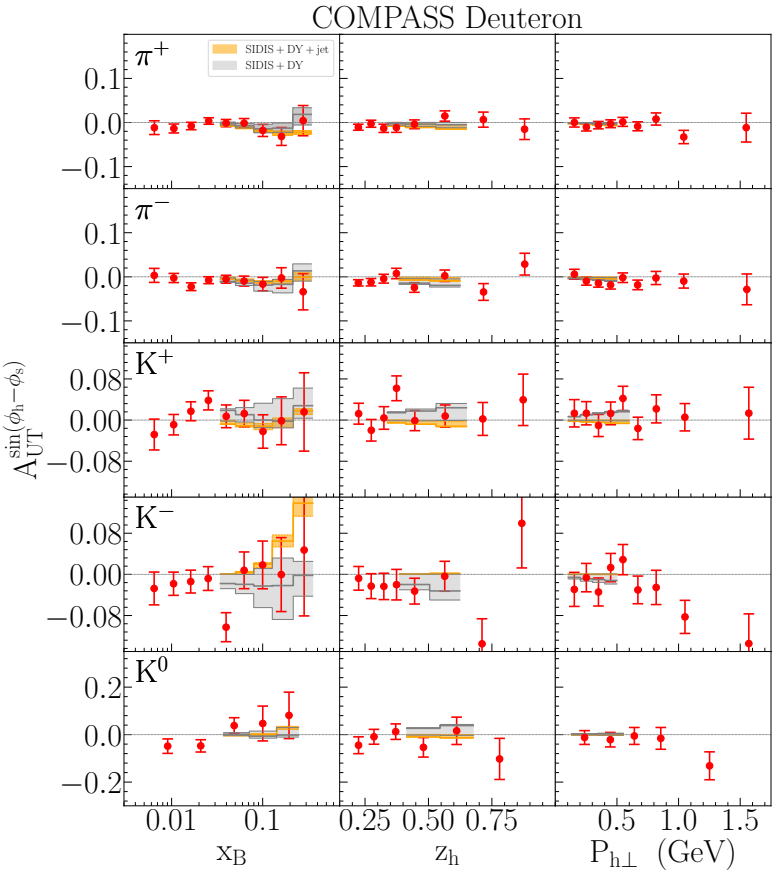

Figure 6.7: The comparison of the fit result without jet $A_N^{(*)}$ data with the fit result with jet $A_N^{(*)}$ data for SIDIS measurements [10] for π^+, π^-, K^+, K^- and K^0. In both cases, the results are plotted as a function of x_B, z_h, and $P_{h\perp}$. The symbol $^{(*)}$ indicates that the jet A_N data consists of STAR data only.

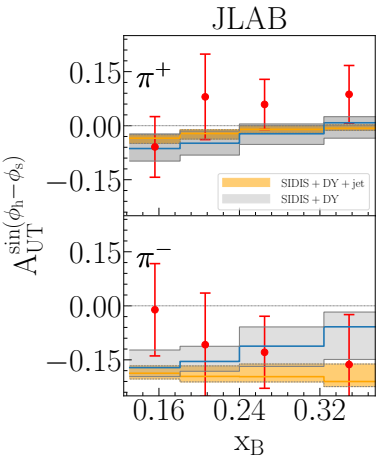

Figure 6.8: The comparison of the fit result without jet $A_N^{(*)}$ data with the fit result with jet $A_N^{(*)}$ data for SIDIS measurements for π^- and π^+ using a neutron target [11]. In both cases, the results are plotted as a function of x_B. The symbol $^{(*)}$ indicates that the jet A_N data consists of STAR data only.

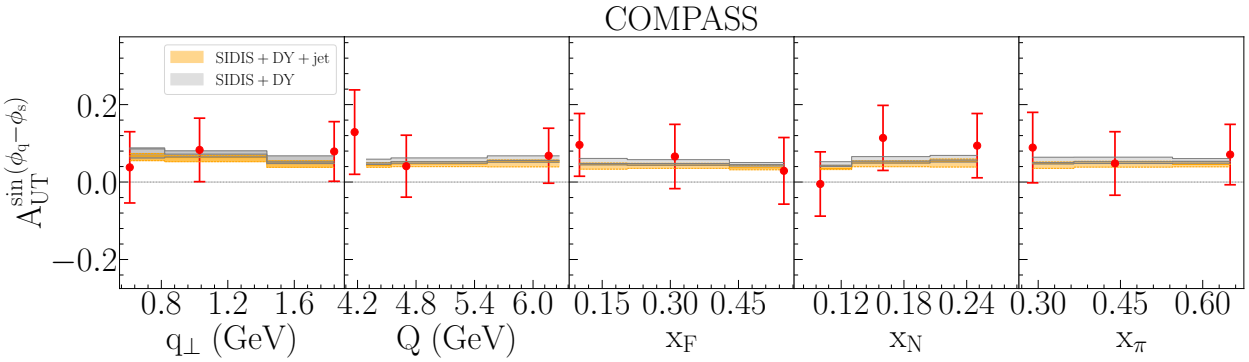

Figure 6.9: The comparison of the fit result without jet $A_N^{(*)}$ data with the fit result with jet $A_N^{(*)}$ data for DY measurement in the $\pi^- p$ collision process [12]. In both cases, the results are plotted as a function of $q_\perp$, Q, x_N, and x_π. The symbol $^{(*)}$ indicates that the jet A_N data consists of STAR data only.

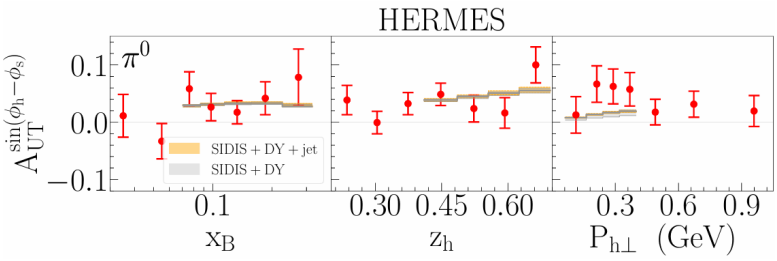

Figure 6.10: The comparison of the fit result without jet $A_N^{(*)}$ data with the fit result with jet $A_N^{(*)}$ data for SIDIS measurements [13] for π^0. In both cases, the results are plotted as a function of x_B, z_h, and $P_{h\perp}$. The symbol $^{(*)}$ indicates that the jet A_N data consists of STAR data only.

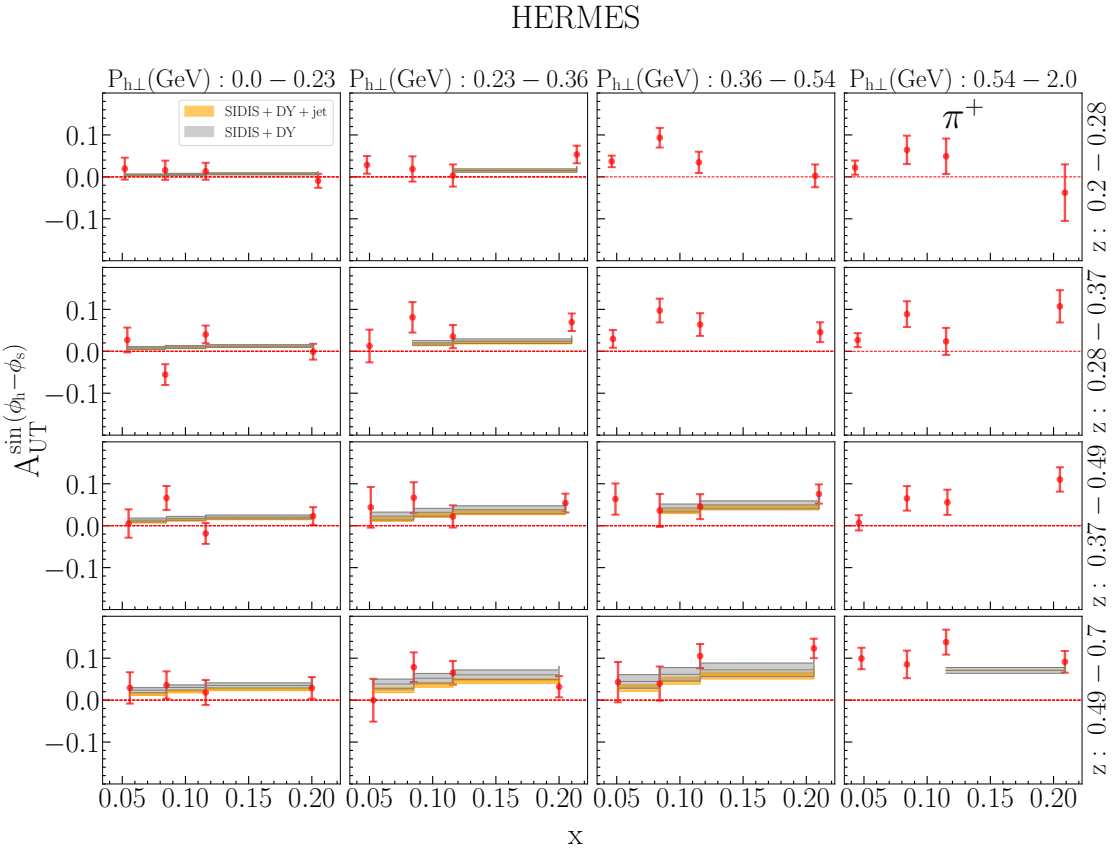

Figure 6.11: The comparison of the fit result without jet $A_N^{(*)}$ data with the fit result with jet $A_N^{(*)}$ data for HERMES π^+ measurement [14]. For both cases, the results are shown for different $P_{h\perp}$- and z-intervals as a function of x. The symbol $^{(*)}$ indicates that the jet A_N data consists of STAR data only.

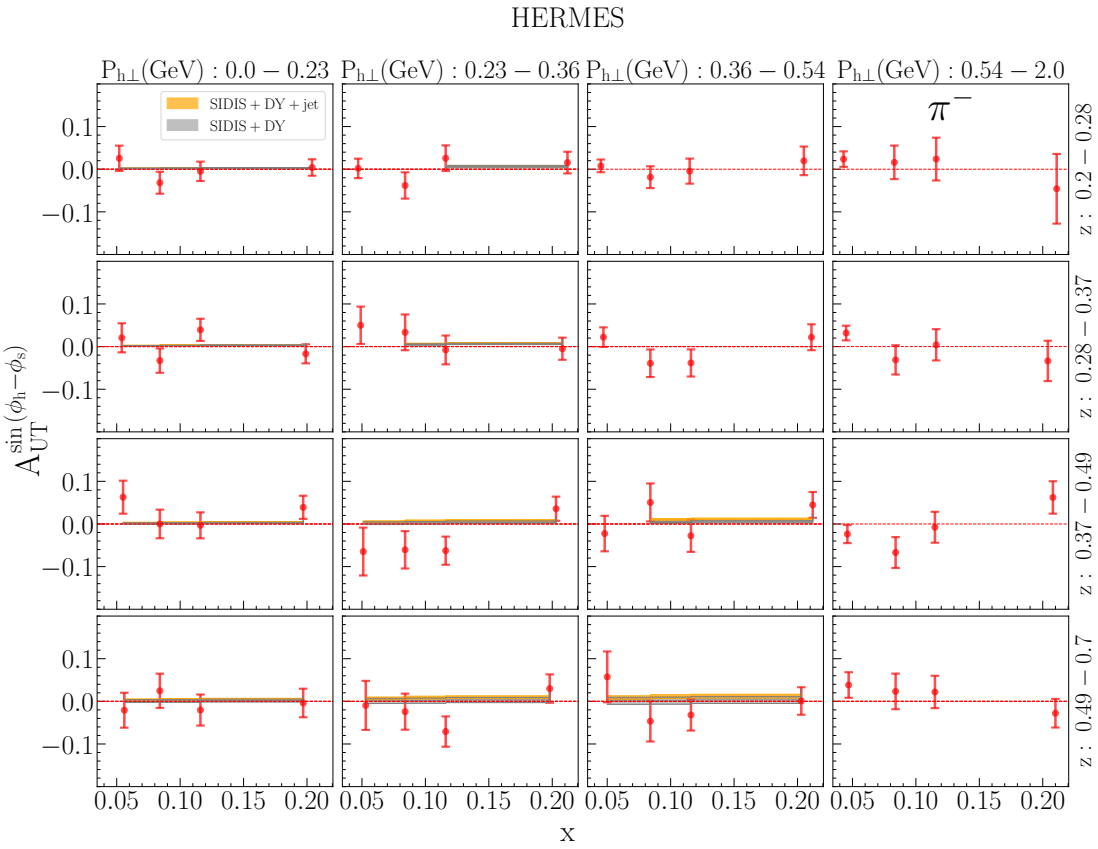

Figure 6.12: The comparison of the fit result without jet $A_N^{(*)}$ data with the fit result with jet $A_N^{(*)}$ data for HERMES π^- measurement [14]. For both cases, the results are shown for different $P_{h\perp}$- and z-intervals as a function of x. The symbol $^{(*)}$ indicates that the jet A_N data consists of STAR data only.

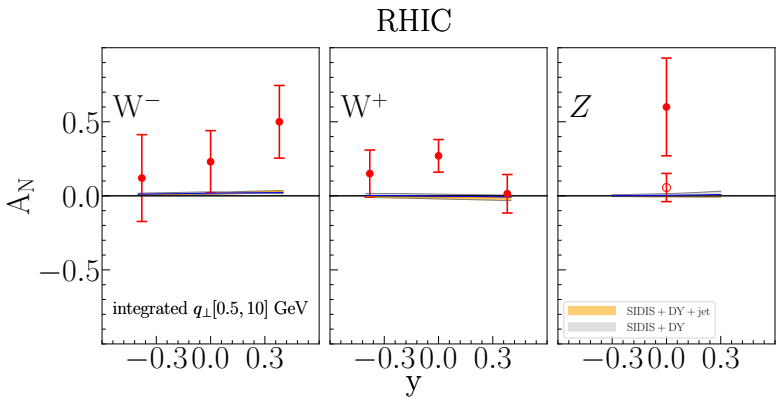

Figure 6.13: The comparison of the fit result with jet $A_N^{(*)}$ data the fit result without jet $A_N^{(*)}$ data for $pp \to W/Z$ measurements [15, 16]. The most recent data for Z is plotted with the empty circle. In both cases, the results are plotted as function of y. The y dependent data integrated in q_T from 0.5 to 10 GeV. The symbol $^{(*)}$ indicates that the jet A_N data consists of STAR data only.

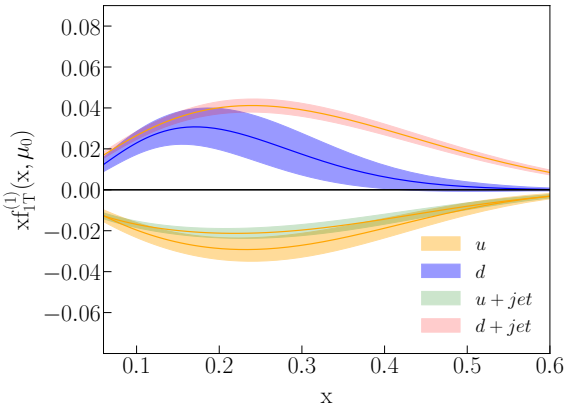

Figure 6.14: The first moment of the Sivers function with and without STAR jet data (also referred to as jet $A_N^{(*)}$ data) as a function of x.

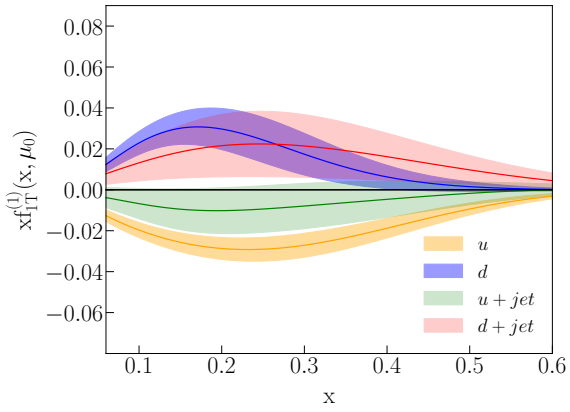

Figure 6.15: The first moment of the sivers function with and without STAR+AnDY jet data (also referred to as jet $A_N^{(*+A)}$ data) as a function of x.

Figure (6.4) shows the A_N for the fit result without jet A_N data and the fit result with jet A_N data in comparison with RHIC data at 200 and 500 GeV for different ranges of jet rapidity η_{jet} and mean jet rapidity $\langle\eta_{jet}\rangle$. This involves STAR measurement at $\sqrt{s}$ = 200 GeV,($3.0 < \eta_{jet} < 3.5$) and $\sqrt{s}$ = 500 GeV, ($3.4 < \eta_{jet} < 3.7$) and AnDY measurement at $\sqrt{s}$ = 500 GeV, ($\langle\eta_{jet}\rangle = 3.31$). It can be seen that the fit result with jet A_N data agree very well with RHIC data for each center-of-mass energy. In addition, the comparison of fit result

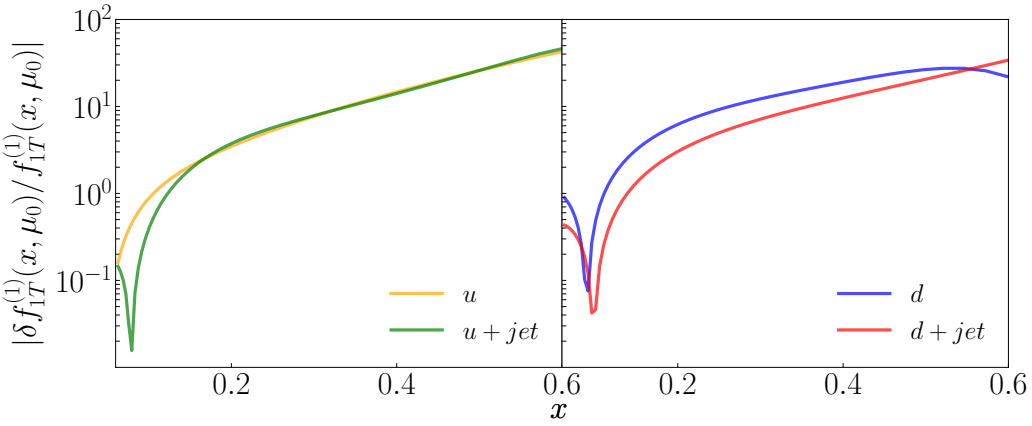

Figure 6.16: The comparison of the ratio of uncertainty of first moment of the Sivers function with jet $A_N^{(*)}$ data and the ratio of uncertainty of the first moment of the Sivers function without jet $A_N^{(*)}$ data. In both cases, the results for u- and d-quarks are plotted as function of x.

without jet A_N data with the fit result with jet A_N data shows that the inclusion of jet A_N data has a tendency to reduce the uncertainty.

Table (6.3) shows the values for fit parameters from both fit with and without jet A_N along with the corresponding χ^2/dof. The uncertainties are obtained by selecting only 68 % of replicas among 201 sets of parameters. Table (6.3) shows that χ^2/dof for the fit without jet A_N data is slightly less than χ^2/dof for the fit with jet A_N data.

Figures (6.5), and (6.6) show the plots of the Sivers asymmetry for different hard scale intervals, $1 < Q^2 < 4$, $4 < Q^2 < 6.25$, $6.25 < Q^2 < 16$, and $16 < Q^2 < 81$ GeV^2 for the fit without jet $A_N^{(*)}$ data and the fit with jet $A_N^{(*)}$ data. Figure (6.5) shows the fit result for the production of hadron h^+, and Figure (6.6) shows the fit result for the production of hadron h^-. For each interval, the asymmetry is plotted as a function of the momentum fractions x_B, z_h, and hadron transverse momentum $P_{h\perp}$. While there is a slight change attributed to the jet $A_N^{(*)}$ data, in both cases, the results show that the fitted asymmetry describe the experimental data very well.

Figure (6.7) shows the plots of the Sivers asymmetry for the hadron production of π^+ , π^-, K^+, K^-, and K^0 for both the fit without jet $A_N^{(*)}$ data and the fit with jet $A_N^{(*)}$ data.

SIDIS+DY	SIDIS+DY+jet
$N_u = 0.068^{+0.015}_{-0.005}$ GeV	$N_u = 0.064^{+0.024}_{-0.074}$ GeV
$N_d = -0.128^{+0.025}_{-0.091}$ GeV	$N_d = -0.267^{+0.290}_{-0.063}$ GeV
$N_s = 0.251^{+0.060}_{-0.147}$ GeV	$N_s = -0.112^{+0.002}_{-3.815}$ GeV
$N_{\bar{u}} = -0.088^{+0.060}_{-0.202}$ GeV	$N_{\bar{u}} = 0.017^{+2.706}_{-0.101}$ GeV
$N_{\bar{d}} = -0.136^{+0.078}_{-0.032}$ GeV	$N_{\bar{d}} = -0.076^{+0.634}_{-0.771}$ GeV
$N_{\bar{s}} = 0.044^{+0.236}_{-0.455}$ GeV	$N_{\bar{s}} = 1.200^{+0.047}_{-0.203}$ GeV
$\alpha_u = 0.832^{+0.132}_{-0.178}$	$\alpha_u = 1.323^{+1.817}_{-0.702}$
$\alpha_d = 1.636^{+0.620}_{-0.922}$	$\alpha_d = 1.206^{+1.053}_{-0.092}$
$\beta_u = 2.633^{+1.353}_{-1.092}$	$\beta_u = 4.067^{+0.440}_{-4.563}$
$\beta_d = 7.397^{+2.519}_{-3.998}$	$\beta_d = 1.709^{+1.020}_{-0.175}$
$\alpha_{\text{sea}} = 0.510^{+0.395}_{-0.010}$	$\alpha_{\text{sea}} = 1.002^{+0.187}_{-0.065}$
$\beta_{\text{sea}} = 0.005^{+0.197}_{-0.031}$	$\beta_{\text{sea}} = 0.595^{+0.481}_{-0.017}$
$g_1^T = 0.024^{+0.085}_{-0.014}$ GeV^2	$g_1^T = 0.085^{+0.254}_{-0.154}$ GeV^2
$\chi^2/dof = 1.017$	$\chi^2/dof = 1.145$

Table 6.3: Summary of the results for the fitted parameters and χ^2/dof. From left, the first column shows the result from the fit without jet A_N data, and the second column shows the result from the fit with jet A_N data. The $\pi^- p \to \gamma^* X$ and $pp \to W/ZX$ processes are considered as DY process.

For each hadron, the asymmetry is plotted as a function of the momentum fractions x_B, z_h, and hadron transverse momentum $P_{h\perp}$. Similar to Figures (6.5) and (6.6), the comparison between the two cases shown in Figure (6.7) also indicates a slight change attributed to the jet $A_N^{(*)}$ data. In both cases, the fitted asymmetry describes the experimental data very well.

Figure (6.8) shows the plots of the Sivers asymmetry for π^-, and π^+ for the fit without jet $A_N^{(*)}$ data and the fit with jet $A_N^{(*)}$ data. The experimental data for the production of π^- and π^+ was obtained using the neutron target. In both cases, the results are plotted as function of the momentum fraction x_B. The comparison between the fit result without jet $A_N^{(*)}$ data and the fit result with jet $A_N^{(*)}$ data shows a difference that is attributed to the jet

$A_N^{(*)}$ data.

Figure (6.9) shows the plots of the Sivers asymmetry for the fit without jet $A_N^{(*)}$ data and the fit with jet $A_N^{(*)}$ data. In both cases, the results are plotted as function of transverse momentum q_T, invariance mass Q, Feynman variable x_F=$x_\pi - x_N$, momentum fraction x_N in the nucleon target, and momentum fraction x_π in the pion target respectively. The effect of jet $A_N^{(*)}$ generates a slight difference, but the results from both cases show that the fitted asymmetry agrees with the experimental data very well.

Figure (6.10) shows the plot of the Sivers asymmetry for π^0 production for the fit without the inclusion of jet $A_N^{(*)}$ data and the fit with jet $A_N^{(*)}$ data. Both fit results are shown as function of x_B, z_h, and $P_{h\perp}$. The comparison shows that both fit results agree very well with the experiment result. The jet $A_N^{(*)}$ data induces a change but the impact is easily noticeable for the fit results as function of $P_{h\perp}$.

Figures (6.11), and (6.12) show the plots of the Sivers asymmetries for π^+, and π^- productions for the fit without jet $A_N^{(*)}$ data and the fit with jet $A_N^{(*)}$ data. For both cases, the fit results are shown for different $P_{h\perp}$- and z-interval ranges as a function of x. In both case, the results show that the fitted asymmetry describes the experimental data very well. In addition, the comparison shows a difference that is attributed to the effect of the jet $A_N^{(*)}$ data. This difference becomes more noticeable in the large z-region.

Figure (6.13) shows the plots of the $A_N^{(*)}$ asymmetry for W^-, W^+, and Z vector bosons for the fit without jet $A_N^{(*)}$ data and the fit with jet $A_N^{(*)}$ data. In both cases, the results are plotted as function of the rapidity y. The most recent data for the Z vector boson [14] is plotted with the empty circle. The transverse momentum of the vector boson is integrated over the range $0.5 < q_\perp < 10$ GeV. In both cases, the uncertainty band is very small especially for for W^- and Z vector bosons. The result also shows that the change due to the jet A_N $^{(*)}$ data is more noticeable for W^+.

The Figure (6.14) shows the plots for the extracted first transverse moment of the Sivers function for u- and d-quarks, $f_{1T}^{\perp(1)}(x, \mu_0)$, and uncertainty bands with and without jet $A_N^{(*)}$

data. And Figure (6.15) shows the plots for the extracted first transverse moment of the Sivers function for u- and d-quarks, $f_{1T}^{\perp(1)}(x,\mu_0)$, and uncertainty bands with and without jet $A_N^{(*+A)}$ data. The first transverse moment of the Sivers function is plotted as function of x at the initial scale $\mu_0 = \sqrt{1.9}$ GeV. In each case, the Sivers d function is positive and the Sivers u function is negative, and the magnitude of the Sivers d function is greater than that of the Sivers u function. The results in both Figure (6.14) and Figure (6.15) clearly show the opposite effect of the jet $A_N^{(*)}$ data and $A_N^{(*+A)}$ data, respectively. The x_F-interval for both jet $A_N^{(*)}$ data and $A_N^{(*+A)}$ data is roughly the large x-region, $0.2 \leq x_F \leq 0.6$. While the jet $A_N^{(*+A)}$ data increases the uncertainty, it can be seen that the jet $A_N^{(*)}$ data reduces significantly the uncertainty on the quark sivers function. The reduction of the uncertainty is an indication that the jet $A_N^{(*)}$ data provides an important information about the quark Sivers function in the large x-region. The result also indicates that the jet $A_N^{(*)}$ data provides a significant complementary information to the low x-region, and there is an excellent compatibility between the jet $A_N^{(*)}$ data and other data. Figure (6.16) shows the comparison of the ratio of uncertainty for the first moment of the Sivers function from the fit with the jet $A_N^{(*)}$ data with that of the Sivers function without the jet $A_N^{(*)}$ data. We realize that the result in Figure (6.16) agrees with result in Figure (6.14), for instance, in the region of roughly $0.2 \leq x \leq 0.5$, there is a significant reduction of uncertainty for d-quarks.

6.4 Conclusions

In this article, we studied for the first time the impact of jet A_N data on the quark Sivers function at NLO+NNLL within the TMD factorization formalism. To achieve this, we first extracted the quark Sivers function from the Sivers asymmetry with and without the jet A_N data, and we then compared the extracted quark Sivers function without the inclusion of jet A_N data with the extracted quark Sivers function with the inclusion of jet A_N data. We found that the inclusion of the jet $A_N^{(*)}$ data allowed to improve and extend the knowledge

of the quark Sivers function in the large x-region which was not explored in other data, the jet $A_N^{(*)}$ data led to the remarkable constraint and reduction of the uncertainty on the Sivers function in such large x-region, especially for d quarks. Our finding was obtained using the most recent experimental data, but we expect that future high-precision measurements with reduced uncertainties at COMPASS, JLAB, RHIC or the future EIC [117, 118] will further constrain the Sivers function. This will allow to gather more information on the impact of the jet $A_N^{(*)}$ data on the Sivers function which is crucial in the model-dependent determination of the nucleon spin.

Chapter 7

Simultaneous extraction of Collins fragmentation function in TMD physics

7.1 Introduction

This chapter is partially based on the paper titled 'A simultaneous global extraction of the Collins function in e^+e^- collisions, semi-inclusive DIS, and hadron-in-jet production', in preparation to submit to JHEP, authored by Zhong-Bo Kang, Fidele J. Twagirayezu, and Yiyu Zhou.

Transverse momentum dependent functions (TMDs) are important objects in TMD physics because they allow to acquire the three-dimensional representation of the internal nucleon structure. In addition, TMDs can facilitate a better understanding of QCD properties such as hadronization described by fragmentation function . The TMD function that describes the hadronization of a transversely polarized hadron into unpolarized hadron is the Collins fragmentation function [70]. The Collins effect is experimentally measurable with Collins asymmetry. The Collins effect can be studied in the semi-inclusive deep inelas-

tic scattering (SIDIS) process [10, 11, 15, 119] where the Collins fragmentation function is coupled to the transversity distribution. The modulation is proportional of $\sin(\phi_s + \phi_h)$ where ϕ_s is the azimuthal angle of the transverse spin of the nucleon and ϕ_h is the azimuthal angle of the hadron transverse momentum in the final state with respect to the reaction plane. The collins effect can be studied in di-hadron productions in semi-inclusive electron-positron annihilation [120, 121, 122, 123]. In the hadronic-plane method, the modulation is proportional to $\cos(2\phi_0)$ where ϕ_0 is the azimuthal angle between the two hadrons. In addition, the Collins effect can be studied in hadron production in a highly energetic jets in proton-proton collisions [124]. For the universality property, the Collins fragmentation function is the same in the SIDIS process and electron-positron annihilation [125]. Also, Kang *et al.*[19] showed the universality of the Collins fragmentation function in hadron production inside jets in proton-proton collisions. To test further the universality property of the Collins fragmentation function, we establish a formalism to extract the Collins fragmentation function from the combination of SIDIS process, electron-positron annihilation and hadron production inside jets in proton-proton collisions.

7.2 Collins Formalism

This section we present the TMD factorization formalism for the Collins asymmetry in semi-inclusive deep inelastic scattering (SIDIS), electron-positron (e^+e^-) processes, and hadron in jet production from proton-proton (pp) collisions. The Collins formalism in SIDIS is presented in (7.2.1), the Collins formalism in e^+e^- process is presented in (7.2.2), and the Collins formalism for hadron in jet production from pp collisions is presented in (7.2.3) respectively.

7.2.1 Collins formalism in SIDIS

We consider an electron e that scatters on a polarized proton p, by exchanging a virtual photon of momentum q, and produce a hadron h in the final state.

$$e(l) + p(P) \rightarrow e(l') + h(P_h) + X \tag{7.1}$$

The exchanged momentum q is directly related to the hard scale Q through the invariant mass, $-q^2 = Q^2$.

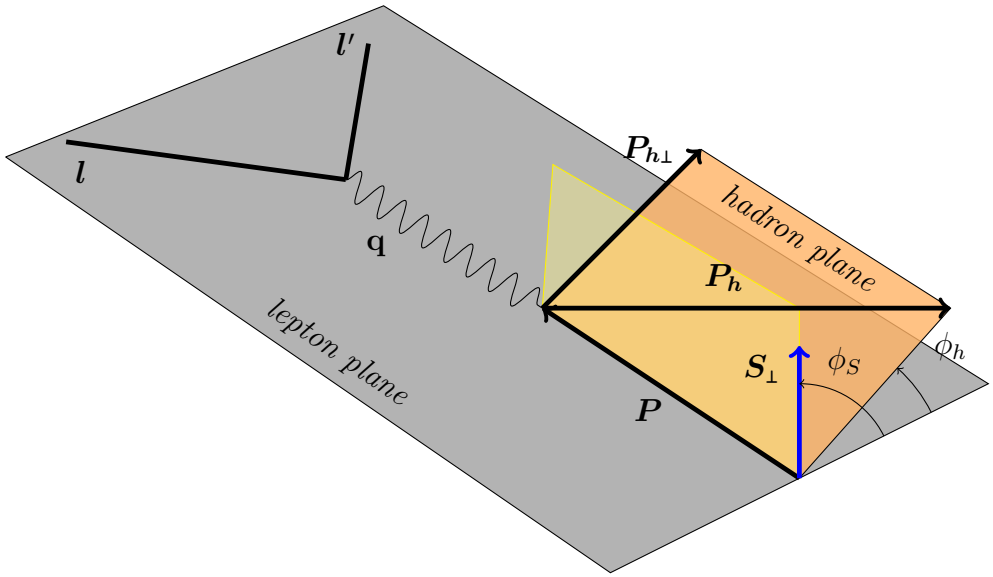

Figure 7.1: The kinematics for Semi-Inclusive DIS. The exchanged photon carries a momentum q. The quantity $\mathbf{S}_\perp$ is the transverse polarization of the proton, ϕ_S is the azimuthal angle between $\mathbf{S}_\perp$ and the lepton plane, and ϕ_h is the azimuthal angle between the hadron plane and the lepton plane. In this case, the modulation depends on the sum of azimuthal angles.

The Collins asymmetry is defined as

$$A_{\mathrm{UT}}^{\sin(\phi_h+\phi_s)} = D_{\mathrm{NN}} \frac{F_{\mathrm{UT}}^{\sin(\phi_h+\phi_s)}}{F_{\mathrm{UU}}}, \tag{7.2}$$

where $D_{\rm NN}$ is the depolarization factor which is given by

$$D_{\rm NN} = \frac{2(1-y)}{1+(1-y)^2}\,, \tag{7.3}$$

while $F_{\rm UU}$ and $F_{\rm UT}^{\sin(\phi_h+\phi_s)}$ denote the unpolarized and polarized structure functions. These structure functions are related to the cross section for Semi-Inclusive DIS as

$$\frac{d\sigma}{d\mathcal{PS}_{\rm DIS}} = \sigma_0(x,y,Q^2)\Big[F_{\rm UU} + \sin(\phi_h+\phi_s) D_{\rm NN}\, F_{\rm UT}^{\sin(\phi_h+\phi_s)} + \cdots,\Big] \tag{7.4}$$

where the dots denote additional structure functions that do not contribute to the Collins asymmetry. The quantity, $\sin(\phi_h+\phi_s)$, is the modulation in the Collins formalism. In this expression, $d\mathcal{PS}_{\rm DIS}$ denotes the phase space, which is given by

$$d\mathcal{PS}_{\rm DIS} = dxdydzd^2\boldsymbol{P}_{h\perp} \tag{7.5}$$

where we have the usual parton fraction variables defined as

$$x = \frac{Q^2}{2P\cdot q}\,, \qquad y = \frac{P\cdot q}{P\cdot l}\,, \qquad z = \frac{P\cdot P_h}{P\cdot q}\,, \tag{7.6}$$

while $P_{h\perp}$ denotes the transverse momentum of the final-state hadron. The structure functions in Eq. (7.4) can be written as convolutions of TMDs as

$$F_{\rm UU} = \mathcal{C}_{\rm DIS}\left[f\,D\right]\,, \qquad F_{\rm UT}^{\sin(\phi_h+\phi_s)} = \mathcal{C}_{\rm DIS}\left[\frac{\hat{P}_{h\perp}\cdot\mathbf{p}_\perp}{zM_h} h_1\, H_1^\perp\right], \tag{7.7}$$

where the convolution integral is given by

$$\begin{aligned}\mathcal{C}_{\rm DIS}[c\,A\,B] = H_{\rm DIS}(Q,\mu)\sum_q e_q^2 \int d^2\boldsymbol{k}_\perp d^2\boldsymbol{p}_\perp\, \delta^2(z\mathbf{k}_\perp + \mathbf{p}_\perp - \mathbf{P}_{\mathbf{h}\perp}) c(\mathbf{k}_\perp,\mathbf{p}_\perp,\hat{\mathbf{P}}_{\mathbf{h}\perp}) \\ \times A_{q/p}(x,k_\perp,\mu,\zeta_1)\, B_{h/q}(z,p_\perp,\mu,\zeta_2)\,,\end{aligned} \tag{7.8}$$

where c denotes an arbitrary kinematic prefactor, A denotes a TMD PDF and B denotes a TMD FF. Namely, f_1 and D_1 denote the unpolarized TMD PDF and TMD FF, while h_1 and $H_1^\perp$ denote the transversity TMD PDF and the Collins fragmentation function. Additionally, $\mathbf{k}_\perp$ denotes the transverse momentum of the incoming quark with respect to the incoming hadron, while $\mathbf{p}_\perp$ denotes the transverse momentum of the final-state hadron with respect to the fragmenting quark. These convolution integrals can be simplified by working in b-space, the conjugate space to $-\mathbf{P}_{h\perp}/z$. After converting these convolutions to b-space, we have the expression for the unpolarized structure function

$$F_{\mathrm{UU}} = H_{\mathrm{DIS}}(Q,\mu)\sum_q e_q^2 \int \frac{bdb}{2\pi} J_0(b\,P_{h\perp}/z) f_{1\,q/p}(x,b,\mu,\zeta_1) D_{1\,q/p}(z,b,\mu,\zeta_2)\,, \tag{7.9}$$

where J_0 is the zeroth Bessel function of the first kind. In this expression, we have introduced and we have introduced H_{DIS}, the hard function for DIS, as well as the b-dependent TMDs, which are defined as

$$f_{1\,q/p}(x,b,\mu,\zeta) = \int d^2\boldsymbol{k}_\perp e^{-i\boldsymbol{b}\cdot\boldsymbol{k}_\perp} f_{1\,q/p}(x,k_\perp,\mu,\zeta)\,, \tag{7.10}$$

$$D_{1\,h/q}(z,b,\mu,\zeta) = \frac{1}{z^2}\int d^2\boldsymbol{p}_\perp e^{-i\boldsymbol{b}\cdot\boldsymbol{p}_\perp/z} D_{1\,h/q}(z,p_\perp,\mu,\zeta)\,. \tag{7.11}$$

For the unpolarized TMDs, we can perturbatively match them onto the collinear distributions as follows

$$\begin{aligned} f_{1\,q/p}(x,b,\mu,\zeta_1) &= [C\otimes f](x,b,\mu,\zeta_1)\,,\\ D_{1\,q/p}(z,b,\mu,\zeta_2) &= \frac{1}{z^2}[\hat{C}\otimes D](z,b,\mu,\zeta_2)\,, \end{aligned} \tag{7.12}$$

where the convolutions for the TMD PDFs and TMD FFs are given by

$$[C \otimes A](x, b, \mu, \zeta) = \sum_i \int_x^1 \frac{d\hat{x}}{\hat{x}} C_{q/i}(\frac{x}{\hat{x}}, b, \mu, \zeta)\, A_{i/p}(\hat{x}, \mu)\,, \tag{7.13}$$

$$[\hat{C} \otimes B](z, b, \mu, \zeta) = \sum_i \int_z^1 \frac{d\hat{z}}{\hat{z}} \hat{C}_{i/q}(\frac{z}{\hat{z}}, b, \mu, \zeta)\, B_{h/i}(\hat{z}, \mu)\,. \tag{7.14}$$

These operator product expansions involve large logarithms which must be resummed. This resummation is captured by the perturbative Sudakov term

$$S_{\text{pert}}(b, \mu_i, \zeta_i, \mu_f, \zeta_f) = \int_{\mu_i}^{\mu_f} \frac{d\mu'}{\mu'} \left[\gamma^V + \Gamma_{\text{cusp}} \ln\left(\frac{\zeta_f}{\mu'^2}\right)\right] + D(b, \mu_i) \ln\left(\frac{\zeta_f}{\zeta_i}\right), \tag{7.15}$$

where γ^V, Γ_{cusp}, and D denote the non-cusp, cusp, and rapidity anomalous dimension. In Appendix (B), we have included the expressions for these anomalous dimensions up to NNLL accuracy.

The convolution entering into the polarized structure function can also be simplified by working in b-space as

$$F_{\text{UT}}^{\sin(\phi_h+\phi_s)} = -\frac{1}{2z} \sum_q e_q^2\, H_{\text{DIS}}(Q, \mu) \int \frac{b^2 db}{2\pi} J_1(b\, P_{h\perp}/z) h_{1\,q/p}(x, b, \mu, \zeta_1)\, H_{1\,q/p}^{\perp}(z, b, \mu, \zeta_2)\,, \tag{7.16}$$

where we have introduced the b-space spin-dependent TMDs which are defined as Fourier transforms of the momentum space ones

$$h_{1\,q/p}(x, b, \mu, \zeta) = \int d^2k_\perp e^{-i\mathbf{b}\cdot\mathbf{k}_\perp} h_{1\,q/p}\,(x, k_\perp, \mu, \zeta)\,, \tag{7.17}$$

$$H_{1\,h/q}^{\perp\,\alpha}(z, b, \mu, \zeta) = \frac{1}{z^2} \int d^2p_\perp e^{-i\mathbf{b}\cdot\mathbf{p}_\perp/z} \frac{p_\perp^\alpha}{M_h} H_{1\,h/q}^{\perp}\,(z, p_\perp, \mu, \zeta)\,. \tag{7.18}$$

We can once again perform an operator product expansion of these distributions onto

collinear ones

$$h_{1\,,q/p}\left(x,b,\mu,\zeta_1\right) = \left[C^h\otimes,h\right]\left(x,b,\mu,\zeta_1\right)\,. \tag{7.19}$$

We note that there is additional complications associated with the matching of the Collins function. This is due to the prefactor of $p_\perp^\alpha$, which causes the Collins function to match onto a higher twist collinear distributions. The matching procedure can be performed as follows

$$H_{1\,q/p}^{\perp\,\alpha}\left(z,b,\mu,\zeta_2\right) = -\frac{ib^\alpha}{2z}H_{1\,q/p}^{\perp}\left(z,b,\mu,\zeta_2\right)\,, \tag{7.20}$$

$$H_{1\,q/p}^{\perp}\left(z,b,\mu,\zeta_2\right) = \frac{1}{z^2}\left[C^H\otimes H^{(3)}\right]\left(z,b,\mu,\zeta_2\right)\,, \tag{7.21}$$

where the $H^{(3)}$ denotes a twist-3 collinear distribution. As in the case of the unpolarized TMDs, this OPE contains large logarithms which need to be resummed by the perturbative Sudakov in Eq. (7.15). After resumming the large logarithms in the unpolarized and polarized TMDs, we have the expressions for the cross section

$$\begin{aligned} F_{UU}(x,z,P_{h\perp},Q) &= H^{\rm DIS}(Q,\mu_f)\frac{1}{z^2}\int_0^\infty \frac{b\,db}{2\pi}J_0\left(bP_{h\perp}/z\right)\sum_q e_q^2 \\ &\times\Big[C\otimes f_1\Big](x,b,\mu_i,\zeta_i)\Big[\hat{C}\otimes D_1\Big](z,b,\mu_i,\zeta_i) \\ &\times\exp\Big[-2S_{\rm pert}(b,\mu_i,\zeta_i,\mu_f,\zeta_f)-S_{\rm NP}^f(x,b,Q_0,\zeta_f)-S_{\rm NP}^D(z,b,Q_0,\zeta_f)\Big], \end{aligned} \tag{7.22}$$

$$\begin{aligned} F_{UT}^{\sin(\phi_h+\phi_s)}(x,z,P_{h\perp},Q) &= -\frac{1}{z}H^{\rm DIS}(Q,\mu_f)\frac{1}{z^2}\int_0^\infty \frac{b^2\,db}{4\pi}J_1\left(bP_{h\perp}/z\right)\sum_q e_q^2 \\ &\times\Big[C^h\otimes h_1\Big](x,b,\mu_i,\zeta_i)\Big[C^H\otimes H^{(3)}\Big](z,b,\mu_i,\zeta_i) \\ &\times\exp\Big[-2S_{\rm pert}(b,\mu_i,\zeta_i,\mu_f,\zeta_f)-S_{\rm NP}^h(x,b,Q_0,\zeta_f)-S_{\rm NP}^H(z,b,Q_0,\zeta_f)\Big]\,, \end{aligned} \tag{7.23}$$

where one usually takes $\mu_i^2=\zeta_i=\mu_b^2$ and $\mu_f^2=\zeta_f=Q^2$. In these expressions, we have introduced the non-perturbative Sudakov terms associated with each TMD as well as the

initial TMD scale Q_0. We will discuss these functions in more depth in Sec. (7.3).

7.2.2 Collins formalism in e^+e^-

In this section we present the Collins formalism of the di-hadron productions in the e^+e^- process,

$$e^+(l_+) + e^-(l_-) \to h_1 h_1 X \tag{7.24}$$

where l_+ and l_- are initial momenta, P_{h1} and P_{h2} are the momenta of hadrons h_1 and h_2 respectively. The center of mass energy is defined as, $S = Q^2 = (l_+ + l_-)^2$. The hard scale Q is expressed in terms of the hadron momentum P_{hi} as, $z_{hi} = 2|P_{hi}|/Q$, where z_{hi} is the longitudinal momentum associated with fragmentation functions. The thrust-axis and hadronic-plane methods are two methods which are frequently utilized to study the collins effects. The thrust-axis method consists of defining a thrust-axis and measure the azimuthal correlation between hadrons, see Figure (7.2), this method corresponds to A_{12} asymmetries. The hadronic-plane method consists of choosing one hadron as a reference to define the azimuthal angle of another hadron, see Figure (7.3); this method that will be the subject of use in our formalism, is the cornerstone for A_0 asymmetries.

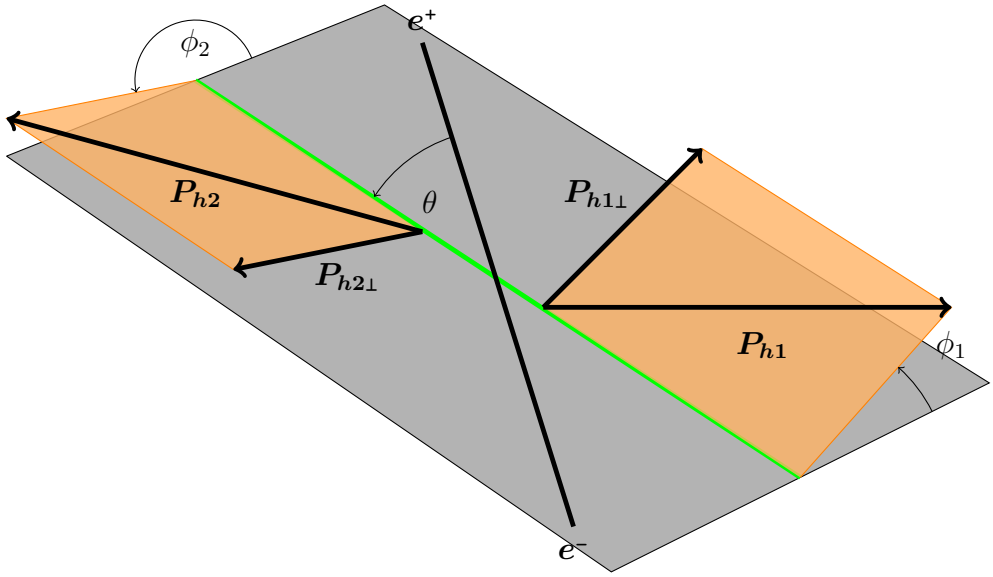

Figure 7.2: The kinematics for double-inclusive annihilation in the thrust-axis method. P_{h1} and P_{h2} are the momenta of the produced hadrons h_1 and h_2 respectively.

In the hadronic-plane method the differential cross section for di-hadron productions in e^+e^- annihilation can be written in terms of the unpolarized structure function $Z_{\rm UU}^{e+e-}$, and the double Collins structure function $Z_{\rm Collins}^{e+e-}$ as follows

$$\frac{d\sigma}{d\mathcal{PS}_{\circledast}} = \sigma_0^{\rm U}\, Z_{\rm UU}^{e+e-} + \cos\left(2\phi_0\right) \sigma_0^{\rm T}\, Z_{\rm Collins}^{e+e-} + \ldots \tag{7.25}$$

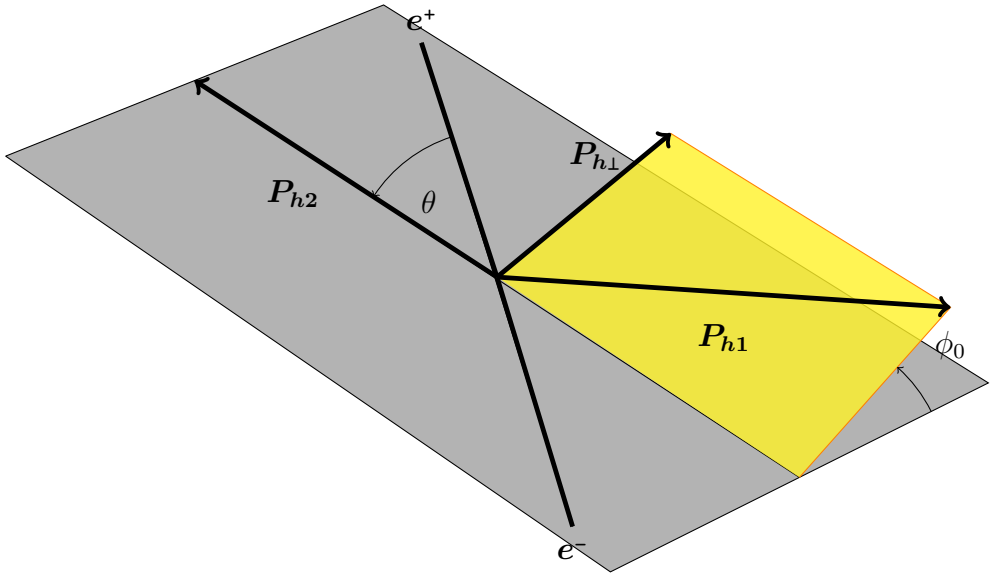

Figure 7.3: The kinematics for double-inclusive annihilation in the hadronic plane method. The hadron h_2 is chosen to be a reference to measure the azimuthal angle ϕ_0 for the hadron h_1.

where the unintegrated phase space is given by $d\mathcal{PS}_{\circledast} = dz_1\, dz_2\, d^2P_{h\perp}\, d\cos\theta$ and the Born cross section for the unpolarized and transversely polarized quarks are given by

$$\sigma_0^{\mathrm{U}} = \frac{N_c \pi \alpha_{\mathrm{em}}^2}{2Q^2}\left(1+\cos^2\theta\right), \qquad \sigma_0^{\mathrm{T}} = \frac{\sin^2\theta}{1+\cos^2\theta}\sigma_0^{\mathrm{U}}. \tag{7.26}$$

The structure functions can be written as a convolution of the unpolarized TMD FF and the Collins function as

$$\begin{aligned} Z_{\mathrm{UU}}^{e+e-} &= \mathcal{C}\left[D_1\, D_2\right], \\ Z_{\mathrm{Collins}}^{e+e-} &= \mathcal{C}\left[\frac{1}{z_{h1} z_{h2} M_1 M_2}\left(2\hat{P}_{h\perp}\cdot\mathbf{p}_{1\perp}\hat{P}_{h\perp}\cdot\mathbf{p}_{2\perp} - \mathbf{p}_{1\perp}\cdot\mathbf{p}_{2\perp}\right) H_1^{\perp}\, H_2^{\perp}\right], \end{aligned} \tag{7.27}$$

where the convolution for e^+e^- is given by

$$\mathcal{C}\left[c\, B_1\, B_2\right] = \sum_q e_q^2\, H\left(Q,\mu\right) \int d^2p_{1\perp}\, d^2p_{2\perp}\, \delta^2\left(\mathbf{P}_{h\perp} - \mathbf{p}_{1\perp} - \frac{z_{h1}}{z_{h2}}\mathbf{p}_{2\perp}\right) \times c\left(\mathbf{p}_{1\perp}, \mathbf{p}_{1\perp}, \hat{P}_{h\perp}\right)\, B_{q/h_1}\left(z_{h1}, p_{1\perp}, \mu, \zeta_1\right)\, B_{q/h_2}\left(z_{h2}, p_{2\perp}, \mu, \zeta_2\right)\,. \tag{7.28}$$

By Fourier transform, the structure functions for the unpolarized and double Collins asymmetries take the following form, from the b-space to the momentum space.

$$Z_{\mathrm{UU}}^{e+e-} = \frac{1}{z_{h1}^2} H_{\mathrm{U}}(Q,\mu) \int \frac{d^2b}{\left(2\pi\right)^2} e^{i\mathbf{b}\cdot\mathbf{P}_{h\perp}/z_1} \sum_q e_q^2 \times D_{h_1/q}\left(z_{h1}, b, \mu, \zeta_1\right)\, D_{h_2/\bar{q}}\left(z_{h2}, b, \mu, \zeta_2\right)\,, \tag{7.29}$$

$$Z_{\mathrm{Collins}}^{e+e-} = \frac{1}{z_{h1}^2} H_{\mathrm{C}}(Q,\mu) \int \frac{d^2b}{\left(2\pi\right)^2} e^{i\mathbf{b}\cdot\mathbf{P}_{h\perp}/z_1} \sum_q e_q^2 \left(2\hat{P}_{h\perp}^{\alpha}\, \hat{P}_{h\perp}^{\beta} - g_{\perp}^{\alpha\beta}\right) \times H_{1\, h_1/q}^{\perp\,\alpha}\left(z_{h1}, b, \mu, \zeta_1\right)\, H_{1\, h_2/\bar{q}}^{\perp\,\beta}\left(z_{h2}, b, \mu, \zeta_2\right)\,. \tag{7.30}$$

After performing the OPE for the TMDs and resumming the large logs, the expressions for

the structure functions are given by

$$Z_{\rm UU}^{e+e-}(P_{h\perp},Q) = H_{\rm U}(Q,\mu_f)\int_0^\infty \frac{b\,db}{2\pi} J_0\left(bP_{h\perp}/z_{h1}\right)\sum_q e_q^2 \\ \times\left[\hat{C}^D\otimes D_1\right](z_{h1},b,\mu_i,\zeta_i)\left[\hat{C}^D\otimes D_1\right](z_{h2},b,\mu_i,\zeta_i) \\ \times\exp\Big[-2S_{\rm pert}(b,\mu_i,\zeta_i,\mu_f,\zeta_f) - S_{\rm NP}^D(z_{h1},b,Q_0,\zeta_f) - S_{\rm NP}^D(z_{h2},b,Q_0,\zeta_f)\Big], \tag{7.31}$$

$$Z_{\rm Collins}^{e+e-}(P_{h\perp},Q) = -\frac{1}{z_{h1}^2}\frac{1}{z_{h1}z_{h2}}H_{\rm C}(Q,\mu_f)\int_0^\infty \frac{b^3\,db}{8\pi} J_2\left(bP_{h\perp}/z\right)\sum_q e_q^2 \\ \times\left[\delta C^C\otimes H^{(3)}\right](x,b,\mu_i,\zeta_i)\left[\delta C^C\otimes H^{(3)}\right](z,b,\mu_i,\zeta_i) \\ \times\exp\Big[-2S_{\rm pert}(b,\mu_i,\zeta_i,\mu_f,\zeta_f) - S_{\rm NP}^C(z_{h1},b,Q_0,\zeta_f) - S_{\rm NP}^C(z_{h2},b,Q_0,\zeta_f)\Big]. \tag{7.32}$$

To eliminate false asymmetries, BELLE and BABAR consider the ratios of unlike-sign "U" , like "L", and conjugate "C" pion pairs in the asymmetries.

$$\mathrm{U}\equiv\left(\pi^+\pi^- + \pi^-\pi^+\right), \qquad \mathrm{L}\equiv\left(\pi^+\pi^+ + \pi^-\pi^-\right), \qquad \mathrm{C}\equiv\left(\pi^+\pi^+ + \pi^-\pi^- + \pi^+\pi^- + \pi^-\pi^+\right). \tag{7.33}$$

The asymmetries $A_0^{\rm UL}$ and $A_0^{\rm UC}$ are written as

$$A_0^{\rm UL}\left(z_{h1},z_{h2},\theta,P_{h\perp}\right) = \frac{\sin^2\theta}{1+\cos^2\theta}\left(P_U - P_L\right), \tag{7.34}$$

$$A_0^{\rm UC}\left(z_{h1},z_{h2},\theta,P_{h\perp}\right) = \frac{\sin^2\theta}{1+\cos^2\theta}\left(P_U - P_C\right) \tag{7.35}$$

where

$$P_U = Z_{\rm COL,U}^{\cos(2\phi_0)}/Z_{\rm UU,U}, \qquad P_L = Z_{\rm COL,L}^{\cos(2\phi_0)}/Z_{\rm UU,L}, \qquad P_C = Z_{\rm COL,C}^{\cos(2\phi_0)}/Z_{\rm UU,C}. \tag{7.36}$$

Here, the subscript COL is simply a shorthand notation for Collins. Similarly, one can define the $P_{h\perp}$-integrated asymmetries as

$$A_0^{\mathrm{UL}}\left(z_{h1}, z_{h2}, \theta\right) = \frac{\sin^2\theta}{1+\cos^2\theta}\left(\frac{\int P_{h\perp} dP_{h\perp} Z_{\mathrm{COL,U}}^{\cos(2\phi_0)}}{\int P_{h\perp} dP_{h\perp} Z_{\mathrm{UU,U}}} - \frac{\int P_{h\perp} dP_{h\perp} Z_{\mathrm{COL,L}}^{\cos(2\phi_0)}}{\int P_{h\perp} dP_{h\perp} Z_{\mathrm{UU,L}}}\right), \tag{7.37}$$

$$A_0^{\mathrm{UC}}\left(z_{h1}, z_{h2}, \theta\right) = \frac{\sin^2\theta}{1+\cos^2\theta}\left(\frac{\int P_{h\perp} dP_{h\perp} Z_{\mathrm{COL,U}}^{\cos(2\phi_0)}}{\int P_{h\perp} dP_{h\perp} Z_{\mathrm{UU,U}}} - \frac{\int P_{h\perp} dP_{h\perp} Z_{\mathrm{COL,C}}^{\cos(2\phi_0)}}{\int P_{h\perp} dP_{h\perp} Z_{\mathrm{UU,C}}}\right). \tag{7.38}$$

For the structure function $Z_{uu}^{e^+e^-}$, the hard factor H_U is the same as that for Drell-Yan lepton pair production but differs for SIDIS. The reason for this is that the virtual photon is time-like ($q^2 > 0$) in e^+e^- and Drell-Yan processes, whereas in SIDIS, the virtual photon is space-like ($q^2 < 0$). Additionally, the hard part H_C of the structure function $Z_{\mathrm{Collins}}^{e^+e^-}$ is the same as that of the structure function $Z_{uu}^{e^+e^-}$ due to the spin-independence of hard interaction in perturbative QCD.

7.2.3 Collins formalism for hadron-in-jet production from proton-proton *pp* collisions

We consider the hadron azimuthal distribution inside jets in transversely polarized $p^{\uparrow}p$ collisions,

$$p^{\uparrow}(P_A, S_T, \phi_{S_A}) + p(P_B) \rightarrow jet(\eta, p_T) h(z_h, j_\perp, \phi_h) + X, \tag{7.39}$$

where P_A is the four-momentum of a transversely polarized proton with a transverse polarization vector S_T moving the $+z$-direction, and P_B is the four-momentum of unpolarized proton moving in the $-z$-direction. The azimuthal angle of S_T with respect to the reaction plane is denoted by ϕ_{S_A}. For the jet function, η is the rapidity, and p_T is the transverse momentum of a jet in the final state. For the hadron function, z_h is the momentum fraction

of a hadron, j_T is the transverse momentum of a hadron inside a jet which forms an angle ϕ_h with the reaction plane. Here, $j_\perp$ is defined with respect to the standard jet axis, the choice of this type of axis is due to the fact that it allows a direct relation to the transverse momentum fragmentation functions (TMDFFs).

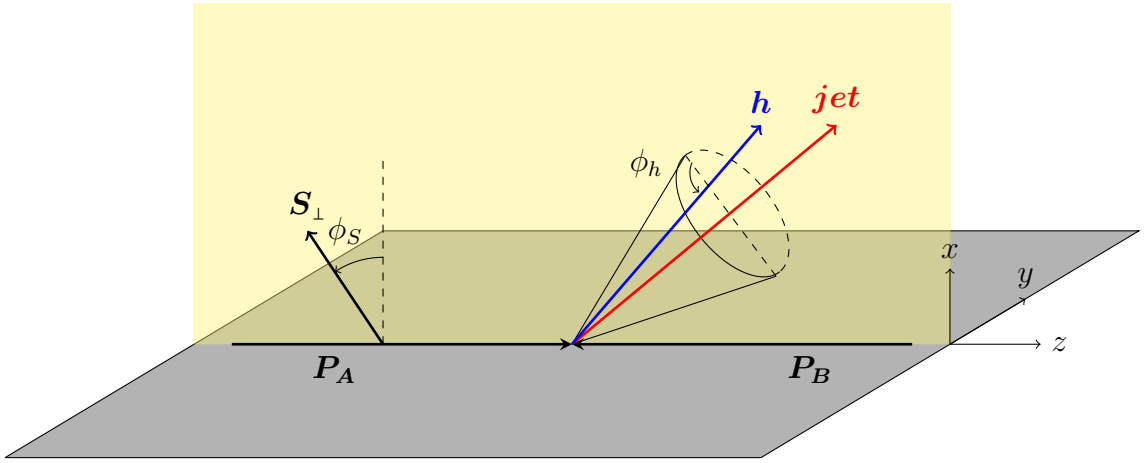

Figure 7.4: Illustration for single inclusive jet production in transversely polarized proton-proton collisions, $p(P_A, \mathbf{S}_\perp) + p(P_B) \to h(\eta, p_T)\text{jet}(z_h, j_\perp, \phi_h) + X$. The azimuthal angle of the transverse spin vector, $\mathbf{S}_\perp$, with respect to the reaction plane is denoted by ϕ_S.

The differential cross-section of hadron azimuthal distribution inside jets in transversely polarized $p^\uparrow p$ collisions can be expressed as

$$\frac{d\sigma}{d\eta d^2p_T dz_h d^2j_\perp} = F_{\mathrm{UU}} + \sin(\phi_S - \phi_h) F_{\mathrm{UT}}^{\sin(\phi_S-\phi_h)} + \cdots, \tag{7.40}$$

where the dots contain additional asymmetries which do not contribute to the Collins asymmetry. Once again F_{UU} and $F_{\mathrm{UT}}^{\sin(\phi_S-\phi_h)}$ denote the spin averaged and spin-dependent structure functions respectively. The Collins azimuthal spin asymmetry can be expressed in terms of structure functions F_{UU} and $F_{\mathrm{UT}}^{\sin(\phi_S-\phi_h)}$ as follows

$$A_{\mathrm{UT}}^{\sin(\phi_S-\phi_h)}(z_h, j_\perp, \eta, p_T) = \frac{F_{\mathrm{UT}}^{\sin(\phi_S-\phi_h)}}{F_{\mathrm{UU}}}. \tag{7.41}$$

The structure functions F_{UU} and $F_{\mathrm{UT}}^{\sin(\phi_S-\phi_h)}$ depend on z_h, $j_\perp$, η, and p_T, but we will

omit η and p_T for simplicity. The QCD factorization at the lowest approximation or leading order (LO) leads to the following expressions for the structures functions

$$F_{\rm UU}(z_h, j_\perp) = \frac{\alpha_s^2}{s} \sum_{a,b,c} \int_{\tilde{x}_1}^1 \frac{dx_1}{x_1} f_{a/A}(x_1,\mu) \int_{\tilde{x}_2}^1 \frac{dx_2}{x_2} f_{b/B}(x_2,\mu) D_{h/c}(z_h, j_\perp, \mu, \zeta_J) \times H^{\rm U}_{ab\to c}(\hat{s},\hat{t},\hat{u},\mu)\,\delta(\hat{s}+\hat{t}+\hat{u}), \tag{7.42}$$

$$F_{\rm UT}^{\sin(\phi_{\rm S}-\phi_{\rm h})}(z_h, j_\perp) = \frac{\alpha_s^2}{s} \sum_{a,b,c} \int_{\tilde{x}_1}^1 \frac{dx_1}{x_1} h_1^a(x_1,\mu) \int_{\tilde{x}_2}^1 \frac{dx_2}{x_2} f_{b/B}(x_2,\mu) \frac{j_\perp}{z_h M_h} H^\perp_{1h/c}(z_h, j_\perp, \mu, \zeta_J) \times H^{\rm Collins}_{ab\to c}(\hat{s},\hat{t},\hat{u},\mu)\,\delta(\hat{s}+\hat{t}+\hat{u}). \tag{7.43}$$

The factorization for the above structure functions involves two steps: the first step is a collinear factorization for the production of the jet and the second step is a TMD factorization for the hadron $j_\perp$-distribution inside the jet. The factorized form for the above structure functions was derived within the standard soft-collinear effective theory (SCET). The hard function $H^U_{ab\to c}$ is related to the unpolarized structure function and the hard function $H^{\rm Collins}_{ab\to c}$ is related to the Collins fragmentation function. The sum is taken over all relevant channels $ab \to c$. The center of mass energy squared is defined by $s = (P_A + P_B)^2$ and M_h is the observed hadron mass inside a jet. The strong coupling constant is denoted by α_s and $\hat{s}$, $\hat{t}$, and $\hat{u}$ are the usual partonic Mandelstam variables. In terms of p_T and η, the Mandelstam variables $\hat{u}$ and $\hat{t}$ are expressed as

$$\hat{u} = -x_1 p_T \sqrt{s} e^{-\eta}, \qquad \hat{t} = -x_2 p_T \sqrt{s} e^{\eta}, \tag{7.44}$$

where x_1 and x_2 are momentum fractions. In the parton massless limit, the expression for the Mandelstam variable $\hat{s}$ is deduced from the condition $\hat{s} + \hat{u} + \hat{t} = 0$. The functions $f_{a/A}(x_1,\mu)$ and $f_{b/B}(x_2,\mu)$ are the unpolarized parton distribution functions (PDFs) for protons A and

B respectively, while the function $h_1^a(x_1,\mu)$ is the collinear transversity distribution function.

$$\tilde{x}_1 = \frac{x_T e^{\eta}}{2 - x_T e^{-\eta}}, \qquad \tilde{x}_2 = x_1 \frac{x_T e^{-\eta}}{2x_1 - x_T e^{\eta}}, \tag{7.45}$$

where $x_T = 2p_T/\sqrt{s}$. The unpolarized TMD fragmentation functions and Collins fragmentation function are denoted by $D_{h/q}(z_h, j_\perp, \mu, \zeta_J)$ and $H_{1h/q}^{\perp}(z_h, j_\perp, \mu, \zeta_J)$ respectively. The momentum scale Q represents the appropriate factorization scale for both the unpolarized TMD fragmentation functions and Collins fragmentation functions. The Q-dependence of these TMD functions is referred as the TMD evolution, thus the TMD evolution is different from the DGLAP evolution associated with the scale μ. The TMD fragmentation functions can be expressed as

$$\begin{aligned} D_{h/q}(z_h, j_\perp, \mu, \zeta_J) =& \frac{1}{z_h^2} \int_0^\infty \frac{bdb}{(2\pi)} J_0(j_\perp b/z_h) \left[\hat{C} \otimes D\right](z_h, \mu_i) \\ & \times \exp\left[-S_{\rm pert}(b, \mu_i, \zeta_i, \mu, \zeta_J) - S_{\rm NP}^{D_1}(z, b, Q_0, \zeta_J)\right], \end{aligned} \tag{7.46}$$

$$\begin{aligned} \frac{j_\perp}{z_h M_h} H_{1h/q}^{\perp}(z_h, j_\perp, \mu, \zeta_J) =& \frac{1}{z_h^2} \int_0^\infty \frac{b^2 db}{(2\pi)} J_1(j_\perp b/z_h) \left[C^H \otimes \hat{H}_1^{\perp(1)}\right](z_h, \mu_i) \\ & \times \exp\left[-S_{\rm pert}(b, \mu_i, \zeta_i, \mu, \zeta_J) - S_{\rm NP}^{H}(z, b, Q_0, \zeta_J)\right], \end{aligned} \tag{7.47}$$

where J_0 and J_1 are the usual Bessel functions, and Q_0 is just the initial scale. The relevant scale Q for TMD fragmentation functions for hadron distribution inside a jet is usually set by the jet dynamics scale $\mu_J \sim p_T R$ where R is the jet size parameter. Thus, one should have a TMD evolution from μ_b to $\mu_J \sim p_T R$ scale to resum double logs to all orders in the strong coupling constant and a DGLAP evolution from $\mu_J \sim p_T R$ to $\mu \sim p_T$ scale to resum single logs to all orders in the strong coupling constant. But, at LO in QCD there is no dependence on the jet parameter R. In this paper, we work at LO so Q is simply set to p_T for TMDs and also we set μ to p_T for collinear PDFs and quark transversity function.

7.3 Non-perturbative parameterization

In order to reconstruct the measured cross-section, one needs to perform the Fourier transform over all values of b. However, the TMD evolution contains a non-perturbative piece in the region where $1/b \gg \Lambda_{\rm QCD}$. This requires the introduction of a certain prescription to extrapolate smoothly between the perturbative small-b region and the non-perturbative large-b region. Similar to our Sivers formalism, we choose the standard b_* prescription of the form

$$b_* = \frac{b}{\sqrt{1 + b^2/b_{MAX}^2}}, \tag{7.48}$$

One can see that $b_* \to b_{MAX}$ for large b. Here, b_{MAX} is the cut-off parameter in the prescription and is usually chosen to be $b_{MAX} = 1.5$ GeV^{-1}. After introducing b_* in the Sudakov factor, the total Sudakov factor is just the sum of a perturbative factor $S_{\rm pert}(Q, b_*)$ and a non-perturbative Sudakov factor $S_{\rm NP}(Q, b)$. In this prescription, the b_* variable lives in the perturbative region. The expressions for $S_{\rm NP}(Q, b)$ for both unpolarized TMD fragmentation functions and Collins fragmentation functions are written as

$$S_{\rm NP}^{D_1}(Q, b) = \frac{g_2}{2} \ln\left(\frac{b}{b_*}\right) \ln\left(\frac{Q}{Q_0}\right) + \frac{g_h}{z_h^2} b^2, \tag{7.49}$$

$$S_{\rm NP}^{\rm C}(Q, b) = \frac{g_2}{2} \ln\left(\frac{b}{b_*}\right) \ln\left(\frac{Q}{Q_0}\right) + \frac{g_h - g_c}{z_h^2} b^2, \tag{7.50}$$

where $Q_0^2 = 2.4$ GeV^2, $g_2 = 0.84$, $g_h = 0.042$ GeV^2, and $g_c = 0.0236 \pm 0.0007$ GeV^2. In the parametrization of the Sudakov function, $\ln(b/b_*) \propto \ln(1 + b^2/b_{MAX}^2)$, which is important for including low-Q^2 data. This parametrization at small b is in agreement with the standard b^2 parametization that was used in high-Q^2 extraction. The favored and unfavored twist-3 Collins fragmentation functions are parametrized in terms of unpolarized collinear

fragmentation functions as follows

$$H_{fav}^{(3)}(z,Q_0) = N_u^c z^{\alpha_u}(1-z)^{\beta_u} D_{\pi^+/u}(z,Q_0), \tag{7.51}$$

$$H_{unf}^{(3)}(z,Q_0) = N_d^c z^{\alpha_d}(1-z)^{\beta_d} D_{\pi^+/d}(z,Q_0), \tag{7.52}$$

The parametrization of the strange quark fragmentation function in terms of its collinear counterpart is given in Ref. [126]. In addition, the quark transversity distribution function h_1^q is parametrized at the initial scale Q_0 as follows

$$h_1^q(x,Q_0) = N_q^h x^{a_q}(1-x)^{b_q}\frac{(a_q+b_q)^{a_q+b_q}}{a_q^{a_q}b_q^{b_q}}\frac{1}{2}(f_1^q(x,Q_0)+g_1^q(x,Q_0)), \tag{7.53}$$

where f_1^q is the collinear quark distribution function and g_1^q is the quark helicity distribution function at the initial scale Q_0.

7.4 Current status

Unpolarized FF with TMD evolution is defined as

$$\begin{aligned} D_{h/q}(z,b,Q) = {} & \frac{1}{z^2}\frac{b}{2\pi}\hat{C}_{i\leftarrow q}^{D_1}\otimes D_{h/i}(z,\mu_b) \\ & \times \exp\left(-\frac{1}{2}S_{\rm pert}(Q,b_*) - S_{\rm NP}^{D_1}(Q,b)\right). \end{aligned} \tag{7.54}$$

Figure (7.5) displays TMD unpolarized FF at $z = 0.4$ and at different scales $Q^2 = 2.4$ (dotted line), $Q^2 = 10$ (solid line), and $Q^2 = 1000$ (dashed line) GeV^2. We observe that the unpolarized FF at $Q^2 = 1000$ (dashed line) peaks in the perturbative region, and the peak shifts towards the non-perturbative region as the energy decreases. The Collins FF with TMD evolution is defined as

$$\begin{aligned} H_{1h/q}^{\perp}(z,b,Q)_{\mathcal{T}} = {} & \frac{1}{z^2}\frac{b^2}{2\pi}\delta\hat{C}_{i\leftarrow q}^{C}\otimes H_{1h/j}^{\perp(1)}(z,\mu_b)_{\mathcal{T}} \\ & \times \exp\left(-\frac{1}{2}S_{\rm pert}(Q,b_*) - S_{\rm NP}^{C}(Q,b)\right). \end{aligned} \tag{7.55}$$

where the subscript $\mathcal{T}$ indicates the use of the Trento convention. Figure (7.6) shows that the TMD Collins FF at Q^2 = 1000 (dashed line) peaks in the perturbative region, and the peak shifts towards the non-perturbative region as the energy decreases.

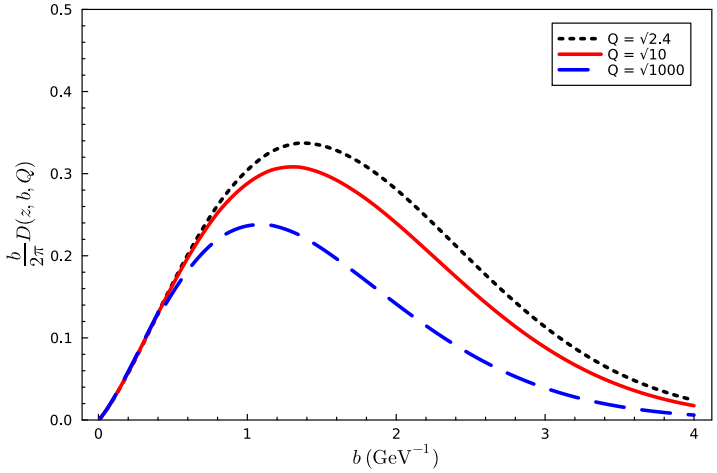

Figure 7.5: Unpolarised FF $u \to \pi^+$ as function of b at three different scales $Q_2 = 2.4$ (dotted line), Q_2 =10 (solid line) and $Q_2 = 1000$ (dashed line) GeV^2.

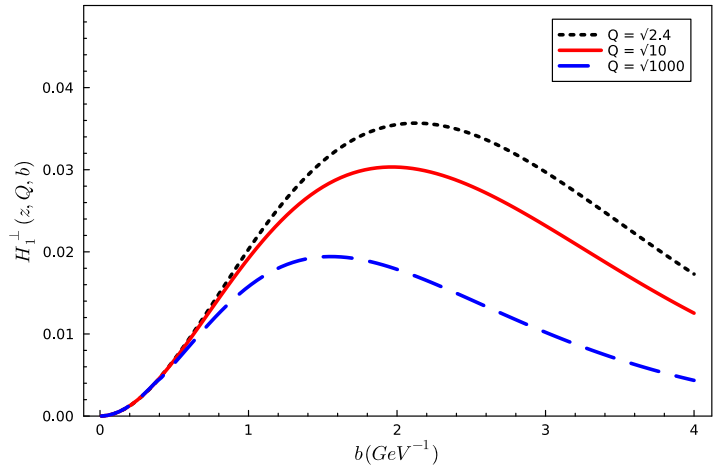

Figure 7.6: Collins FF $u \to \pi^+$ as function of b at three different scales $Q_2 = 2.4$ (dotted line), Q_2 =10 (solid line) and $Q_2 = 1000$ (dashed line) GeV^2.

STAR collaboration at RHIC has performed measurement for Collins asymmetry of hadron-in-jet in transversely polarized proton-proton collisions. The experimental data was compared with the theory prediction based on the Collins functions extracted from e^+e^- collisions and SIDIS process.

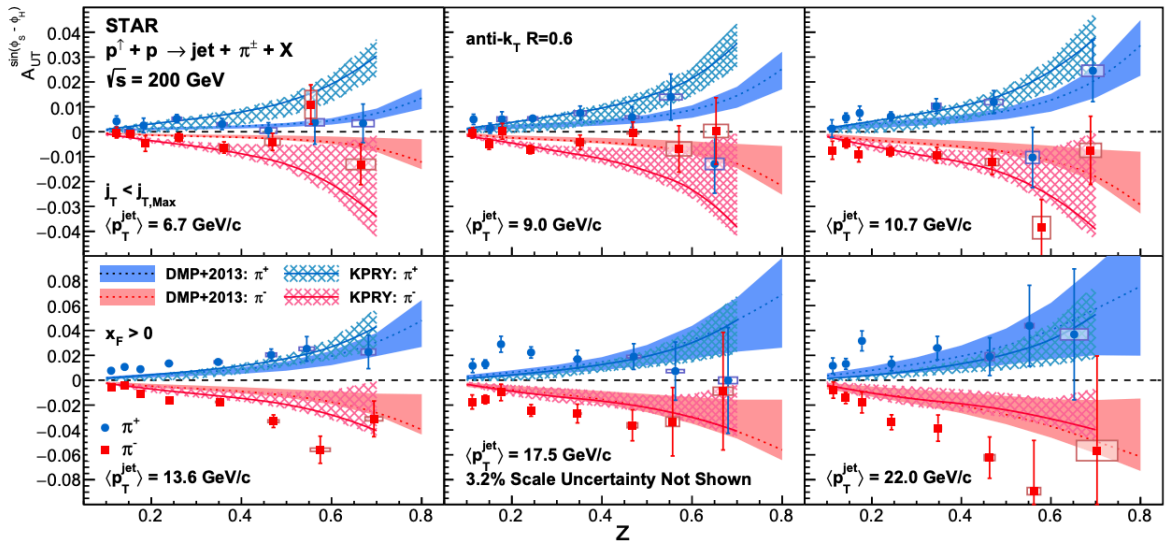

Figure 7.7: The comparison of STAR measurements [17] to the previous theoretical calculations with the DMP+2013 model of Ref. [18] and the KPRY model of Ref. [19] .

Figure (7.7) clearly shows that the theory curves do not describe the Collins asymmetry very well, especially for π^- at large z region. This indicates that the previous extraction of the Collins function based on e^+e^- and SIDIS do not give a good constrain on the Collins function at large z, most likely the d-quark Collins functions. This points to the new direction we are undertaking in the future, that is, to perform a global analysis of the Collins function by including the data from e^+e^-, SIDIS and hadron-in-jet in proton-proton collisions.

Chapter 8

Summary

Asymmetries and transverse polarization effects offer vital insights into the internal architecture of hadrons and the intricacies of the hadronization process, particularly with respect to parton distribution and fragmentation functions. Early investigations primarily examined collinear parton distribution and fragmentation functions; however, it soon became evident that these collinear functions alone were insufficient to fully elucidate the internal structure of hadrons. This realization underscored the need for a more comprehensive understanding, leading to the development of transverse momentum-dependent functions (TMDs).

In the introductory section of this dissertation, we explore the concept of transverse single spin asymmetry (TSSA), highlighting its essential role in deriving the TMD functions central to our study. We also delve into Soft-Collinear Effective Theory (SCET), valued for its robust framework that systematically addresses processes involving diverse modes, particularly within the realm of high-energy hadronic physics. SCET enables us to exclude modes irrelevant to the asymptotic behavior of Quantum Chromodynamics (QCD), thereby providing an effective description. Given the recurring significance of Wilson lines in gauge theories, we elaborate on their relevance to non-local operators, delineating various types of Wilson lines and offering some physical interpretations.

As our TMD frameworks incorporate twist-2 and twist-3 functions, we detail their deriva-

tions from correlation functions (correlators). We also examine TMD factorization theorems—a potent tool in quantum field theory (QFT)—which facilitate the expression of cross sections through a combination of perturbatively calculable and non-perturbative quantities. Furthermore, we address the use of the η regulator to mitigate rapidity divergences. Given that our TMD frameworks involve QCD evolutions, we outline the derivations of evolution equations and their solutions. The significance of SCET prompts further discussion on TMD factorization and evolution within this context.

The primary objective of this dissertation is to develop TMD formalisms for the concurrent global extraction of Sivers and Collins asymmetries. Initially, we establish a TMD formalism for the simultaneous global extraction of Sivers asymmetries across Semi-Inclusive Deep Inelastic Scattering (SIDIS), the Drell-Yan (DY) process, and W/Z production, with and without jet A_N data from proton-proton (pp) collisions. In both scenarios, the fitted asymmetries align exceptionally well with experimental data, and the Sivers function is consistently extracted. Comparing outcomes with and without jet A_N data reveals a marked reduction in uncertainty for the Sivers function when jet A_N data is included. The results are found in Sec. (6.3). Subsequently, we formulate a TMD framework for the simultaneous extraction of Collins asymmetries in the SIDIS process, e^+e^- annihilation, and hadron production within jets in pp collisions.

A Mellin Transformation

In this section, we outline the approach for streamlining the OPE and DGLAP evolution of the transversity TMD PDF and the Collins TMD FF through the use of Mellin space techniques. The transversity TMD PDF can be perturbatively matched to the collinear transversity PDF using Eq. (7.19). In this equation, the matching is implemented as a convolution that can be simplified by employing Mellin space techniques.

$$h_{1\,q/P}\left(N,\mu_b,\mu_i,\zeta_i\right) = C^h\left(N,\mu_b,\mu_i,\zeta_i\right) h\left(x,\mu_i\right)\,, \tag{1}$$

where we have introduced the Mellin transform, which is explicitly given by

$$A(N) = \int_0^1 dx x^{N-1} A(x)\,, \tag{2}$$

while the inverse Mellin transform is defined as

$$A(x) = \frac{1}{\pi}\int_0^\infty dz \Im\Big[e^{i\phi}x^{-c-ze^{i\phi}}A(N)\Big]. \tag{3}$$

Taking the canonical scale choice for the TMDs, $\mu_i^2 = \mu_b^2 = \zeta_i$, the Mellin-space $\bar{\text{MS}}$ matching coefficient for the transversity TMD PDF is given by:

$$C^h\left(N,\mu_b,\mu_i,\zeta_i\right) = 1 + \frac{\alpha_s C_F}{4\pi}\frac{\pi^2}{6} + \mathcal{O}\left(\alpha_s^2\right)\,. \tag{4}$$

Thus the Mellin-space formalism reduces the integration in x to an integration in the complex plane. However, the Mellin-space formalism also simplifies the evolution of the collinear transversity TMD PDF as well. Namely, the evolution equation of this distribution is given by

$$\frac{\partial h(x,\mu)}{\partial \ln \mu^2} = \alpha_s \left[P^h_{qq} \otimes h\right](x,\mu)\,, \tag{5}$$

which can be simplified in Mellin space. The solution to the Mellin transform of this equation is given by

$$h(N,\mu) = h(N,\mu_0)\left(\frac{\alpha_s(\mu)}{\alpha_s(\mu_0)}\right)^{-\frac{1}{\beta_0}P^h_{qq}(N)} \tag{6}$$

where we have introduced the Mellin transform of the transversity PDFs splitting function

$$P^h_{qq}(N) = \int x^{N-1} P^h_{qq}(x) = -2H(N) + \frac{3}{2}\,, \tag{7}$$

for the harmonic number, $H(n)$. OPE of the transversity TMD PDF can be written as a single integral in the complex plane as

$$\left[C^h \otimes h_1\right]\left(x,\mu_b,\mu_b,\zeta_b^2\right) = \frac{1}{\pi}\int_0^\infty dz \Im\left[e^{i\phi}x^{-c-ze^{i\phi}} C^h\left(N,\mu_b,\mu_b,\mu_b^2\right) h\left(N,\mu_b\right)\right]. \tag{8}$$

Following the same procedure, the expression for the Collins TMD FF is given by

$$\left[C^H \otimes H^{(3)}\right]\left(z,\mu_b,\mu_b,\zeta_b^2\right) = \frac{1}{\pi}\int_0^\infty dz \Im\left[e^{i\phi}x^{-c-ze^{i\phi}} C^H\left(N,\mu_b,\mu_b,\mu_b^2\right) H^{(3)}\left(N,\mu_b\right)\right], \tag{9}$$

where the Mellin-space matching coefficient is given by

$$C^H\left(N,\mu_b,\mu_b,\mu_b^2\right) = 1 + \frac{\alpha_s C_F}{4\pi}\left[-8\psi^1(1+n) - \frac{\pi^2}{6}\right], \tag{10}$$

where ψ^1 is the tri-gamma function while the twist-3 collinear FF follows the same evolution

equation as the transversity PDF such that

$$H^3(N,\mu) = H^3(N,\mu_0)\left(\frac{\alpha_s(\mu)}{\alpha_s(\mu_0)}\right)^{-\frac{1}{\beta_0}P^h_{qq}(N)} . \tag{11}$$

B Anomalous dimensions

Below we give the expressions for the anomalous dimensions and the QCD β-function, in the $\overline{\text{MS}}$ renormalization scheme. We use the following expansions

$$\Gamma_{\text{cusp}} = \sum_{n=1}^{\infty}\Gamma_{n-1}\left(\frac{\alpha_s}{4\pi}\right)^n , \tag{12}$$

$$\gamma^V = \sum_{n=1}^{\infty}\gamma^V_{n-1}\left(\frac{\alpha_s}{4\pi}\right)^n , \tag{13}$$

$$\beta = -2\alpha_s\sum_{n=1}^{\infty}\beta_{n-1}\left(\frac{\alpha_s}{4\pi}\right)^n . \tag{14}$$

The coefficients for the cusp anomalous dimension Γ_{cusp} are

$$\Gamma_0 = 4C_F, \tag{15}$$

$$\Gamma_1 = 4C_F\left[\left(\frac{67}{9}-\frac{\pi^2}{3}\right)C_A - \frac{20}{9}T_F n_f\right], \tag{16}$$

$$\begin{aligned}\Gamma_2 = 4C_F\Bigg[&C_A^2\left(\frac{245}{6}-\frac{134\pi^2}{27}+\frac{11\pi^4}{45}+\frac{22}{3}\zeta_3\right)\\ &+C_A T_F n_f\left(-\frac{418}{27}+\frac{40\pi^2}{27}-\frac{56}{3}\zeta_3\right)\\ &+C_F T_F n_f\left(-\frac{55}{3}+16\zeta_3\right)\\ &-\frac{16}{27}T_F^2 n_f^2\Bigg].\end{aligned} \tag{17}$$

The anomalous dimension γ^V can be determined up to three-loop order from the partial

three-loop expression for the on-shell quark form factor in QCD. We have

$$\gamma_0^V = -6C_F, \tag{18}$$

$$\gamma_1^V = C_F^2\left(-3+4\pi^2-48\zeta_3\right)+C_FC_A\left(-\frac{961}{27}-\frac{11\pi^2}{3}+52\zeta_3\right)+C_FT_Fn_f\left(\frac{260}{27}+\frac{4\pi^2}{3}\right). \tag{19}$$

The rapidity anomalous dimension, Collins-Soper kernel, is defined perturbatively as

$$D(b,\mu) = \sum_{n=1}^{\infty}\sum_{k=0}^{n} d^{(n,k)}\left(\frac{\alpha_s}{4\pi}\right)^n L^k\,, \tag{20}$$

where the coefficients up to NNLL are given by

$$d^{(1,0)} = 0, \qquad d^{(1,1)} = \Gamma_0/2, \tag{21}$$

$$d^{(2,0)} = C_AC_F\left(\frac{404}{27}-14\zeta_3\right)-\frac{112}{27}C_FT_Fn_f, \tag{22}$$

$$d^{(2,1)} = \Gamma_1/2, \qquad d^{(2,2)} = \Gamma_0\beta_0/4. \tag{23}$$

The description of the perturbative TMD evolution requires finding the analytic solution to the following expression

$$\mathrm{I} = \int_{\mu_L}^{\mu_U}\frac{d\bar{\mu}}{\bar{\mu}}\left[\gamma^V+\Gamma_{\mathrm{cusp}}\ln\left(\frac{\mu_U^2}{\bar{\mu}^2}\right)\right] \tag{24}$$

where the coefficients of perturbative expansions of the anomalous dimensions up to NNLL accuracy are found in Ref. [81].

Bibliography

[1] David J. Gross and Frank Wilczek. Ultraviolet behavior of non-abelian gauge theories. *Phys. Rev. Lett.*, 30:1343–1346, Jun 1973. doi: 10.1103/PhysRevLett.30.1343. URL https://link.aps.org/doi/10.1103/PhysRevLett.30.1343.

[2] H. David Politzer. Reliable perturbative results for strong interactions? *Phys. Rev. Lett.*, 30:1346–1349, Jun 1973. doi: 10.1103/PhysRevLett.30.1346. URL https://link.aps.org/doi/10.1103/PhysRevLett.30.1346.

[3] A. Accardi, J.L. Albacete, M. Anselmino, et al. Electron-ion collider: The next qcd frontier. *Eur. Phys. J. A*, 52:268, 2016. doi: 10.1140/epja/i2016-16268-9. URL https://arxiv.org/abs/1212.1701.

[4] Khachatryan et al. Measurement of the inclusive 3-jet production differential cross section in proton–proton collisions at 7 tev and determination of the strong coupling constant in the tev range. *The European Physical Journal C*, 75(5), May 2015. ISSN 1434-6052. doi: 10.1140/epjc/s10052-015-3376-y. URL http://dx.doi.org/10.1140/epjc/s10052-015-3376-y.

[5] K. A. Olive et al. Review of Particle Physics. *Chin. Phys. C*, 38:090001, 2014. doi: 10.1088/1674-1137/38/9/090001.

[6] I. Arsene, I. G. Bearden, D. Beavis, S. Bekele, C. Besliu, B. Budick, H. Bøggild, C. Chasman, H. H. Dalsgaard, R. Debbe, B. Fox, J. J. Gaardhøje, K. Hagel, A. Jipa, E. B. Johnson, R. Karabowicz, N. Katryńska, E. J. Kim, T. M. Larsen, J. H. Lee, G. Løvhøiden, Z. Majka, M. Murray, C. Nygaard, J. Natowitz, B. S. Nielsen, D. Pal, A. Qviler, C. Ristea, D. Röhrich, S. J. Sanders, P. Staszel, T. S. Tveter, F. Videbæk, H. Yang, and R. Wada. Single-transverse-spin asymmetries of identified charged hadrons in polarized pp collisions at $\sqrt{s}$ = 62.4 GeV. *Phys. Rev. Lett.*, 101:042001, Jul 2008. doi: 10.1103/PhysRevLett.101.042001. URL https://link.aps.org/doi/10.1103/PhysRevLett.101.042001.

[7] J. Adam et al. Measurement of transverse single-spin asymmetries of neutral pion and electromagnetic jets at forward rapidity in 200 and 500 gev transversely polarized proton-proton collisions. *Physical Review D*, 103(9), May 2021. ISSN 2470-0029. doi: 10.1103/physrevd.103.092009. URL http://dx.doi.org/10.1103/PhysRevD.103.092009.

[8] L.C. Bland, E.J. Brash, H.J. Crawford, A.A. Derevschikov, K.A. Drees, J. Engelage, C. Folz, M.K. Jones, E.G. Judd, X. Li, N.K. Liyanage, Y. Makdisi, N.G. Minaev, R.N. Munroe, L. Nogach, A. Ogawa, C.F. Perdrisat, C. Perkins, M. Planinic, V. Punjabi, G. Schnell, G. Simatovic, T.G. Throwe, C. Van Hulse, and A.N. Vasiliev. Cross sections and transverse single-spin asymmetries in forward jet production from proton collisions. *Physics Letters B*, 750:660–665, November 2015. ISSN 0370-2693. doi: 10.1016/j.physletb.2015.10.001. URL http://dx.doi.org/10.1016/j.physletb.2015.10.001.

[9] C. Adolph et al. Sivers asymmetry extracted in sidis at the hard scales of the drell–yan process at compass. *Physics Letters B*, 770:138–145, July 2017. ISSN 0370-2693. doi: 10.1016/j.physletb.2017.04.042. URL http://dx.doi.org/10.1016/j.physletb.2017.04.042.

[10] M. Alekseev et al. Collins and sivers asymmetries for pions and kaons in muon–deuteron dis. *Physics Letters B*, 673(2):127–135, March 2009. ISSN 0370-2693. doi: 10.1016/j.physletb.2009.01.060. URL http://dx.doi.org/10.1016/j.physletb.2009.01.060.

[11] X. Qian et al. Single spin asymmetries in charged pion production from semi-inclusive deep inelastic scattering on a transversely polarized target. *Physical Review Letters*, 107(7), August 2011. ISSN 1079-7114. doi: 10.1103/physrevlett.107.072003. URL http://dx.doi.org/10.1103/PhysRevLett.107.072003.

[12] G. D. Alexeev et al. Final compass results on the transverse-spin-dependent azimuthal asymmetries in the pion-induced drell-yan process, 2023. URL https://arxiv.org/abs/2312.17379.

[13] A. Airapetian et al. Observation of the naive-odd sivers effect in deep-inelastic scattering. *Physical Review Letters*, 103(15), October 2009. ISSN 1079-7114. doi: 10.1103/physrevlett.103.152002. URL http://dx.doi.org/10.1103/PhysRevLett.103.152002.

[14] HERMES Collaboration, A. Airapetian, et al. Azimuthal single- and double-spin asymmetries in semi-inclusive deep-inelastic lepton scattering by transversely polarized protons, 2020. URL https://arxiv.org/abs/2007.07755.

[15] L. Adamczyk et al. Measurement of the transverse single-spin asymmetry at rhic. *Physical Review Letters*, 116(13), April 2016. ISSN 1079-7114. doi: 10.1103/physrevlett.116.132301. URL http://dx.doi.org/10.1103/PhysRevLett.116.132301.

[16] STAR Collaboration. Measurements of the z^0/γ^* cross section and transverse single spin asymmetry in 510 gev p+p collisions, 2023. URL https://arxiv.org/abs/2308.15496.

[17] M.S. Abdallah et al. Azimuthal transverse single-spin asymmetries of inclusive jets and identified hadrons within jets. *Physical Review D*, 106(7), October 2022. ISSN 2470-0029. doi: 10.1103/physrevd.106.072010. URL http://dx.doi.org/10.1103/PhysRevD.106.072010.

[18] Umberto D'Alesio, Francesco Murgia, and Cristian Pisano. Testing the universality of the collins function in pion-jet production at rhic. *Physics Letters B*, 773:300–306, October 2017. ISSN 0370-2693. doi: 10.1016/j.physletb.2017.08.023. URL http://dx.doi.org/10.1016/j.physletb.2017.08.023.

[19] Zhong-Bo Kang, Alexei Prokudin, Felix Ringer, and Feng Yuan. Collins azimuthal asymmetries of hadron production inside jets. *Physics Letters B*, 774:635–642, November 2017. ISSN 0370-2693. doi: 10.1016/j.physletb.2017.10.031. URL http://dx.doi.org/10.1016/j.physletb.2017.10.031.

[20] Murray Gell-Mann. Nonleptonic weak decays and the eightfold way. *Phys. Rev. Lett.*, 12:155–156, Feb 1964. doi: 10.1103/PhysRevLett.12.155. URL https://link.aps.org/doi/10.1103/PhysRevLett.12.155.

[21] Murray Gell-Mann. A Schematic Model of Baryons and Mesons. *Phys. Lett.*, 8:214–215, 1964. doi: 10.1016/S0031-9163(64)92001-3.

[22] G. Zweig. *An SU(3) model for strong interaction symmetry and its breaking. Version 2*, pages 22–101. 2 1964. doi: 10.17181/CERN-TH-412.

[23] G. Zweig. An SU(3) model for strong interaction symmetry and its breaking. Version 1. 1 1964.

[24] E. D. Bloom, D. H. Coward, H. DeStaebler, J. Drees, G. Miller, L. W. Mo, R. E. Taylor, M. Breidenbach, J. I. Friedman, G. C. Hartmann, and H. W. Kendall. High-energy inelastic $e-p$ scattering at 6° and 10°. *Phys. Rev. Lett.*, 23:930–934, Oct 1969. doi: 10.1103/PhysRevLett.23.930. URL https://link.aps.org/doi/10.1103/PhysRevLett.23.930.

[25] M. Breidenbach, J. I. Friedman, H. W. Kendall, E. D. Bloom, D. H. Coward, H. DeStaebler, J. Drees, L. W. Mo, and R. E. Taylor. Observed behavior of highly inelastic electron-proton scattering. *Phys. Rev. Lett.*, 23:935–939, Oct 1969. doi: 10.1103/PhysRevLett.23.935. URL https://link.aps.org/doi/10.1103/PhysRevLett.23.935.

[26] C. N. Yang and R. L. Mills. Conservation of isotopic spin and isotopic gauge invariance. *Phys. Rev.*, 96:191–195, Oct 1954. doi: 10.1103/PhysRev.96.191. URL https://link.aps.org/doi/10.1103/PhysRev.96.191.

[27] L.D. Faddeev and V.N. Popov. Feynman diagrams for the yang-mills field. *Physics Letters B*, 25(1):29–30, 1967. ISSN 0370-2693. doi: https://doi.org/10.1016/0370-2693(67)90067-6. URL https://www.sciencedirect.com/science/article/pii/0370269367900676.

[28] David J. Gross and Frank Wilczek. Asymptotically free gauge theories. i. *Phys. Rev. D*, 8:3633–3652, Nov 1973. doi: 10.1103/PhysRevD.8.3633. URL https://link.aps.org/doi/10.1103/PhysRevD.8.3633.

[29] H. David Politzer. Asymptotic Freedom: An Approach to Strong Interactions. *Phys. Rept.*, 14:129–180, 1974. doi: 10.1016/0370-1573(74)90014-3.

[30] S. Navas et al. Review of particle physics. *Phys. Rev. D*, 110:030001, Aug 2024. doi: 10.1103/PhysRevD.110.030001. URL https://link.aps.org/doi/10.1103/PhysRevD.110.030001.

[31] Igor Olegovich Cherednikov, Tom Mertens, and Frederik F. Van der Veken. *Wilson Lines in Quantum Field Theory*, volume 24 of *De Gruyter Studies in Mathematical Physics*. De Gruyter, 9 2014. ISBN 978-3-11-030921-8, 978-3-11-030910-2. doi: 10.1515/9783110309218.

[32] Piotr Kotko. Wilson lines and gauge invariant off-shell amplitudes. *Journal of High Energy Physics*, 2014(7), July 2014. ISSN 1029-8479. doi: 10.1007/jhep07(2014)128. URL http://dx.doi.org/10.1007/JHEP07(2014)128.

[33] P.J Mulders and R.D Tangerman. The complete tree-level result up to order 1/q for polarized deep-inelastic leptoproduction. *Nuclear Physics B*, 461(1–2):197–237, February 1996. ISSN 0550-3213. doi: 10.1016/0550-3213(95)00632-x. URL http://dx.doi.org/10.1016/0550-3213(95)00632-X.

[34] K. Goeke, A. Metz, and M. Schlegel. Parameterization of the quark–quark correlator of a spin-1/2 hadron. *Physics Letters B*, 618(1–4):90–96, July 2005. ISSN 0370-2693. doi: 10.1016/j.physletb.2005.05.037. URL http://dx.doi.org/10.1016/j.physletb.2005.05.037.

[35] D. Boer, R. Jakob, and P.J. Mulders. Asymmetries in polarized hadron production in e+e- annihilation up to order. *Nuclear Physics B*, 504(1–2):345–380, October 1997. ISSN 0550-3213. doi: 10.1016/s0550-3213(97)00456-2. URL http://dx.doi.org/10.1016/S0550-3213(97)00456-2.

[36] Jian Zhou, Feng Yuan, and Zuo-Tang Liang. Transverse momentum dependent quark distributions and polarized drell-yan processes. *Physical Review D*, 81(5), March 2010. ISSN 1550-2368. doi: 10.1103/physrevd.81.054008. URL http://dx.doi.org/10.1103/PhysRevD.81.054008.

[37] Jian-wei Qiu and George F. Sterman. Single transverse spin asymmetries. *Phys. Rev. Lett.*, 67:2264–2267, 1991. doi: 10.1103/PhysRevLett.67.2264.

[38] John C. Collins and Davison E. Soper. Back-To-Back Jets in QCD. *Nucl. Phys. B*, 193:381, 1981. doi: 10.1016/0550-3213(81)90339-4. [Erratum: Nucl.Phys.B 213, 545 (1983)].

[39] John C. Collins and Davison E. Soper. Back-To-Back Jets: Fourier Transform from B to K-Transverse. *Nucl. Phys. B*, 197:446–476, 1982. doi: 10.1016/0550-3213(82)90453-9.

[40] John C. Collins, Davison E. Soper, and George F. Sterman. Transverse Momentum Distribution in Drell-Yan Pair and W and Z Boson Production. *Nucl. Phys. B*, 250:199–224, 1985. doi: 10.1016/0550-3213(85)90479-1.

[41] John Collins. *Foundations of Perturbative QCD*, volume 32 of *Cambridge Monographs on Particle Physics, Nuclear Physics and Cosmology*. Cambridge University Press, 7 2023. ISBN 978-1-00-940184-5, 978-1-00-940183-8, 978-1-00-940182-1. doi: 10.1017/9781009401845.

[42] Thomas Becher and Matthias Neubert. Drell–yan production at small q t , transverse parton distributions and the collinear anomaly. *The European Physical Journal C*, 71 (6), June 2011. ISSN 1434-6052. doi: 10.1140/epjc/s10052-011-1665-7. URL http://dx.doi.org/10.1140/epjc/s10052-011-1665-7.

[43] Thomas Becher, Matthias Neubert, and Daniel Wilhelm. Electroweak gauge-boson production at small qt: Infrared safety from the collinear anomaly. *Journal of High Energy Physics*, 2012(2), February 2012. ISSN 1029-8479. doi: 10.1007/jhep02(2012)124. URL http://dx.doi.org/10.1007/JHEP02(2012)124.

[44] Thomas Becher, Matthias Neubert, and Daniel Wilhelm. Higgs-boson production at small transverse momentum. *Journal of High Energy Physics*, 2013(5), May 2013. ISSN 1029-8479. doi: 10.1007/jhep05(2013)110. URL http://dx.doi.org/10.1007/JHEP05(2013)110.

[45] Miguel G. Echevarría, Ahmad Idilbi, and Ignazio Scimemi. Factorization theorem for drell-yan at low qt and transverse-momentum distributions on-the-light-cone. *Journal of High Energy Physics*, 2012(7), July 2012. ISSN 1029-8479. doi: 10.1007/jhep07(2012)002. URL http://dx.doi.org/10.1007/JHEP07(2012)002.

[46] Miguel G. Echevarría, Ahmad Idilbi, and Ignazio Scimemi. Soft and collinear factorization and transverse momentum dependent parton distribution functions. *Physics Letters B*, 726(4–5):795–801, November 2013. ISSN 0370-2693. doi: 10.1016/j.physletb.2013.09.003. URL http://dx.doi.org/10.1016/j.physletb.2013.09.003.

[47] Miguel G. Echevarria, Ahmad Idilbi, and Ignazio Scimemi. Unified treatment of the qcd evolution of all (un-)polarized transverse momentum dependent functions: Collins function as a study case. *Physical Review D*, 90(1), July 2014. ISSN 1550-2368. doi: 10.1103/physrevd.90.014003. URL http://dx.doi.org/10.1103/PhysRevD.90.014003.

[48] John Collins and Ted C. Rogers. Connecting different tmd factorization formalisms in qcd. *Physical Review D*, 96(5), September 2017. ISSN 2470-0029. doi: 10.1103/physrevd.96.054011. URL http://dx.doi.org/10.1103/PhysRevD.96.054011.

[49] Renaud Boussarie, Matthias Burkardt, Martha Constantinou, William Detmold, Markus Ebert, Michael Engelhardt, Sean Fleming, Leonard Gamberg, Xiangdong Ji, Zhong-Bo Kang, Christopher Lee, Keh-Fei Liu, Simonetta Liuti, Thomas Mehen, Andreas Metz, John Negele, Daniel Pitonyak, Alexei Prokudin, Jian-Wei Qiu, Abha Rajan, Marc Schlegel, Phiala Shanahan, Peter Schweitzer, Iain W. Stewart, Andrey Tarasov, Raju Venugopalan, Ivan Vitev, Feng Yuan, and Yong Zhao. Tmd handbook, 2023. URL https://arxiv.org/abs/2304.03302.

[50] Davison E. Soper. Partons and Their Transverse Momenta in QCD. *Phys. Rev. Lett.*, 43:1847, 1979. doi: 10.1103/PhysRevLett.43.1847.

[51] John C. Collins and F. V. Tkachov. Breakdown of dimensional regularization in the Sudakov problem. *Phys. Lett. B*, 294:403–411, 1992. URL https://arxiv.org/abs/hep-ph/9208209.

[52] John Collins. Rapidity divergences and valid definitions of parton densities, 2008. URL https://arxiv.org/abs/0808.2665.

[53] Jui-yu Chiu, Ambar Jain, Duff Neill, and Ira Z. Rothstein. Rapidity renormalization group. *Physical Review Letters*, 108(15), April 2012. ISSN 1079-7114. doi: 10.1103/physrevlett.108.151601. URL http://dx.doi.org/10.1103/PhysRevLett.108.151601.

[54] John C. Collins and Davison E. Soper. Back-to-back jets: Fourier transform from b to kt. *Nuclear Physics B*, 197(3):446–476, 1982. ISSN 0550-3213. doi: https://doi.org/10.1016/0550-3213(82)90453-9. URL https://www.sciencedirect.com/science/article/pii/0550321382904539.

[55] John C. Collins and Davison E. Soper. Parton Distribution and Decay Functions. *Nucl. Phys. B*, 194:445–492, 1982. doi: 10.1016/0550-3213(82)90021-9.

[56] John Collins and Ted Rogers. Understanding the large-distance behavior of transverse-momentum-dependent parton densities and the Collins-Soper evolution kernel. *Phys. Rev. D*, 91(7):074020, 2015. doi: 10.1103/PhysRevD.91.074020.

[57] Huey-Wen Lin et al. Parton distributions and lattice qcd calculations: A community white paper. *Progress in Particle and Nuclear Physics*, 100:107–160, May 2018. ISSN 0146-6410. doi: 10.1016/j.ppnp.2018.01.007. URL http://dx.doi.org/10.1016/j.ppnp.2018.01.007.

[58] Martha Constantinou, Aurore Courtoy, Markus A. Ebert, Michael Engelhardt, Tommaso Giani, Tim Hobbs, Tie-Jiun Hou, Aleksander Kusina, Krzysztof Kutak, Jian Liang, Huey-Wen Lin, Keh-Fei Liu, Simonetta Liuti, Cédric Mezrag, Pavel Nadolsky, Emanuele R. Nocera, Fred Olness, Jian-Wei Qiu, Marco Radici, Anatoly Radyushkin, Abha Rajan, Ted Rogers, Juan Rojo, Gerrit Schierholz, C.-P. Yuan, Jian-Hui Zhang, and Rui Zhang. Parton distributions and lattice-qcd calculations: Toward 3d structure. *Progress in Particle and Nuclear Physics*, 121:103908, November 2021. ISSN 0146-6410. doi: 10.1016/j.ppnp.2021.103908. URL http://dx.doi.org/10.1016/j.ppnp.2021.103908.

[59] Xiang-dong Ji, Jian-ping Ma, and Feng Yuan. QCD factorization for semi-inclusive deep-inelastic scattering at low transverse momentum. *Phys. Rev. D*, 71:034005, 2005. doi: 10.1103/PhysRevD.71.034005.

[60] Thomas Becher, Matthias Neubert, and Ben D Pecjak. Factorization and momentum-space resummation in deep-inelastic scattering. *Journal of High Energy Physics*, 2007 (01):076–076, January 2007. ISSN 1029-8479. doi: 10.1088/1126-6708/2007/01/076. URL http://dx.doi.org/10.1088/1126-6708/2007/01/076.

[61] S. Mert Aybat and Ted C. Rogers. Transverse momentum dependent parton distribution and fragmentation functions with qcd evolution. *Physical Review D*, 83 (11), June 2011. ISSN 1550-2368. doi: 10.1103/physrevd.83.114042. URL http://dx.doi.org/10.1103/PhysRevD.83.114042.

[62] John C. Collins. Leading-twist single-transverse-spin asymmetries: Drell–yan and deep-inelastic scattering. *Physics Letters B*, 536(1–2):43–48, May 2002. ISSN 0370-2693. doi: 10.1016/s0370-2693(02)01819-1. URL http://dx.doi.org/10.1016/S0370-2693(02)01819-1.

[63] D. Boer et al. Gluons and the quark sea at high energies: distributions, polarization, tomography, 2011. URL https://arxiv.org/abs/1108.1713.

[64] A. Accardi et al. Electron ion collider: The next qcd frontier - understanding the glue that binds us all, 2014. URL https://arxiv.org/abs/1212.1701.

[65] R. Abdul Khalek et al. Science requirements and detector concepts for the electron-ion collider. *Nuclear Physics A*, 1026:122447, October 2022. ISSN 0375-9474. doi: 10.1016/j.nuclphysa.2022.122447. URL http://dx.doi.org/10.1016/j.nuclphysa.2022.122447.

[66] Dennis Sivers. Hard-scattering scaling laws for single-spin production asymmetries. *Phys. Rev. D*, 43:261–263, Jan 1991. doi: 10.1103/PhysRevD.43.261. URL https://link.aps.org/doi/10.1103/PhysRevD.43.261.

[67] Dennis Sivers. Single-spin production asymmetries from the hard scattering of pointlike constituents. *Phys. Rev. D*, 41:83–90, Jan 1990. doi: 10.1103/PhysRevD.41.83. URL https://link.aps.org/doi/10.1103/PhysRevD.41.83.

[68] Alessandro Bacchetta and Marco Radici. Quark angular momentum and the sivers asymmetry, 2012. URL https://arxiv.org/abs/1206.2565.

[69] Stanley J. Brodsky, Dae Sung Hwang, and Ivan Schmidt. Final-state interactions and single-spin asymmetries in semi-inclusive deep inelastic scattering. *Physics Letters B*, 530(1–4):99–107, March 2002. ISSN 0370-2693. doi: 10.1016/s0370-2693(02)01320-5. URL http://dx.doi.org/10.1016/S0370-2693(02)01320-5.

[70] John Collins. Fragmentation of transversely polarized quarks probed in transverse momentum distributions. *Nuclear Physics B*, 396(1):161–182, May 1993. ISSN 0550-3213. doi: 10.1016/0550-3213(93)90262-n. URL http://dx.doi.org/10.1016/0550-3213(93)90262-N.

[71] D. Boer, P.J. Mulders, and F. Pijlman. Universality of t-odd effects in single spin and azimuthal asymmetries. *Nuclear Physics B*, 667(1–2):201–241, September 2003. ISSN 0550-3213. doi: 10.1016/s0550-3213(03)00527-3. URL http://dx.doi.org/10.1016/S0550-3213(03)00527-3.

[72] C.J. Bomhof, P.J. Mulders, and F. Pijlman. The construction of gauge-links in arbitrary hard processes. *The European Physical Journal C*, 47(1):147–162, May 2006. ISSN 1434-6052. doi: 10.1140/epjc/s2006-02554-2. URL http://dx.doi.org/10.1140/epjc/s2006-02554-2.

[73] Zhong-Bo Kang, Jian-Wei Qiu, Werner Vogelsang, and Feng Yuan. Observation concerning the process dependence of the sivers functions. *Physical Review D*, 83 (9), May 2011. ISSN 1550-2368. doi: 10.1103/physrevd.83.094001. URL http://dx.doi.org/10.1103/PhysRevD.83.094001.

[74] Zhong-Bo Kang and Jian-Wei Qiu. Single transverse spin asymmetry of dilepton production near pole. *Physical Review D*, 81(5), March 2010. ISSN 1550-2368. doi: 10.1103/physrevd.81.054020. URL http://dx.doi.org/10.1103/PhysRevD.81.054020.

[75] Stanley J. Brodsky, Dae Sung Hwang, Yuri V. Kovchegov, Ivan Schmidt, and Matthew D. Sievert. Single-spin asymmetries in semi-inclusive deep inelastic scattering and drell-yan processes. *Physical Review D*, 88(1), July 2013. ISSN 1550-2368. doi: 10.1103/physrevd.88.014032. URL http://dx.doi.org/10.1103/PhysRevD.88.014032.

[76] Ignazio Scimemi and Alexey Vladimirov. Analysis of vector boson production within tmd factorization. *The European Physical Journal C*, 78(2), January 2018. ISSN 1434-6052. doi: 10.1140/epjc/s10052-018-5557-y. URL http://dx.doi.org/10.1140/epjc/s10052-018-5557-y.

[77] Ignazio Scimemi and Alexey Vladimirov. Non-perturbative structure of semi-inclusive deep-inelastic and drell-yan scattering at small transverse momentum. *Journal of High Energy Physics*, 2020(6), June 2020. ISSN 1029-8479. doi: 10.1007/jhep06(2020)137. URL http://dx.doi.org/10.1007/JHEP06(2020)137.

[78] Alessandro Bacchetta, Valerio Bertone, Chiara Bissolotti, Giuseppe Bozzi, Matteo Cerutti, Fulvio Piacenza, Marco Radici, and Andrea Signori. Unpolarized transverse momentum distributions from a global fit of drell-yan and semi-inclusive deep-inelastic scattering data. *Journal of High Energy Physics*, 2022(10), October 2022. ISSN 1029-8479. doi: 10.1007/jhep10(2022)127. URL http://dx.doi.org/10.1007/JHEP10(2022)127.

[79] Valentin Moos, Ignazio Scimemi, Alexey Vladimirov, and Pia Zurita. Extraction of unpolarized transverse momentum distributions from fit of drell-yan data at n^4ll, 2024. URL https://arxiv.org/abs/2305.07473.

[80] Alessandro Bacchetta, Valerio Bertone, Chiara Bissolotti, Giuseppe Bozzi, Matteo Cerutti, Filippo Delcarro, Marco Radici, Lorenzo Rossi, and Andrea Signori. Flavor dependence of unpolarized quark transverse momentum distributions from a global fit. *Journal of High Energy Physics*, 2024(8), August 2024. ISSN 1029-8479. doi: 10.1007/jhep08(2024)232. URL http://dx.doi.org/10.1007/JHEP08(2024)232.

[81] Miguel G. Echevarria, Zhong-Bo Kang, and John Terry. Global analysis of the sivers functions at nlo+nnll in qcd. *Journal of High Energy Physics*, 2021(1), January 2021. ISSN 1029-8479. doi: 10.1007/jhep01(2021)126. URL http://dx.doi.org/10.1007/JHEP01(2021)126.

[82] Alessandro Bacchetta, Filippo Delcarro, Cristian Pisano, and Marco Radici. The 3-dimensional distribution of quarks in momentum space. *Physics Letters B*, 827:136961, April 2022. ISSN 0370-2693. doi: 10.1016/j.physletb.2022.136961. URL http://dx.doi.org/10.1016/j.physletb.2022.136961.

[83] Marcin Bury, Alexei Prokudin, and Alexey Vladimirov. Extraction of the sivers function from sidis, drell-yan, and w±/z boson production data with tmd evolution. *Journal of High Energy Physics*, 2021(5), May 2021. ISSN 1029-8479. doi: 10.1007/jhep05(2021)151. URL http://dx.doi.org/10.1007/JHEP05(2021)151.

[84] C. Adolph et al. Ii – experimental investigation of transverse spin asymmetries in mu-p sidis processes: Sivers asymmetries. *Physics Letters B*, 717(4–5):383–389, October 2012. ISSN 0370-2693. doi: 10.1016/j.physletb.2012.09.056. URL http://dx.doi.org/10.1016/j.physletb.2012.09.056.

[85] M. Aghasyan et al. First measurement of transverse-spin-dependent azimuthal asymmetries in the drell-yan process. *Physical Review Letters*, 119(11), September 2017. ISSN 1079-7114. doi: 10.1103/physrevlett.119.112002. URL http://dx.doi.org/10.1103/PhysRevLett.119.112002.

[86] Xiangdong Ji, Jian-Ping Ma, and Feng Yuan. Qcd factorization for semi-inclusive deep-inelastic scattering at low transverse momentum. *Physical Review D*, 71(3), February 2005. ISSN 1550-2368. doi: 10.1103/physrevd.71.034005. URL http://dx.doi.org/10.1103/PhysRevD.71.034005.

[87] Alessandro Bacchetta, Markus Diehl, Klaus Goeke, Andreas Metz, Piet J Mulders, and Marc Schlegel. Semi-inclusive deep inelastic scattering at small transverse momentum. *Journal of High Energy Physics*, 2007(02):093–093, February 2007. ISSN 1029-8479. doi: 10.1088/1126-6708/2007/02/093. URL http://dx.doi.org/10.1088/1126-6708/2007/02/093.

[88] Alessandro Bacchetta, Umberto D'Alesio, Markus Diehl, and C. Miller. Single-spin asymmetries: The trento conventions. *Physical Review D*, 70(11), December 2004. ISSN 1550-2368. doi: 10.1103/physrevd.70.117504. URL http://dx.doi.org/10.1103/PhysRevD.70.117504.

[89] Aneesh V. Manohar. Deep inelastic scattering as x using soft-collinear effective theory. *Physical Review D*, 68(11), December 2003. ISSN 1089-4918. doi: 10.1103/physrevd.68.114019. URL http://dx.doi.org/10.1103/PhysRevD.68.114019.

[90] Ahmad Idilbi and Xiangdong Ji. Threshold resummation for the drell-yan process in the soft-collinear effective theory. *Physical Review D*, 72(5), September 2005. ISSN 1550-2368. doi: 10.1103/physrevd.72.054016. URL http://dx.doi.org/10.1103/PhysRevD.72.054016.

[91] Alexey Vladimirov. Structure of rapidity divergences in soft factors, 2017. URL https://arxiv.org/abs/1707.07606.

[92] Jianwei Qiu and George Sterman. Single transverse-spin asymmetries in hadronic pion production. *Physical Review D*, 59(1), November 1998. ISSN 1089-4918. doi: 10.1103/physrevd.59.014004. URL http://dx.doi.org/10.1103/PhysRevD.59.014004.

[93] A. V. Efremov and O. V. Teryaev. THE TRANSVERSAL POLARIZATION IN QUANTUM CHROMODYNAMICS. *Sov. J. Nucl. Phys.*, 39:962, 1984.

[94] Justin Cammarota, Leonard Gamberg, Zhong-Bo Kang, Joshua A. Miller, Daniel Pitonyak, Alexei Prokudin, Ted C. Rogers, and Nobuo Sato. Origin of single transverse-spin asymmetries in high-energy collisions. *Physical Review D*, 102(5), September 2020. ISSN 2470-0029. doi: 10.1103/physrevd.102.054002. URL http://dx.doi.org/10.1103/PhysRevD.102.054002.

[95] S. Arnold, A. Metz, and M. Schlegel. Dilepton production from polarized hadron hadron collisions. *Physical Review D*, 79(3), February 2009. ISSN 1550-2368. doi: 10.1103/physrevd.79.034005. URL http://dx.doi.org/10.1103/PhysRevD.79.034005.

[96] M. Anselmino, M. Boglione, U. D'Alesio, S. Melis, F. Murgia, and A. Prokudin. Sivers effect in drell-yan processes. *Physical Review D*, 79(5), March 2009. ISSN 1550-2368. doi: 10.1103/physrevd.79.054010. URL http://dx.doi.org/10.1103/PhysRevD.79.054010.

[97] Jin Huang, Zhong-Bo Kang, Ivan Vitev, and Hongxi Xing. Spin asymmetries for vector boson production in polarized collisions. *Physical Review D*, 93(1), January 2016. ISSN 2470-0029. doi: 10.1103/physrevd.93.014036. URL http://dx.doi.org/10.1103/PhysRevD.93.014036.

[98] John C. Collins, Davison E. Soper, and George Sterman. Factorization of hard processes in qcd, 2004. URL https://arxiv.org/abs/hep-ph/0409313.

[99] J. F. Owens. Large Momentum Transfer Production of Direct Photons, Jets, and Particles. *Rev. Mod. Phys.*, 59:465, 1987. doi: 10.1103/RevModPhys.59.465.

[100] Chris Kouvaris, Jian-Wei Qiu, Werner Vogelsang, and Feng Yuan. Single transverse-spin asymmetry in high transverse momentum pion production in pp collisions. *Physical Review D*, 74(11), December 2006. ISSN 1550-2368. doi: 10.1103/physrevd.74.114013. URL http://dx.doi.org/10.1103/PhysRevD.74.114013.

[101] Leonard Gamberg and Zhong-Bo Kang. Process dependent sivers function and implication for single spin asymmetry in inclusive hadron production. *Physics Letters B*, 696 (1–2):109–118, January 2011. ISSN 0370-2693. doi: 10.1016/j.physletb.2010.11.066. URL http://dx.doi.org/10.1016/j.physletb.2010.11.066.

[102] Xiaoyu Wang, Zhun Lu, and Ivan Schmidt. Transverse momentum spectrum of dilepton pair in the unpolarized π- n drell-yan process within tmd factorization. *Journal of High Energy Physics*, 2017(8), August 2017. ISSN 1029-8479. doi: 10.1007/jhep08(2017)137. URL http://dx.doi.org/10.1007/JHEP08(2017)137.

[103] P.C. Barry, N. Sato, W. Melnitchouk, and Chueng-Ryong Ji. First monte carlo global qcd analysis of pion parton distributions. *Physical Review Letters*, 121(15), October 2018. ISSN 1079-7114. doi: 10.1103/physrevlett.121.152001. URL http://dx.doi.org/10.1103/PhysRevLett.121.152001.

[104] H1 and ZEUS Collaborations. Combination of measurements of inclusive deep inelastic $e^{\pm}p$ scattering cross sections and qcd analysis of hera data, 2015. URL https://arxiv.org/abs/1506.06042.

[105] Daniel de Florian, R. Sassot, Manuel Epele, Roger J. Hernández-Pinto, and Marco Stratmann. Parton-to-pion fragmentation reloaded. *Physical Review D*, 91(1), January 2015. ISSN 1550-2368. doi: 10.1103/physrevd.91.014035. URL http://dx.doi.org/10.1103/PhysRevD.91.014035.

[106] Daniel de Florian, Manuel Epele, Roger J. Hernández-Pinto, R. Sassot, and Marco Stratmann. Parton-to-kaon fragmentation revisited. *Physical Review D*, 95(9), May 2017. ISSN 2470-0029. doi: 10.1103/physrevd.95.094019. URL http://dx.doi.org/10.1103/PhysRevD.95.094019.

[107] Jian Zhou, Feng Yuan, and Zuo-Tang Liang. Qcd evolution of the transverse momentum dependent correlations. *Physical Review D*, 79(11), June 2009. ISSN 1550-2368. doi: 10.1103/physrevd.79.114022. URL http://dx.doi.org/10.1103/PhysRevD.79.114022.

[108] Werner Vogelsang and Feng Yuan. Next-to-leading order calculation of the single transverse spin asymmetry in the drell-yan process. *Physical Review D*, 79(9), May 2009. ISSN 1550-2368. doi: 10.1103/physrevd.79.094010. URL http://dx.doi.org/10.1103/PhysRevD.79.094010.

[109] V. M. Braun, A. N. Manashov, and B. Pirnay. Scale dependence of twist-three contributions to single spin asymmetries. *Physical Review D*, 80(11), December 2009. ISSN 1550-2368. doi: 10.1103/physrevd.80.114002. URL http://dx.doi.org/10.1103/PhysRevD.80.114002.

[110] Zhong-Bo Kang and Jian-Wei Qiu. Qcd evolution of naive-time-reversal-odd parton distribution functions. *Physics Letters B*, 713(3):273–276, July 2012. ISSN 0370-2693. doi: 10.1016/j.physletb.2012.06.021. URL http://dx.doi.org/10.1016/j.physletb.2012.06.021.

[111] Zhong-Bo Kang, Enke Wang, Xin-Nian Wang, and Hongxi Xing. Next-to-leading order qcd factorization for semi-inclusive deep inelastic scattering at twist 4. *Physical Review Letters*, 112(10), March 2014. ISSN 1079-7114. doi: 10.1103/physrevlett.112.102001. URL http://dx.doi.org/10.1103/PhysRevLett.112.102001.

[112] Andreas Schäfer and Jian Zhou. Note on the scale evolution of the efremov-teryaev-qiu-sterman function. *Physical Review D*, 85(11):117501, 2012. ISSN 1550-2368. doi: 10.1103/PhysRevD.85.117501. URL http://dx.doi.org/10.1103/PhysRevD.85.117501.

[113] J.P. Ma, Q. Wang, and G.P. Zhang. Qcd evolutions of twist-3 chirality-odd operators. *Physics Letters B*, 718(4–5):1358–1363, January 2013. ISSN 0370-2693. doi: 10.1016/j.physletb.2012.12.007. URL http://dx.doi.org/10.1016/j.physletb.2012.12.007.

[114] Ling-Yun Dai, Zhong-Bo Kang, Alexei Prokudin, and Ivan Vitev. Next-to-leading order transverse momentum-weighted sivers asymmetry in semi-inclusive deep inelastic scattering: The role of the three-gluon correlator. *Physical Review D*, 92(11), December 2015. ISSN 1550-2368. doi: 10.1103/physrevd.92.114024. URL http://dx.doi.org/10.1103/PhysRevD.92.114024.

[115] Daniel Callos, Zhong-Bo Kang, and John Terry. Extracting the transverse momentum dependent polarizing fragmentation functions. *Physical Review D*, 102(9), November 2020. ISSN 2470-0029. doi: 10.1103/physrevd.102.096007. URL http://dx.doi.org/10.1103/PhysRevD.102.096007.

[116] Cristian Pisano, Alessandro Bacchetta, Filippo Delcarro, Marco Radici, and Andrea Signori. A first determination of the unpolarized quark tmds from a global analysis, 2018. URL https://arxiv.org/abs/1801.08443. arXiv:1801.08443 [hep-ph].

[117] R. Abdul Khalek et al. Snowmass 2021 white paper: Electron ion collider for high energy physics, 2022. URL https://arxiv.org/abs/2203.13199.

[118] C. Allaire, R. Ammendola, E.C. Aschenauer, and et al. Artificial intelligence for the electron ion collider (ai4eic). *Computational Software in Big Science*, 8 (5), 2024. doi: 10.1007/s41781-024-00113-4. URL https://doi.org/10.1007/s41781-024-00113-4.

[119] Y. X. Zhao et al. Single spin asymmetries in charged kaon production from semi-inclusive deep inelastic scattering on a transversely polarized he target. *Physical Review C*, 90(5), November 2014. ISSN 1089-490X. doi: 10.1103/physrevc.90.055201. URL http://dx.doi.org/10.1103/PhysRevC.90.055201.

[120] R. Seidl et al. Measurement of azimuthal asymmetries in inclusive production of hadron pairs. *Physical Review D*, 78(3), August 2008. ISSN 1550-2368. doi: 10.1103/physrevd.78.032011. URL http://dx.doi.org/10.1103/PhysRevD.78.032011.

[121] J.P. Lees et al. Measurement of collins asymmetries in inclusive production of charged pion pairs in e+e- annihilation atbabar. *Physical Review D*, 90(5), September 2014. ISSN 1550-2368. doi: 10.1103/physrevd.90.052003. URL http://dx.doi.org/10.1103/PhysRevD.90.052003.

[122] J.P. Lees et al. Collins asymmetries in inclusive charged pairs produced kaons and kaon pion in annihilation. *Physical Review D*, 92(11), December 2015. ISSN 1550-2368. doi: 10.1103/physrevd.92.111101. URL http://dx.doi.org/10.1103/PhysRevD.92.111101.

[123] M. Ablikim et al. Measurement of azimuthal asymmetries in inclusive charged dipion production in e+e- annihilations. *Physical Review Letters*, 116(4), January 2016. ISSN 1079-7114. doi: 10.1103/physrevlett.116.042001. URL http://dx.doi.org/10.1103/PhysRevLett.116.042001.

[124] L. Adamczyk et al. Azimuthal transverse single-spin asymmetries of inclusive jets and charged pions within jets from polarized-proton collisions at 500 gev. *Physical Review D*, 97(3), February 2018. ISSN 2470-0029. doi: 10.1103/physrevd.97.032004. URL http://dx.doi.org/10.1103/PhysRevD.97.032004.

[125] Feng Yuan. Asymmetric azimuthal distribution of hadrons inside a jet from hadron-hadron collisions. *Physical Review Letters*, 100(3), January 2008. ISSN 1079-7114. doi: 10.1103/physrevlett.100.032003. URL http://dx.doi.org/10.1103/PhysRevLett.100.032003.

[126] Zhong-Bo Kang, Alexei Prokudin, Peng Sun, and Feng Yuan. Extraction of quark transversity distribution and collins fragmentation functions with qcd evolution. *Physical Review D*, 93(1), January 2016. ISSN 2470-0029. doi: 10.1103/physrevd.93.014009. URL http://dx.doi.org/10.1103/PhysRevD.93.014009.